



## **Report of the Ad Hoc Team Tsunami Generated by Volcanoes (TGV) (V1.3 24<sup>th</sup> February 2023)**

### **0 Introduction**

After the destructive tsunamis in Greenland in 2017 and Indonesia in 2018 that were generated by landslides, volcanic eruptions and earthquakes outside subduction zones, the Intergovernmental Oceanographic Commission (IOC) of UNESCO on Tsunamis and Other Hazards related to Sea Level Warning and Mitigation Systems (TOWS-WG) identified the need to provide to Member States a report summarizing relevant information and knowledge on tsunami warning systems for tsunami events generated by non-seismic and complex sources, which have made up 13% of the world's confirmed tsunamis.

Non-seismic and complex sources of tsunamis are volcanic sources, such as underwater explosions, pyroclastic flows, large scale collapses, etc., underwater landslides, and tsunamis triggered by meteorological perturbations (meteotsunamis).

In 2020, an Ad Hoc Team on Atypical Tsunamis was established by the TOWS-WG Task Team on Tsunami Watch Operations (TT-TWO). The mandate of the team was to investigate these events, document the current state of monitoring and warning for such events, and provide guidance and recommendation to IOC Member States. The ad hoc team presented its final report on February 2022, which was accepted by the TT-TWO Task Team and endorsed by the 15<sup>th</sup> Session of the TOWS-WG. That report is in the process of publication by the IOC.

Due to the importance of the tsunami hazard related to volcanism, in February 2022 the TT TWO decided to establish a new Ad Hoc Team on Tsunamis Generated by Volcanoes (TGV Team).

The purpose was, as recommended by IOC General Assembly in 2021, to document the current state of monitoring and warning of volcanic tsunamis and provide guidance to Member States and IOC on this topic.

François Schindelé was nominated as Chair of the TGV Team. The TGV Team is composed by 6 Members :

- François Schindelé (FS), France, international expert on seismology and tsunami warning systems
- Laura Kong (LK), USA, Director International Tsunami Information Center (ITIC)
- Emily Lane (EL), New-Zealand, physicist, modelling of tsunami

- Raphaël Paris (RP), France, volcanologist, expert on volcanic tsunamis
- Maurizio Rippepe (MR), Italy, geophysicist responsible of the tsunami warning at the Stromboli
- Vasily Tito (VT), USA, physicist, modelling of tsunamis

Rick Bailey (RB), Head of Secretariat for the IOC-UNESCO Intergovernmental Coordination Group for the Indian Ocean Tsunami Warning & Mitigation System (ICG/IOTWMS), contributed to the TGV Team activities as IOC Technical Secretariat.

The TGV Team met six times by video-conference, from April 2022 to February 2023.

During its first meeting, the TGV Team decided that in order to collect as much information as possible related to volcanic tsunami monitoring, warning systems, and hazard assessment, a survey with specific questions should be sent to persons-in-charge of Volcano Observatories and Institutes responsible for monitoring volcanoes close to the sea or ocean and/or agencies currently providing tsunami warnings for tsunamis generated by volcanoes.

In the message sent to the volcano observatories and tsunami warning agencies, it was specified that :

*A primary objective of the TGV Team is to make a list of the volcano observatories and agencies that monitor and warn of volcanoes that may generate tsunamis, including what type of networks and methods are using to do so*

*The TGV Team has accordingly prepared a specific questionnaire on the issue. We would very much appreciate if you could respond to the questionnaire and provide as much information or documents you can related to volcano tsunami monitoring and warning. **Your feedback will help guide us in developing best practice guidelines of how to warn communities at-risk of the threat from tsunamis generated by volcanic related sources.***

The questionnaire consisted of three parts (see Appendix 1) : (i) Volcanoes monitored; (ii) Description of the monitoring systems; and (iii) Description of the tsunami warning system.

The TGV Team prepared the following documents:

- a) Questionnaire sent to Volcano Observatories (see Appendix 1X)
- b) List of Volcano Observatories
- c) Report on volcanic tsunamis, including a summary of the responses to the Questionnaire.
- d) List of potentially tsunamigenic volcanoes

This present report includes the following chapters (main contributors' initials):

- 0 Introduction and background (include summary from questionnaire) (FS, LK, RB)
- 1 Tsunami generated by volcanic activity (RP, EL)
- 2 Numerical modelling of volcanic tsunamis (EL, VT, RP)
- 3 Volcanic tsunami hazard assessment Stromboli (MR)
- 4 Volcano monitoring requirements for tsunami warning (Stromboli following chapter 1) (MR, RP)
- 5 Volcanic tsunami warning systems and SOPs (Stromboli SOP example, Indonesia) (MR, LK, RB)

6 Recommendations (FS, LK)

Appendix 1 Volcano observatory questionnaire - quick summary (LK et al)

Appendix 2 : list of tsunamigenic volcanoes (RP)

A draft report was finalised in early February 2023 and sent to the TT TWO for review. The Chair of the TGV Team, and members presented the report during the TT-TWO meeting on 27 February 2023. The recommendations to the TT-TWO are :

***The TGV Team recommends*** that the TOWS-WG:

- 1) Accepts the recommendations of the report.
- 2) Requests the IOC to publish the report in 2023 as IOC Technical Manual or other IOC publication.

All TGV Team members participated in the video-conferences and provided material and documents to prepare the different components of this report.

DRAFT

## Chapter 1– Tsunamis generated by volcano activity and instability

What we commonly call a “volcanic tsunami” corresponds to a tsunami that is generated by either eruptive processes, rapid ground deformation, or flank instability of volcanoes (Day, 2015; Paris, 2015). Following this definition, volcanic tsunamis represent ~6% of all listed tsunamis during the last four centuries (NCEI, ITIC, 2022). Historical examples and theoretical studies on tsunami generation have made it possible to distinguish different types of volcanic tsunamis (Fig. 1). Here we provide background information on the physical phenomena associated with each of these tsunami sources, as well as examples of historical and recent case-studies.

### A- Subaerial landslide

Flank instability of volcanoes has been widely documented. Indeed, volcano flanks display a broad variety of instabilities, from rock falls, cliff collapses and small landslides (with volumes typically in the order of  $10^5$ - $10^6$  m<sup>3</sup>) to large debris avalanches ( $10^8$ - $10^9$  m<sup>3</sup>). Volcano flanks are particularly unstable as a result of both endogenous (structural discontinuities, hydrothermal alteration, and magmatic intrusions inside the edifice, rapid growth by accumulation of tephra and lava flows) and exogenous factors (earthquake, tectonic uplift, climatic event, sea level variations).

In the case of a subaerial landslide, the entrance of a mass flow into water generates an impulsive wave, which then propagates away from the source. The water above the flow is pushed upward, and the water in front is pushed forward. The impulse (forced) wave first travels at the speed of the slide front, and then becomes a free wave. In the near-field, this leading wave is usually the largest wave, because it received most of the energy transferred from the landslide at impact. The height of the first wave increases with increasing landslide Froude number, relative thickness, mass flux and volume (e.g., Fritz et al., 2004; Viroulet et al., 2013; Yavari-Ramshe & Ataie-Ashtiani, 2016; Lee & Huang, 2020). In terms of tsunami generation, there is no specific difference between landslides observed on the flank of volcanoes and other landslides, each event having its own structural setting, lithology, and rheology. Landslides on the flanks of a volcano may occur separately from an eruption (e.g., following heavy rains), but the largest landslides are related to increased volcanic activity or major eruptions (e.g., debris avalanche). Note that some of the landslides listed below (Table 1) involved both subaerial and submarine material (e.g., Stromboli 2002, Anak Krakatau 2018).

Table 1 – Examples of tsunamis generated by volcano flank instability.

Volcano	Location	Year	Landslide volume	Max tsunami runup (dist. from source)	Reference
Anak Krakatau	Sunda Strait, Indonesia	2018	$210 \times 10^6$ m <sup>3</sup>	85 m (4 km)	Muhari et al. (2019), Walter et al. (2019), Borrero et al. (2020), Perttu et al. (2020), Putra et al. (2020), Hunt et al. (2021)
Stromboli	Aeolian Islands, Italy	2002	$17 \times 10^6$ m <sup>3</sup> and $5 \times 10^6$ m <sup>3</sup>	11 m (1.5 km)	Bonaccorso et al. (2003), Maramai et al. (2005)
Kilauea	Hawaii, USA	1994	$\sim 10^5$ m <sup>3</sup>	15 m (50 m)	Mattox and Mangan (1997)
Iliwerung	Lembata, Indonesia	1979	$50 \times 10^6$ m <sup>3</sup>	9 m (18 km)	Lassa (2009), Yudhicara et al. (2015)
Ritter Island	Papua New Guinea	1888	5 km <sup>3</sup>	15 m (9 km)	Johnson (1987), Ward and Day (2003), Kartens et al. (2019)
Unzen-Mayuyama	Kyushu, Japan	1792	$340 \times 10^6$ m <sup>3</sup>	57 m (7 km)	Tsuji and Hino (1993), Inoue (2000)
Oshima-Oshima	Japan Sea, Japan	1741	2.4 km <sup>3</sup>	13 m (50 km)	Satake & Kato (2001), Satake (2007)

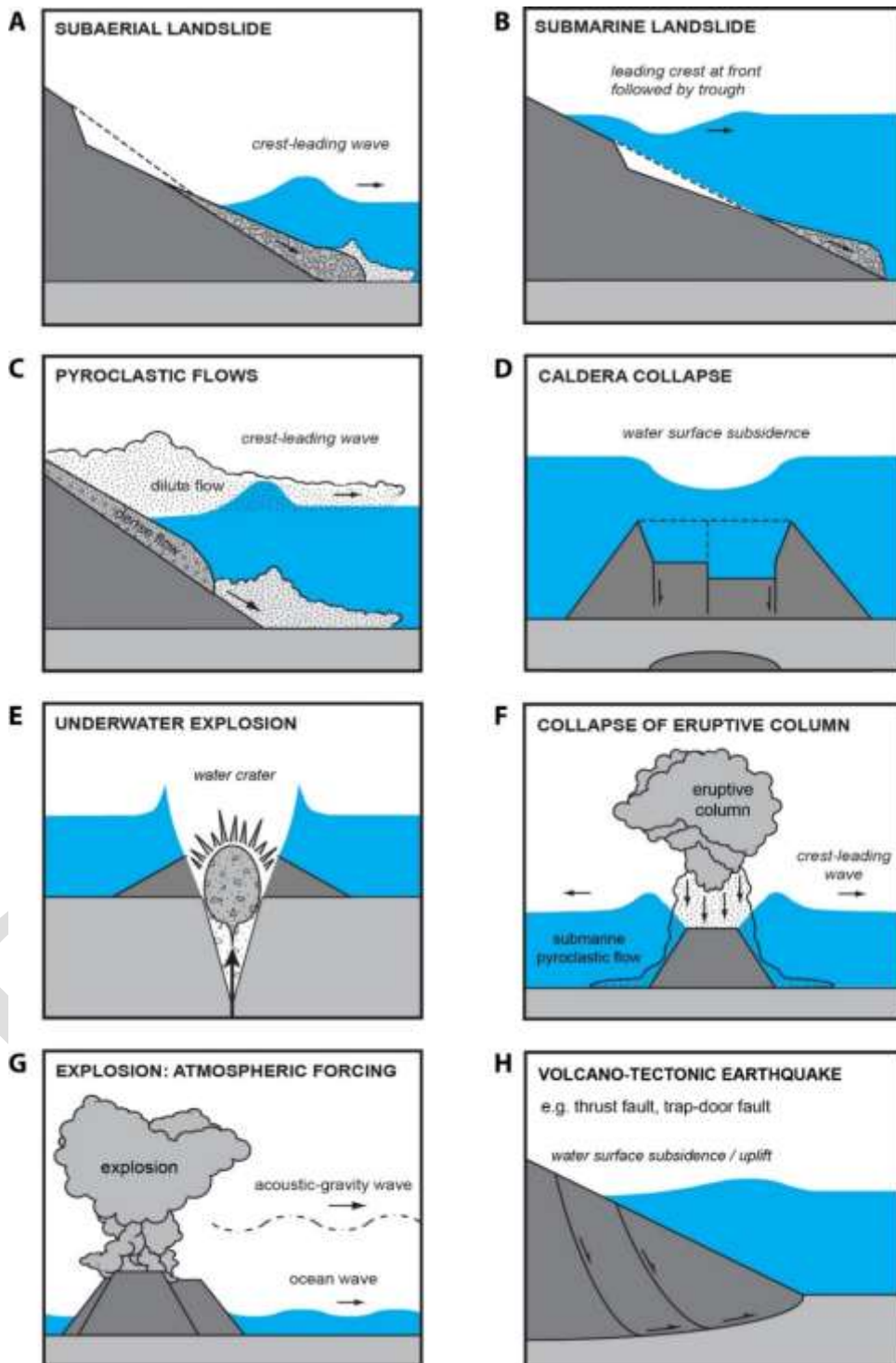


Figure 1 – Different types of volcanic tsunamis, i.e., tsunamis generated by volcano activity and instability (updated from Paris et al., 2014a).

## B- Submarine landslide

Many volcanoes are entirely (volcanic seamounts) or partly (volcanic islands) submarine or sublacustrine. As for subaerial landslides, the volumes implied by submarine landslides range from small-scale ( $10^5$ - $10^6$  m<sup>3</sup>) events (e.g., collapses of coastal lava deltas, landslides in submarine canyons) to massive collapses on the submarine flanks of ocean islands (up to tens of km<sup>3</sup>). The number of tsunamis generated by submarine landslide on volcanoes is probably underestimated due to a lack of observations and data. For this reason, there are few unequivocal historical examples (Table 1: Ritter Island 1888).

In the case of a submarine landslide, the main parameters are the volume of the sliding mass, its initial acceleration, and its maximum velocity (Ward, 2001; Grilli & Watts, 2005; Harbitz et al., 2006, Yavari-Ramshe & Ataie-Ashtiani, 2016). Tsunamis generated by submarine landslides typically display three successive waves: (1) A first crest ahead of the landslide front, as a consequence of the energy transferred from the slide, (2) followed by a large trough propagating at the speed of the landslide front, and (3) a final crest which later represents the main cause of inundation.

## C- Pyroclastic flow

Pyroclastic flows are hot mixtures of gas and particles generated by volcanic eruptions, particularly in the case of a dome collapse or a plume (eruptive column) collapse. Pyroclastic flows can generate tsunamis, as demonstrated by recent examples (Table 2: Montserrat 2003, Stromboli 2019), but the conditions required to generate a tsunami and the mechanisms of interaction between the flow and the water are still poorly understood, due to a lack of observations and the absence of a physical model.

The dense basal component of the pyroclastic flow is the main source of tsunami generation, but other phenomena such as steam explosion, flow pressure and shear, and pressure impulse could theoretically generate small waves (Watts and Waythomas, 2003). The important parameters controlling the generation of a tsunami by pyroclastic flows are the flow volume and mass flux, together with the flow density and permeability (ash-rich flows being more tsunamigenic because of their low permeability), the angle of incidence, and the transport distance from the eruptive vent (Watts and Waythomas, 2003; Bougouin et al., 2020). High-velocity pyroclastic flows with a bulk density near or even below that of water may generate waves, whatever their temperature (Bougouin et al., 2020; Freundt et al., 2003).

Table 2 – Examples of tsunami generated by pyroclastic flow.

Volcano	Location	Year	Volume (flux)	Max tsunami runup (dist. from source)	Reference
Stromboli	Aeolian Islands, Italy	2019	$10^5 - 10^6$ m <sup>3</sup>	0.3 m (2 km)	Italian Civil Protection
Soufriere Hills	Montserrat, Antilles	2003	$200 \times 10^6$ m <sup>3</sup> ( $13 \times 10^4$ m <sup>3</sup> /s)	4 m (4 km)	Pelinovsky et al. (2004), Herd et al. (2005)
Soufriere Hills	Montserrat, Antilles	1997	$20 \times 10^6$ m <sup>3</sup>	3 m (10 km)	Lander et al. (2002), Pelinovsky et al. (2004)
Rabaul	Papua New Guinea	1994	nd	8 m (4 km)	Blong and McKee (1995), Nishimura et al. (2005)
Krakatau	Sunda Strait, Indonesia	1883	nd ( $10^7$ m <sup>3</sup> /s?)	40 m (67 km)	Simkin & Fiske (1983), Carey et al. (2000), Maeno & Imamura (2011), Paris et al. (2014b)

## D- Caldera collapse

Large explosive eruptions may result in the collapse of the central part of the edifice, thus forming a caldera. For an underwater eruption, the caldera collapse produces a subsidence of the water surface that initiates the propagation of a leading trough. The amplitude of the water subsidence depends on the volume and geometry of the collapse, and above all on its duration (Gray and Monaghan, 2003; Maeno et al., 2006; Ulvrova et al., 2016). Large collapses lasting a few minutes are theoretically tsunamigenic, but probably unrealistic. Based on recent examples, the duration of a caldera collapse during an explosive eruption typically lasts more than 30 minutes (Stix & Kobayashi, 2008). There are different types of geometry and collapse mechanisms (Roche et al., 2000; Stix & Kobayashi, 2008). Consequently, there is no unequivocal examples of tsunamis generated by a caldera collapse. Other phenomena, such as underwater explosions, eruptive column collapse, and pyroclastic flows may generate tsunamis during an explosive caldera-forming eruption, which makes it difficult to determine the source of the tsunami(s), as illustrated by the near-field tsunami that impacted the Tonga Islands during the 2022 eruption of Hunga Tonga Hunga A'Apai (HTHH) volcano.

## E- Underwater explosion

The theory of water waves generated by underwater explosions is well documented, and it was applied to nuclear, chemical, and volcanic explosions (Le Méhauté, 1971; Mirchina & Pelinovsky, 1988; Duffy, 1992; Le Méhauté & Wang, 1996; Egorov, 2007). After an underwater explosion and while different jet flows are ejected, the development of an underwater crater might be initiated, depending on water depth and energy of explosion. The subsequent expansion, rise and gravitational collapse of the crater create two successive bores followed by a number of smaller undulations propagating radially from the source.

In theory, all volcanic eruptions above 500 m water depth are potentially tsunamigenic, but in fact only a few of them are tsunamigenic. Compared to other sources of underwater explosions, the dynamics of phreatomagmatic eruptions is complex. The physics of magma-water interactions is controlled by many parameters: water depth, geometry of the vent and magma-water interface, transfer of thermal energy, processes of intermingling and mixing between magma and water, metastability of superheated water, and quantity of gas in the ascending magma (Kokelaar, 1986; Wohletz, 1986; Valentine and White, 2012). Field observations of underwater eruptions and laboratory experiments show two different types of fountains at the water surface, dome-regime, and finger-regime fountains, depending on explosion intensity and water depth (Shen et al., 2021a).

There is a critical water depth at which an explosion with a given intensity generate the largest waves (Shen et al., 2021b). Underwater explosions in the ocean typically generate waves of short period and great dispersion compared to earthquakes, thus reducing their far-field impact (Table 3: Myojin-Sho 1952). On the contrary, violent explosions in shallow waters, and more particularly in lakes, have the potential to produce high-runup local tsunamis (Table 3: Karymskoye Lake 1996).

Table 3 – Examples of tsunami generated by volcanic underwater explosion.

Volcano	Location	Year	Explosion energy	Max tsunami runup (dist. from source)	Reference
Karymskoye Lake	Kamchatka, Russia	1996	$5 \times 10^{14}$ J	19 m (840 m)	Belousov et al. (2000), Torsvik et al. (2010), Ulvrova et al. (2014), Falvard et al. (2018)
Myojin-Sho	Izu, Japan	1952	$10^{15}$ - $10^{16}$ J	1.5 m (130 km)	Dietz and Sheehy (1954), Nakano et al. (1954), Lipiejko et al. (2021)
Anak Krakatau	Sunda Strait, Indonesia	1928	nd	4 m (3.5 km)	Stehn (1929)

## F- Collapse of eruptive column

An eruption column or eruption plume is a cloud of volcanic tephra (mostly ash) suspended in gases emitted during an explosive eruption. The column may rise several kilometers in the atmosphere, up to 40-50 km in the stratosphere for the largest explosive eruptions. Continuous eruptions or closely spaced, discrete explosions will form sustained columns, whereas discrete explosions will produce transient columns. The collapse of an eruptive column is controlled by the evolution of buoyancy in the column. The column starts to collapse when the initial upward momentum is not sufficient to carry the flow up to the point of buoyancy inversion (Woods, 1988; Carazzo et al., 2015). As a consequence, the material (i.e., the tephra) can no longer be supported by convection and falls under gravity, forming a pyroclastic flow on the flanks of the volcano. The critical condition at which an eruptive column collapses depends on magma gas content, temperature, and magma discharge rate. The intensity of the collapse is variable from one eruption to another and, for stable plumes, it may evolve as a function of the buoyancy ratio (Carazzo et al., 2015).

If the eruption comes from a small island or a shallow-water volcano, the eruptive column may collapse directly in the water. Pyroclastic flows resulting from the collapse are then subaqueous and the collapse itself becomes the main source of tsunami. Although there is considerable literature on eruptive column collapse in volcanology, it is not commonly addressed as a source of volcanic tsunami. However, this neglected mechanism may have played a role in the generation of near-field tsunami during explosive eruptions such as Krakatau 1883 and HTHH 2022.

## G- Atmospheric forcing following explosion

The atmospheric waves that are produced during a major volcanic explosion can generate tsunami. This rare phenomenon was first documented for the 1883 eruption of Krakatau and extremely-well recorded for the 2022 eruption of HTHH volcano in the Tonga Islands. Tsunamis generated by such an atmospheric forcing represent the only type of volcanic tsunamis that may have a global reach.

The largest explosive eruptions generate a broad range of waves in the atmosphere, including acoustic-gravity waves that may reach the ionosphere (Astafyeva et al., 2022). Among these different types of atmospheric waves, compressional surface-guided Lamb waves travelling at the speed of sound can produce long-period waves in the ocean (Kubota et al., 2022; Omira et al., 2022). The air-water waves phase coupling lasts hours to days and so the associated tsunami lasts longer than usual earthquake-induced tsunamis. The leading tsunami wave also travels faster (i.e., at the speed of sound) than usual tsunamis (Carvajal et al., 2022). The following wave trains travel at the theoretical velocity of a tsunami ( $c=\sqrt{gh}$ ) in the ocean (Kubota et al., 2022; Omira et al., 2022).

Table 4 – Examples of tsunami generated by atmospheric forcing following an explosion.

Volcano	Location	Year	Explosion energy	Max tsunami runup (dist. from source)	Reference
HTHH	Tonga Islands	2022	$3.2 \times 10^{16}$ to $1.5 \times 10^{16}$ J	3.4 m (10300 km)	Astafyeva et al. (2022), Carvajal et al. (2022), Kubota et al. (2022), Omira et al. (2022)
Krakatau	Sunda Strait, Indonesia	1883	$10^{16}$ - $10^{17}$ J	1.6 m (8600 km)	Harkrider & Press (1967, Pelinovsky et al. (2005)



## H- Volcano-tectonic earthquake

Although earthquakes are often mentioned as a source of tsunami preceding or during a volcanic eruption, historical examples are poorly documented because the distinction between tectonic earthquakes, volcanic earthquakes, or other source mechanisms of tsunami (e.g., landslide) is often unclear. Among all kinds of earthquakes related to volcanic and magmatic processes, only volcano-tectonic (high-frequency) earthquakes can involve ground deformation large enough to generate tsunami. Volcano-tectonic earthquakes result from the accumulation of stress induced by magma ascent. They are characterized by seismic swarms at shallow depth (<10 km), with magnitudes typically lower than  $M_s = 6$ , thus generating very small-magnitude tsunamis, if any (Paris, 2015).

Two special cases are mentioned here (Table 5). First, earthquakes with magnitude  $M > 6$  on large thrust faults at the base of the oceanic shield volcanoes (e.g., Hawaii) can produce local tsunamis, as demonstrated by the 1975 Kalapana earthquake at Kilauea volcano, Hawaii (Ando, 1979; Ma et al., 1999; Day et al., 2005). Second, earthquakes with magnitude  $M_w < 6$  resulting from trapdoor faulting of submarine caldera floor can generate small-amplitude tsunamis, as frequently observed around the Sumisu caldera, Japan (Sandanbata et al., 2022)

Table 5 – Examples of tsunami generated by volcano-tectonic earthquake.

Volcano	Location	Year	Earthquake magnitude	Max tsunami runup	Reference
Sumisu (Smith) caldera	Izu-Bonin Islands, Japan	2015	$M_w = 5.7$	1 m (180 km)	Sandanbata et al. (2022)
Kilauea	Hawaii, USA	1975	$M_s = 7.2$	14.6 m (~20 km)	Ando (1969), Ma et al. (1999), Day et al. (2005)

**Conclusion:** The great majority of volcanic eruptions do not generate tsunami, but a single eruption might combine different sources of tsunamis (Table 6). Thus, the source of a tsunami observed during an eruption is often difficult to characterize. All source mechanisms listed here have different characteristics in terms of location, duration, volume, mass flux, and energy, which have consequences on the waves generated. Landslides are the most frequent sources of volcanic tsunamis. From all points of view, volcanic islands (arcs) are the most exposed to volcanic tsunamis.

Table 6 – Types of potentially tsunamigenic volcanoes and associated source mechanisms of tsunamis (updated from Paris et al., 2014a).

		Volcano type			
		Coastal / island stratovolcano	Submarine stratovolcano	Shallow-water caldera	Oceanic shield volcano
Tsunami source	Subaerial landslide				
	Submarine landslide				
	Underwater explosion				
	Caldera collapse				
	Column collapse				
	Pyroclastic flow				
	Volcano-tectonic earthquake				
	Atmospheric forcing				
Examples		Stromboli, Italy	HTHH, Tonga	Taal, Philippines	Kilauea, Hawaii
		Soufriere Hills, Montserrat	Kick'em Jenny, Grenada	Rabaul, Papua New Guinea	Fournaise, Reunion Island
		Unzen, Japan	Kolumbo, Greece	Krakatau, Indonesia	Fogo, Cape Verde

## References

- Ando, M., 1979. The Hawaii earthquake November 29, 1975: low dip angle faulting due to forceful injection of magma. *Journal of Geophysical Research* 84 (B13), 7616-7626.
- Astafyeva, E., Maletckii, B., Mikesell, T.D., Munaibari, E., Ravanelli, M., Coisson, P., et al., 2022. The 15 January 2022 Hunga Tonga eruption history as inferred from ionospheric observations. *Geophysical Research Letters* 49, e2022GL098827.
- Blong, R.J., McKee, C.O., 1995. The Rabaul eruption 1994 - Destruction of a town. *Natural Hazards Research Center, Macquarie University, Australia*, 52 p.
- Bonaccorso, A., Calvari, S., Garfi, L., Lodato, L., Patanè, D., 2003. Dynamics of the December 2002 flank failure and tsunami at Stromboli volcano inferred by volcanological and geophysical observations. *Geophysical Research Letters* 30, 1941.
- Borrero, J.C., Solihuddin, T., Fritz, H.M., Lynett, P.J., Prasetya, G.S., Skanavis, V., Husrin, S., Kushendratno, Kongko, W., Istiyanto, D.C., Daulat, A., Purbani, D., Salim, H.L., Hidayat, R., Asvaliantina, V., Usman, M., Kodijat, A., Son, S., Synolakis, C.E., 2020. Field Survey and Numerical Modelling of the December 22, 2018, Anak Krakatau Tsunami. *Pure Applied Geophysics*. 177, 2457–2475.
- Bougouin, A., Paris, R., Roche, O., 2020. Impact of fluidized granular flows into water: implications for tsunamis generated by pyroclastic flows. *Journal of Geophysical Research, Solid Earth* 125, e2019JB018954.
- Carazzo, G., Kaminski, E., Tait, S., 2015. The timing and intensity of column collapse during explosive volcanic eruptions. *Earth and Planetary Science Letters* 411, 208-217.
- Carey, S., Sigurdsson, H., Mandeville, C., Bronto, S., 2000. Volcanic hazards from pyroclastic flow discharge into the sea: examples from the 1883 eruption of Krakatau, Indonesia. *Geological Society of America Special Publication* 345, 1-14.
- Carvajal, M., Sepúlveda, I., Gubler, A., Garreaud, R., 2022. Worldwide signature of the 2022 Tonga volcanic tsunami. *Geophysical Research Letters* 49, e2022GL098153.
- Day, S.J., Watts, P., Grilli, S.T., Kirby, J.T., 2005. Mechanical models of the 1975 Kalapana, Hawaii earthquake and tsunami. *Marine geology* 215, 59-92.
- Day, S.J., 2015. Volcanic tsunamis. In: Sigurdson (Ed.), *Encyclopedia of Volcanoes*, Academic Press, Elsevier, 993-1009.
- Duffy, D.G., 1992. On the generation of oceanic surface waves by underwater volcanic explosions. *Journal of Volcanology and Geothermal Research* 50, 323-344.
- Egorov, Y., 2007. Tsunami wave generation by the eruption of underwater volcano. *Natural Hazards and Earth System Sciences* 7, 65-69.
- Falvard, S., Paris, R., Belousova, M., Belousov, A., Giachetti, T., Cuven, S., 2018. Scenario of the 1996 volcanic tsunamis in Karymskoye Lake, Kamchatka, inferred from X-ray tomography of heavy minerals in tsunami deposits. *Marine Geology* 396, 160-170.
- Fritz, H., Hager, W., Minor, H., 2004. Near Field Characteristics of Landslide Generated Impulse Waves. *Journal of Waterway Port Coastal and Ocean Engineering* 130, 287-302.
- Gray, J.P., Monaghan, J.J., 2003. Caldera collapse and the generation of waves. *Geochemistry, Geophysics, Geosystems* 4, 1015.

- Grilli, S. T., Watts, P., 2005. Tsunami generation by submarine mass failure. In: Modelling, Experimental Validation, and Sensitivity Analyses. *Journal of Waterway, Port, Coastal, and Ocean Engineering* 131, 283–297.
- Harbitz, C.B., Løvholt, F., Pedersen, G., Masson, D.G., 2006. Mechanisms of tsunami generation by submarine landslides: a short review. *Norw. J. Geol.* 86, 255–264.
- Harkrider, D.G., Press, F., 1967. The Krakatoa air-sea waves: an example of pulse propagation in coupled systems. *Geophys. J. R. Astron. Soc.* 13, 149-159.
- Herd, R.A., Edmonds, M., Bass, V.A., 2005. Catastrophic lava dome failure at Soufriere Hills Volcano, Montserrat, 12-13 July 2003. *Journal of Volcanology and Geothermal Research* 148, 234-252.
- Hunt, J.E., Tappin, D.R., Watt, S.F.L., Susilohadi, S., Novellino, A., Ebmeier, S.K., Cassidy, M., Engwell, S.L., Grilli, S.T., Hanif, M., Priyanto, W.S., Clare, M.A., Abdurrachman, M., Udrek, U., 2021. Submarine landslide megablocks show half of Anak Krakatau island failed on December 22nd, 2018. *Nature Communications* 12, 2827.
- Inoue, K., 2000. Shimabara–Shigatusaku earthquake and topographic change by Shimabara Catastrophe in 1792. *Geographical Reports of Tokyo Metropolitan University*, 35, 59–69.
- Johnson, R.W., 1987. Large-scale volcanic cone collapse; the 1888 slope failure of Ritter volcano. *Bulletin of Volcanology* 49, 669-679.
- Karstens, J., Berndt, C., Urlaub, M., Watt, S.F.L., Micallef, A., Ray, M., Klauke, I., Muff, S., Klaeschen, D., Kühn, M., Roth, T., Böttner, C., Schramm, B., Elger, J., Brune, S., 2019. From gradual spreading to catastrophic collapse – reconstruction of the 1888 Ritter Island volcanic sector collapse from high-resolution 3D seismic data. *Earth and Planetary Science Letters* 517, 1-13.
- Kokelaar, P., 1986. Magma-water interactions in subaqueous and emergent basaltic volcanism. *Bulletin of Volcanology* 48, 275-289.
- Kubota, T., Saito, T., Nishida, K., 2022. Global fast-traveling tsunamis driven by atmospheric Lamb waves on the 2022 Tonga eruption. *Science* 10.1126/science.abo4364
- Le Méhauté, B.L., 1971. Theory of explosion-generated water waves. In: Chow VT (Ed.) *Advances in Hydroscience* 7, Academic Press, New York, London, pp 1-79.
- Le Méhauté, B.L., Wang, S., 1996. Water waves generated by underwater explosion. *Advanced Series on Ocean Engineering* 10, World Scientific Publishing, New Jersey, 384 p.
- Lander, J.F., Whiteside, L.S., Lockridge, P.A., 2002. A brief history of tsunami in the Caribbean Sea. *Science of Tsunami Hazards* 20, 57-94.
- Lassa, J., 2009. The forgotten disaster? Remembering the Larantuka and Lembata disaster 1979-2009. *Journal of NTT Studies* 1, 159-184 (in Indonesian).
- Lee, C.H., Huang, Z., 2020. Multi-phase flow simulation of impulsive waves generated by a sub-aerial granular landslide on an erodible slope. *Landslides*, s10346-020-01527-y.
- Lipiejko, N., Whittaker, C.N., Lane, E.M., White, J.D.L., Power, W.L., 2021. Tsunami generation by underwater volcanic explosions: application to the 1952 explosions of Myojinsho volcano. *Pure and Applied Geophysics* 178, 4743-4761.
- Ma, K.F., Kanamori, H., Satake, K., 1999. Mechanism of the 1975 Kalapana, Hawaii, earthquake inferred from tsunami data. *Journal of Geophysical Research* 104 (B6), 13153-13167.
- Maeno, F., Imamura, F., Taniguchi, H., 2006. Numerical simulations of tsunamis generated by caldera collapse during the 7.3 ka Kikai eruption, Kyushu, Japan. *Earth Planets Space* 58, 1013-1024.

- Maeno, F., Imamura, F., 2011. Tsunami generation by a rapid entrance of pyroclastic flow into the sea during the 1883 Krakatau eruption, Indonesia. *Journal of Geophysical Research* 116, B09205.
- Maramai, A., Graziani, L., Alessio, G., Burrato, P., Colini, L., Cucci, L., Nappi, R., Nardi, A., Vilardo, G., 2005. Near- and far-field survey report of the 30 December 2002 Stromboli Southern Italy tsunami. *Marine Geology* 215, 93-106.
- Mattox, T.N., Mangan, M.T., 1997. Littoral hydrovolcanic explosions: a case-study of lava-seawater interaction at Kilauea volcano. *Journal of Volcanology and Geothermal Research* 75, 1-17.
- Mirchina, N.R., Pelinovsky, E.N., 1988. Estimation of underwater eruption energy based on tsunami wave data. *Natural Hazards* 1, 277–283.
- Muhari, A., Heidarzadeh, M., Susmoro, H., Nugroho, H.D., Kriswati, E., Supartoyo, Wijanarto, A.B., Imamura, F., Arikawa, T., 2019. The December 2018 Anak Krakatau Volcano Tsunami as Inferred from Post-Tsunami Field Surveys and Spectral Analysis. *Pure Applied Geophysics*. 176, 5219–5233.
- Nishimura, Y., Nakagawa, M., Kuduon, J., Wukawa, J., 2005. Timing and scale of tsunamis caused by the 1994 Rabaul eruption, East New Britain, Papua New Guinea. In: K. Satake (ed.) *Tsunamis: case studies and recent developments*, Springer, 43-56.
- Omira, R., Ramalho, R.S., Kim, J., González, P.J., Kadri, U., Miranda, J.M., carrilho, F., Baptista, M.A., 2022. Global Tonga tsunami explained by a fast-moving atmospheric source. *Nature* 609, 734–740.
- Paris, R., 2015. Source mechanisms of volcanic tsunamis. *Philosophical Transactions of the Royal Society A* 373, 20140380.
- Paris, R., Switzer, A.D., Belousova, M., Belousov, A., Ontowirjo, B., Whelley, P.L., Ulvrova, M., 2014a. Volcanic tsunami: a review of source mechanisms, past events, and hazards in Southeast Asia (Indonesia, Philippines, Papua New Guinea). *Natural Hazards* 70 (1), 447-470.
- Paris, R., Wassmer, P., Lavigne, F., Belousov, A., Belousova, M., Iskandarsyah, Y., Benbakkar, M., Ontowirjo, B., Mazzoni, N., 2014b. Coupling eruption and tsunami records: the Krakatau 1883 case-study, Indonesia. *Bulletin of Volcanology* 76, 814.
- Pelinovsky, E., Zahibo, N., Dunkley, P., Edmonds, M., Herd, R., Talipova, T., Kozelkov, A., Nikolkina, I., 2004. Tsunamis generated by the volcano eruption on July 12-13, 2003, at Montserrat, Lesser Antilles. *Science of Tsunami Hazards* 22, 44-57.
- Pelinovsky, E., Choi, B.H., Stromkov, A., Didenkulova, I., Kim, H.S., 2005. Analysis of tide-gauge records of the 1883 Krakatau tsunami. In: Satake, K. (Ed.) *Tsunamis: case studies and recent developments*. Springer, 57-78.
- Perttu, A., Caudron, C., Assink, J.D., Metz, D., Tailpied, D., Perttu, B., Hibert, C., Nurfiani, D., Pilger, C., Muzli, M., Fee, D., Andersen, O.L., Taisne, B., 2020. Reconstruction of the 2018 tsunamigenic flank collapse and eruptive activity at Anak Krakatau based on eyewitness reports, seismo-acoustic and satellite observations. *Earth and Planetary Science Letters* 541, 116268.
- Putra, P.S., Aswan, A., Maryunani, K.A., Yulianto, E., Nugroho, S.H., Setiawan, V., 2020. Post-Event Field Survey of the 22 December 2018 Anak Krakatau Tsunami. *Pure Applied Geophysics* 177, 2477–2492.
- Roche, O., Druitt, T.H., Merle, O., 2000. Experimental study of caldera formation. *Journal of Geophysical Research* 105, 395-416.
- Satake, K., 2007. Volcanic origin of the 1741 Oshima-Oshima tsunami in Japan Sea. *Earth Planets Space* 59, 381-390.

- Sandanbata, O., Watada, S., Satake, K., Kanamori, H., Rivera, L., Zhan, Z., 2022. Sub-decadal volcanic tsunamis due to submarine trapdoor faulting at Sumisu caldera in the Izu–Bonin Arc. *Journal of Geophysical Research: Solid Earth*, 127, e2022JB024213.
- Satake, K., Kato, Y., 2001. The 1741 Oshima-Oshima eruption: extent and volume of submarine debris avalanche. *Geophysical Research Letters* 28, 427-430.
- Shen, Y., Whittaker, C.N., Lane, E.M., White, J.D.L., Power, W., Nomikou, P., 2021a. Laboratory experiments on tsunamigenic discrete subaqueous volcanic eruptions. Part 1: Free surface disturbances. *Journal of Geophysical Research, Oceans* 126, e2020JC016588.
- Shen, Y., Whittaker, C.N., Lane, E.M., White, J.D.L., Power, W., Nomikou, P., 2021a. Laboratory experiments on tsunamigenic discrete subaqueous volcanic eruptions. Part 2: Properties of generated waves. *Journal of Geophysical Research, Oceans* 126, e2020JC016587.
- Simkin, T., Fiske, R.S., 1983. Krakatau 1883: The volcanic eruption and its effects. Smithsonian Institution Press, Washington DC, 464 p.
- Stehnn, C.E., 1929 The geology and volcanism of the Krakatau group. *Proceedings of the Fourth Pacific Science Congress, Batavia*, 1-55.
- Stix, J., Kobayashi, T., 2008. Magma dynamics and collapse mechanisms during four historic caldera-forming events. *Journal of Geophysical Research* 113, B09205.
- Torsvik, T., Paris, R., Didenkulova, I., Pelinovsky, E., Belousov, A., Belousova, M., 2010. Numerical simulation of explosive tsunami wave generation and propagation in Karymskoye Lake, Russia. *Natural Hazards and Earth System Sciences* 10, 2359-2369.
- Tsuji, Y., Hino, T., 1993. Damage and inundation height of the 1792 Shimabara landslide tsunami along the coast of Kumamoto prefecture. *Bulletin of the Earthquake Research Institute, University of Tokyo*, 682, 91-176.
- Ulvrova, M., Paris, R., Nomikou, P., Kelfoun, K., Leibbrandt, S., Tappin, D.R., McCoy, F.W., 2016. Source of the tsunami generated by the 1650 AD eruption of Kolumbo submarine volcano (Aegean Sea, Greece). *Journal of Volcanology and Geothermal Research* 321, 125-139.
- US NOAA National Centers for Environmental Information and International Tsunami Information Center, Tsunami Sources 1610 B.C. to A.D. 2022 , From Earthquakes, Volcanic Eruptions, Landslides, and Other Causes, 2022, [http://itic.ioc-unesco.org/images/stories/awareness\\_and\\_education/map\\_posters/2022\\_tsu\\_poster\\_20220823\\_a2.pdf](http://itic.ioc-unesco.org/images/stories/awareness_and_education/map_posters/2022_tsu_poster_20220823_a2.pdf)
- Valentine, G., A., White, J.D.L., 2012. Revised conceptual model for maar-diatremes: subsurface processes, energetics, and eruptive products. *Geology* 40, 1111-1114.
- Viroulet, S., Cébron, D., Kimmoun, O., & Kharif, C. (2013). Shallow water waves generated by subaerial solid landslides. *Geophysical Journal International*, 193, 747–762.
- Walter, T.R., Haghshenas Haghghi, M., Schneider, F.M., Coppola, D., Motagh, M., Saul, J., Babeyko, A., Dahm, T., Troll, V.R., Tilmann, F., Heimann, S., Valade, S., Triyono, R., Khomarudin, R., Kartadinata, N., Laiolo, M., Massimetti, F., Gaebler, P., 2019. Complex hazard cascade culminating in the Anak Krakatau sector collapse. *Nature Communications* 10, 4339.
- Ward, S.N., 2001. Landslide tsunami. *Journal of Geophysical Research* 6, 11201-11215.
- Watts, P., Waythomas, C.F., 2003. Theoretical analysis of tsunami generation by pyroclastic flows. *Journal of Geophysical Research* 108 B112, 2563.
- Wohletz, K.H., 1986. Explosive magma-water interactions: thermodynamics, explosion mechanisms, and field studies. *Bulletin of Volcanology* 48, 245-2654.

- Woods, A.W., 1988. The fluid dynamics and thermodynamics of eruption columns. *Bulletin of Volcanology* 50, 169-193.
- Yavari-Ramshe S., Ataie-Ashtiani B., 2016. Numerical modelling of subaerial and submarine landslide-generated tsunami waves - recent advances and future challenges. *Landslides* 13(6), 1325-1368.
- Yudhicara, Y. , Bani, P., Darmawan, A., 2015. Geothermal System as the Cause of the 1979 Landslide Tsunami in Lembata Island, Indonesia. *Indonesian Journal on Geoscience* 2 (2), 91-99.

DRAFT

## Chapter 2 - Numerical Modelling of volcanic tsunamis

### General consideration of model applications for volcanic tsunamis

Modelling tools may provide unique opportunities for volcanic tsunami hazard mitigation. In contrast with the seismically generated tsunamis, volcanic tsunamis mostly occur at well-defined locations of known volcanos, and the generation time could often be constrained (albeit with large uncertainties) within certain time periods of transient volcanic eruptions. Such a priori source information could be used for modelling potential volcanic tsunamis to provide actionable forecast information for near-term and long-term tsunami hazard assessment. A combination of research model studies, hazard assessment modelling products, and real-time forecast modelling could provide timely forecast information that is yet unachievable for much more random seismically generated tsunami.

Numerical models provide tools to evaluate impacts of possible volcanic tsunamis. Three main applications of the volcanic tsunami modelling are: (1) Research analysis to interpret data and improve scientific understanding of volcanic tsunami phenomena; (2) Tsunami hazard assessment to evaluate long-term risk from volcanic tsunamis and (3) real-time tsunami forecasting for tsunami warning and threat mitigation purposes. These different modelling goals dictate different numerical methods and different specifics of the models' applications.

Modelling for the research analysis of the volcanic tsunamis requires the least number of constraints regarding the numerical methods that can be used. The main limitation is the available computational resources. For this type of application, considering the complexity of the processes involved in the volcanic tsunami generation, sophisticated models are often needed. Since volcanic tsunami generation processes may involve multiple densities of fluids, phase-shifts, very fast, often supersonic flows, models based on various types of discretization and closures of the Navier-Stokes Equations are often used. Higher order approximations of these basic equations can also be applied. These models are often used as guidance for appropriate approximations to be used for more practical modelling applications that have more computational constraints.

Model studies for tsunami hazard analyses often involve many computations to perform multi-scenario ensemble runs for probabilistic or sensitivity analyses. In addition, the computations usually require high resolution of model discretization. These requirements substantially limit the numerical techniques that can be used. The Navier-Stokes Equations are rarely suitable for performing such studies due to large computational resources needed to solve them. Appropriate approximations must be made so that numerical analysis is achievable computationally but also suitable in terms of accuracy.

Real-time forecast applications are the most demanding in terms of numerical efficiency, since such applications required accurate forecasts in limited time. This requirement demands the use of highly efficient numerical implementation of models with optimal approximation of the Navier-Stokes Equations. Most volcanic tsunami generation mechanisms (see Chapter 1) create shorter waves in comparison with the seismically generated tsunamis. Shorter waves generally attenuate faster, even if the initial amplitudes are much larger. Therefore, most of volcanic tsunamis would impact only local coastlines. Local tsunami impact makes the real-time modelling applications especially challenging due to short time for forecast and often pre-modelled scenarios are the only feasible option. One notable exception is the tsunami generation by the atmospheric pressure forcing from the volcanic explosion, which, creates a global tsunami (e.g., Krakatau 1883, HTHH 2022). The local tsunami forecast is well-recognized problem of tsunami warning and forecast, however, this problem is especially acute for the volcano tsunamis.

All model applications require testing and validation, but this is especially important for the practical applications of tsunami hazard assessment and real-time forecasting. The simplifications of model formulations required for such studies must be validated before the model products can be trusted. The tsunami scientific community has developed the process of model validations (Synolakis et al., 2008), which has included a series of benchmarking workshops for specific tsunami applications over the years (see for example Lynett et al., 2017). Real-time applications must go through additional tests for operational suitability and the process of operational implementation, which put additional demands on model performance (Titov et al., 2016). Many of the characteristics of volcanic tsunamis are similar to those seen in landslide-generated tsunamis and so the extensive literature on that subject should also be considered (see Løvholt et al., 2015 and references therein)

Modelling of tsunamis in general is divided into three phases: generation, propagation, and inundation. The main differences between modelling seismic tsunamis and volcanic tsunamis are in the generation phase, therefore the bulk of this chapter will be dedicated to outlining different methods with volcanic tsunami generation for the different mechanisms outlined in chapter 1. We will also consider some aspects of the propagation of volcanic tsunamis, especially in the case of atmospheric forcing following the explosion where the propagation and forcing are linked.

### **Tsunami generation and initialization modelling**

There are many different processes by which volcanos can generate tsunamis, as are outlined in the previous chapter. Many of these are very complex processes that are still not fully understood and often several processes may occur simultaneously. While some numerical modelling attempts to model the details of the eruption and generation processes, for numerical modelling of volcanic tsunamis it is more important to focus on modelling the processes that displace large amount of water and produce long waves (tsunamis) rather than modelling the full eruption sequence.

Not only can multiple generation mechanisms play a role in the generation of a tsunami, but they may occur at different times over the course of the eruption and the tsunami evolution, which causes additional challenges of incorporating multiple forcing throughout the simulation.

#### ***Instantaneous initialization***

Often, the forcing that generates the tsunami happens rapidly compared to the shallow water wave speed, in these cases it may be appropriate to use an instantaneous initialization of the tsunami by specifying an initially deformed water surface (and potentially an initial velocity field although this is not so common). The assumption behind this sort of initialization is that

$$t_{init} < L / \sqrt{gH} \tag{1}$$

where  $t_{init}$  is the time initialization takes,  $L$  is a characteristic spatial scale of the forcing,  $g$  is acceleration due to gravity and  $H$  is the characteristic water depth in the generation zone. This can also be thought of as analogous to a Froude number comparing the forcing rate to the shallow water wave speed,  $L / t_{init} \sqrt{gH}$ , when this value is large, it is reasonable to assume instantaneous initialization.

A common initialization for volcanic tsunamis is a cavity, this could represent the area remaining after a submarine eruption has blown the surrounding water away. Le Méhauté (1971) and Le Méhauté and Wang (1996) used a combination of theoretical calculations and experiments from underwater explosions to develop relationships between the size and depth of an underwater



explosion and the size of the theoretical cavity it would generate that could then be used to initialize a tsunami generated by a submarine eruption. Le Méhauté (1971) proposes three different initializations, the first is simply the removal of a parabolic cavity of water with a net volume loss and two other cavities with no net volume loss, a shifted parabola with a discontinuous rim, and a fourth-degree polynomial with a more rounded continuous rim.

Different classifications of shallow-, intermediate- and deep-water explosions are given based on the relationship between the depth and the explosive energy released. The constants are defined in relationship to those classifications. Further assumptions are also required to estimate the effective explosive energy released from volcanic parameters which might include the crater diameter or the ejecta volume (Sato and Taniguchi, 1997). This methodology has been used to initialize volcanic tsunamis for Kolumbo, Greece (Ulrova et al., 2016) the Campi Flegrei caldera, Italy (Paris et al., 2019), Lake Taal, Philippines (Pakoksung et al., 2021), Lake Taupō, New Zealand, (Hayward et al., 2022) and Hunga Tonga-Hunga Ha’apai (Lynett et al., 2022).

Tsunamis generated by volcano-tectonic earthquakes can also be initialized by instantaneous ground deformation similar to what is done in the case of standard earthquake generated tsunamis. Because ground deformation from earthquakes generally occurs over tens of seconds at most, Equation (1) holds for a wide range of initialization parameters (e.g., in 1,000m deep water, a 1km wide forcing would need to occur within 10s). Generally, in these situations the ground deformation from the earthquake is applied instantaneously to the water surface at the start of the simulation. Care must be taken with volcano-tectonic tsunamis as, sometimes larger tsunamis than expected can result from volcanic earthquakes, potentially caused by mechanisms such as hydro-fracturing of heated water in shallow sediments, which could cause greater ground deformation than the earthquake alone (Gusman et al., 2020).

Caldera collapse is also sometimes modelled as an instantaneous ground deformation, where the initialization of the water surface either directly replicates the shape of the collapsed caldera or some filtered version (Ulrova et al., 2016). This may be reasonable if the caldera collapse occurs rapidly compared to Equation (1), but most collapses are thought to occur over tens of minutes or more, meaning for most scenarios the finite time initialization described below is more appropriate.

Other volcanic tsunami scenarios have also been modelled using instantaneous changes to the sea surface. The 2018 tsunami generated by the collapse of a large part of Anak Krakatau during an eruption has been modelled as a Gaussian mass of water of approximately the same size as the original volcano (Heidarzadeh et al., 2020; Firdaus et al., 2022). While this is a relatively crude initialization, it can produce waves of a similar magnitude to the event if the magnitude of initialization is correct.

#### *Analytical models, empirical models, and hand-off from more complicated models as instantaneous model initialization*

Tsunami models can be initialized by water surface and possibly also velocity field information taken from either a more complicated numerical model ( e.g., Chang and Wang 2015), analytical model (e.g., Duffy, 1992; Egorov 2007), or an empirical model. An example of an empirical model is the TOPICS model, which is used for initializing landslide tsunamis (Watts et al., 2003) and PDCs (Waythomas and Watts 2003). In this case the water surface and velocity fields for the initialization are estimated using empirical formulas based on the characteristics of the landslide and previous physical and numerical modelling. TOPICS has formulations for submarine and subaerial landslides, as well as PDCs (see <http://www.appliedfluids.com/geowave.html> for further details).

The volcanic eruption (or an aspect of it) could be modelled using Navier Stokes VoF or other 3D models close to the eruption zone. Sometimes this model may have a more simplified representation of the bathymetry and volcano, or modelled as a 2D vertical slice assuming rotational symmetry, or

some approximation into 3D (Mader and Gittings 2006; Gisler et al., 2006; Morrissey et al., 2010; Lane et al., 2016). The water levels and velocity field from this modelling could then be transferred to a simpler and faster (generally 2D) model for the propagation phase. This should occur at the point when the forcing from the volcanic eruption is no longer significantly influencing the tsunami waves. This type of initialization could be used for flank collapse and other landslide-tsunami (Gauer et al., 2005; Abadie et al., 2012) or for PDC using results such as from (Battershill et al., 2021). In these cases, we are not assuming that the initialization is instantaneous, but rather we are initializing a snapshot in time after the generation mechanism has occurred, but before the tsunami has travelled too far, so Equation (1) does not need to hold. These initialization techniques work best for modelling tsunamis outside of their generation area because they often assume simplified geometry in the generation zone and so may need.

### ***Finite time initialization***

#### *Ground deformation*

For situations where Equation (1) does not hold it might be more appropriate to use a finite time initialization, where the forcing happens over a specified time at the start of the modelling, rather than instantaneously.

One example of this is by forcing with a specified bottom motion. Depth-integrated equations generally solve for changes in the sea surface elevation over time, assuming that the bathymetry stays constant with time. But any temporal changes to the sea floor can simply be added as a forcing term.

$$\frac{\partial \eta}{\partial t} = F(\eta, u, v, H) - \frac{\partial H}{\partial t}$$

(2)

where  $F(\eta, u, v, H)$  represents an equation of sea surface motion being used (e.g., Saint Venant Shallow Water Equations, Boussinesq Equations etc.). This method relies on being able to describe the sea floor motion. In the case of finite time caldera collapse this could be achieved by using pre- and post-event bathymetry and assuming that the bathymetry varies linearly between these two end members over a specified time (Maeno et al., 2006). Alternatively, for a piston collapse type caldera collapse, a region of collapse (say a circle in the simplest case) and a collapse rate could be specified, and the collapse occur at that rate over the given time. More complicated time histories of the collapse could also be used, but given the sparsity of knowledge about caldera collapse it is uncertain whether we would have the observations needed to either confirm or refute more complicated models.

This type of bottom forcing can also be used to initialize eruptive column collapse, flank collapse, or PDC entry into the sea (de Lange et al., 2001). This type of initialization relies on assumptions being made about the speed and thickness of the flank collapse or PDC and so, usually, a simplified version of the motion will be used on the assumption that if the general size and timescale of the seafloor motion is captured then the wave motion will likewise be the right order of magnitude. By modelling these changes happening over time it allows the sea surface to adjust to the changes at its natural speed.

In all these sea floor deformation scenarios it is important that the bathymetry being used is updated to maintain consistency with the forcing.

#### *Two-layer models*

In many flank collapse and PDC scenarios, the details of how the mass failure occurs (acceleration, flow paths, etc.) may not be known *a priori*, and so this may want to be modelled together with the

overlying ocean. One methodology for achieving this is to use a two-layer model where both the forcing and the ocean response are modelled as separated, depth-integrated layers that can influence each other (Voellemey 1955; Savage and Hutter 1989, Maeno and Imamura 2011). Potential benefits of this method include being able to model the near-field effects of this tsunami forcing where other initialization techniques such as TOPICS, or initializing from a simplified 3D model, might not be appropriate, as the near-field influences of the bathymetry are not considered. These models generally assume that the flank collapse or PDC is represented by a denser layer of fluid overlain by sea water. In some cases, the less dense component of the PDC has also been considered (Watt and Waythomas, 2003). Different rheologies can be specified for the underlying fluid depending on the sophistication of the equations being used (e.g., Kelfoun 2011). In the simplest case this is specifying different density and viscosity. In the case of flank collapse a more viscous underlying fluid is likely to be more realistic, but for PDCs, experimental modelling has suggested that their behavior is well captured by a dense fluid with a similar viscosity to water (Bougouin et al., 2021).

### *Ongoing forcing*

Volcanic meteotsunamis are generated when the volcano produces a pressure anomaly (such as a Lamb wave) that can travel long distances in the atmosphere at high speeds. This mechanism forced the global tsunami generated from the Hunga Tonga-Hunga Ha'apai eruption (Omira et al., 2022). This forces the ocean surface over large distances due to the pressure gradient. To properly model this, ongoing forcing is required throughout the propagation phase, rather than being able to separate into a generation phase and a propagation phase. For these volcanic meteotsunamis, the generation and propagation phases are combined because the forcing occurs over the entire deep-water propagation of the tsunami. The pressure anomaly forcing is incorporated into the equations as  $-\frac{1}{\rho g} \nabla P$  similar to storm surge models. The Proudman expression (Proudman, 1929) for ocean surface amplification due to moving pressure describes the mechanism of tsunami amplification during such process is:

$$\eta = \frac{c^2 \eta_s}{c^2 - U^2} \quad (3)$$

where  $\eta$  is the sea surface displacement,  $c = \sqrt{gD}$  is tsunami wave celerity at depth  $D$ ,  $U$  is the speed of the atmospheric disturbance and  $\eta_s = P/\rho g$ , where  $P$  is the pressure disturbance,  $\rho$  the seawater density and  $g$  acceleration due to gravity.

This amplification is most effective when the speed of the atmospheric forcing is the same as the shallow water wave speed (Proudman resonance) where:

$$\eta(x, t) \approx -\frac{x}{2\rho g} P_x \quad (4)$$

initially growing linearly before nonlinear effects come into play (Williams et al., 2021).

As Lamb waves move faster ( $\sim 310$ - $320$ m/s) than shallow water waves ( $\sqrt{gH}$ ) over most of the world oceans, it is over deepest parts of the ocean with depths around 10 km where the most effective energy coupling occurs and highest amplitude gravity waves are generated. The first arrivals of pressure-forced tsunamis are timed with the Lamb wave arrival, with heights determined by the off-shore value of Equation (3). However, these first waves can be followed by gravity driven tsunami waves that were generated as the atmospheric disturbance passed over deep ocean trenches due to the Proudman

resonance according to Equation (4). These later gravity-driven tsunamis can arrive hours after the initial arrival and may have much higher amplitudes (Carvajal et al., 2022).

Modelling of such tsunami propagation process, while straightforward (just add additional forcing term described above), is very different from the “traditional” tsunami modelling techniques, when sources are defined (often pre-computed) and source modelling is not part of the propagation simulation. The generation process of Lamb wave pressure waves from the volcano explosion is not yet fully understood. Nevertheless, the propagation of the Lamb wave pressure disturbance in the atmosphere is well-described by a simple shallow-water wave model (Themens et al., 2022). This has been verified with ample number of observations for the 2022 Tonga HTHH volcano tsunami (Wright et al., 2022). The Lamb wave propagation can also be prescribed with even simpler model with constant propagation speed (~310 m/s) and pressure disturbance amplitudes scaled to observations (Lynett et al., 2022).

Therefore, modelling of a Lamb wave-generated tsunami for a particular event is now possible using techniques similar to the meteotsunami simulations, especially if scaled by the measurements of the pressure wave amplitudes.

The scaling laws for volcanic-meteotsunamis are more difficult to realize, since the generation of gravity waves by propagating pressure forcing depends on so many parameters. Tsunamis from sources with instantaneous, and even finite time initialization, scale well with the magnitude of the source. That is, however, not true for the continuous initiation, and especially for the Lamb wave forcing, which is complicated by the Proudman resonance effects. The tsunami arrival, tsunami amplitudes decay and amplification may depend on the location of the source, the depth of the ocean between the source and the location of interest, and the parameters of the Lamb wave in very complex way. Even interpretation of the direct tsunami amplitude is not straightforward. Therefore, modelling of such events remains as the main (and so far, the only) tool for tsunami prediction for such events. Finding simplified interpretation tools for the tsunami warning operations for such event requires sensitivity analyses studies using multi-scenario ensemble runs. This work is only just starting by the scientific community.

### **Tsunami propagation modelling**

In general, volcanic tsunami propagation is similar to the more common seismically generated tsunamis, therefore, most tsunami propagation models can be suitable for volcanic tsunami propagation simulations. However, the specifics of many of the volcanic tsunami generation mechanisms (described in Chapter 1) usually create shorter wavelengths than seismically generated tsunamis. This means that dispersive effects may need to be considered during the propagation phase (see Glimsdal et al., 2013 for further details). This should be considered when applying traditional depth-averaged tsunami models for volcanic tsunami propagation simulations. Most tsunami models are tested for seismic tsunamis, which often have longer wave lengths and/or periods, especially in the case of tsunamis generated by large subduction zone earthquakes. Because the Shallow Water Equations do not resolve dispersive effects, higher order approximations of the depth-averaged models (e.g., Boussinesq Equations and other dispersive approximations (Watts et al., 2003)) or multi-layer models (Haywards et al., 2022) are needed for modelling volcanic tsunamis where dispersive effects are important.

### **Tsunami inundation modelling**

Inundation dynamics for volcanic tsunamis is essentially the same as for any long wave inundation. Volcanic tsunamis are generally a local phenomenon with higher initial amplitudes at the source and impact areas that are much closer to the tsunami source than for seismic tsunamis. As a result, the local inundation from volcanic tsunamis can be far more intense. Standard tsunami inundation models

are generally suitable to simulate inundation by volcanic tsunamis. However, testing and additional validations need to be performed, since volcanic tsunamis may be of higher amplitude and higher flow velocities than seismic tsunamis.

Often for seismic tsunamis the inundation phase is modeled separately from initialization and propagation. With proliferation of the nesting grid techniques for increased resolution nearshore, the separate inundation modelling has become a standard technique. This may simplify the inundation modelling, but care must be taken when the source and inundation areas are nearby. In these situations, a single high-resolution grid or an adaptive grid might be more appropriate.

Other issues that should be considered for inundation modelling is ensuring an accurate wetting and drying scheme that does not cause instabilities. The on-land friction formulations may also need special care, as inundation and shallow water flows are far more sensitive to friction than in deeper water.

### **Other modelling considerations**

When modelling volcanic tsunamis, as with other tsunamis, it is important to have sufficient resolution to properly resolve the tsunami waves throughout the modelling process. This may require high resolution, especially at the initialization and inundation phases where the tsunami waves may have especially steep gradients. A variety of different modelling techniques exist to ensure high enough resolution where it is required. One technique is the use of nesting (sometimes two-way nesting) of Cartesian grids (e.g., MOST (Titov et al., 2016), COMCOT (Liu et al. 2005; Wang and Power 2011)). This nested grid approach may need to be adapted for the near-field volcanic tsunami simulations, since high resolution is needed not only at the inundation site, but also around the source location – not all nested grids models provide such capabilities. Another option is adaptive grids, which can adapt the resolution as required over the simulation, such as quad-tree grids (e.g., Basilisk (Popinet, 2011, 2012)) or block uniform grids (e.g. (Vacondio et al., 2017) or BG-Flood (Bosslerelle et al, 2021)). Yet another option is the use of an unstructured triangular or quad grid, where the grid is static but it can be specifically designed with higher resolution at the source and inundation locations as desired (e.g., SELFE (Zhang and Baptista, 2008)).

Tsunami modelling is often computationally very expensive and so achieving faster, more efficient runtimes is very desirable in many situations. Faster run-times can often be achieved by models that can run in parallel (either OpenMP, or, especially for large domain, or high-resolution models MPI) or models that are able to run on General Purpose GPUs (Qin et al., 2019; Bosslerelle et al., 2021).

**Conclusion:** Tsunami modelling tools are ripe for use in volcanic tsunami hazard mitigation. There are a number of modelling studies that show the potential of accurate tsunami simulations of multiple generation mechanisms of volcanic tsunamis. The fact that many potentially dangerous volcano locations are known, can help with providing very precise hazard assessment products for long-term forecasts. The data overview in this report (Chapter 4) and the results of the questionnaire (Appendix 1) show that the real-time data for many (if not most) known hazardous volcanos are available. These real-time data can be used as input for the real-time forecast modelling.

A combination of tsunami hazard assessment modelling, which is done beforehand based on the historical data, with the more precise “near-real-time” modelling based on real-time monitoring data, could provide an actionable tsunami forecast for local and distant coastlines with timing that is still unachievable for most seismically generated tsunamis.

To obtain this modelling forecast capability, the coordination between the volcano monitoring services and the tsunami warning operations is necessary. While many volcanos are being monitored in real-time, these data generally are not available for tsunami forecast operations.

Connecting the volcano monitoring data with the data of tsunami warning operations could provide necessary input for models to produce timely and actionable forecast for volcano tsunamis.

## References

- Abadie, S. M., Harris, J. C., Grilli, S. T., & Fabre, R. (2012). Numerical modelling of tsunami waves generated by the flank collapse of the Cumbre Vieja Volcano (La Palma, Canary Islands): Tsunami source and near field effects. *Journal of Geophysical Research-Oceans*, 117. doi:10.1029/2011jc007646
- Battershill, L., Whittaker, C. N., Lane, E. M., Popinet, S., White, J. D. L., Power, W. L., & Nomikou, P. (2021). Numerical simulations of a fluidized granular flow entry into water: insights into modelling tsunami generation by pyroclastic density currents. *Journal of Geophysical Research: Solid Earth*, 126(11). doi:10.1029/2021JB022855
- Bosserelle, C. D., Lane E. M., Harang A. (2021) BG-Flood: A GPU adaptive, open-source, general inundation hazard model. *Proceedings of the Australasian Coasts and Ports Conference 2021*. [https://www.coastsandports.org/papers/2021/150\\_bosserelle\\_finalpaper.pdf](https://www.coastsandports.org/papers/2021/150_bosserelle_finalpaper.pdf)
- Bougouin, A., Paris, R., Roche, O., 2020. Impact of fluidized granular flows into water: implications for tsunamis generated by pyroclastic flows. *Journal of Geophysical Research, Solid Earth* 125, e2019JB018954.
- Chang, C.H. and K.H. Wang, (2015) Numerical study on three-dimensional waves produced by a bottom jet. *Applied Ocean Research*, 50: 141-154.
- De Lange, W.P., G.S. Prasetya, and T.R. Healy, (2001) Modelling of tsunamis generated by pyroclastic flows (Ignimbrites). *Natural Hazards*, 24(3): 251-266.
- Duffy, D.G., (1992) On the generation of oceanic surface-waves by underwater volcanic explosions. *Journal of Volcanology and Geothermal Research*, 50(3): 323-344.
- Egorov, Y., (2007) Tsunami wave generation by the eruption of underwater volcano. *Natural Hazards and Earth System Sciences*, 7(1): 65-69.
- Firdaus, K., Matin, M. A., Nurisman, N., & Magdalena, I. (2022) Numerical study for Sunda Strait Tsunami wave propagation and its mitigation by mangroves in Lampung, Indonesia. *Results in Engineering* 16. 100605. [doi:10.1016/j.rineng.2022.100605](https://doi.org/10.1016/j.rineng.2022.100605)
- Gauer P, Kvalstad TK, Forsberg CF, Bryn P, Berg K. (2005) The last phase of the Storegga Slide: simulation of retrogressive slide dynamics and comparison with slide-scar morphology. *Mar. Petroleum Geol.* 22, 171–178. (doi:10.1016/j.marpetgeo.2004.10.004)
- Glimsdal, S., G. K. Pedersen, C. B. Harbitz, and F. Løvholt (2013), Dispersion of tsunamis: Does it really matter? *Nat. Hazards Earth Syst. Sci.*, 13, 1507–1526.
- Gusman, A. R., Kaneko, Y., Power, W., & Burbidge, D. (2020). Source Process for Two Enigmatic Repeating Vertical-T CLVD Tsunami Earthquakes in the Kermadec Ridge. *Geophysical Research Letters*, 47(16). doi:10.1029/2020gl087805
- Hayward, M. W., Whittaker, C. N., Lane, E. M., Power, W. L., Popinet, S., & White, J. D. L. (2022). Multilayer modelling of waves generated by explosive subaqueous volcanism. *Natural Hazards and Earth System Sciences*, 22(2), 617-637. doi:10.5194/nhess-22-617-2022
- Heidarzadeh M., Ishibe T., Sandanbata O., Muhari A., Wijanarto A. (2020) Numerical modelling of the subaerial landslide source of the 22 December 2018 Anak Krakatoa volcanic tsunami, Indonesia *Ocean Eng.*, 195 10.1016/j.oceaneng.2019.106733
- Kelfoun, K., (2011) Suitability of simple rheological laws for the numerical simulation of dense pyroclastic flows and long-runout volcanic avalanches. *Journal of Geophysical Research-Solid Earth*, 116(B8).

- Lane E.M., Mountjoy J.M., Power, W.L. and Popinet S. (2016) Initialising landslide-generated tsunamis for probabilistic tsunami hazard assessment in Cook Strait. *International Journal of Ocean and Climate Systems*. p4-13, doi: 10.1177/1759313115623162
- Le Mehaute, B.: (1971). Theory of explosion-generated water waves, in Ven te Chow (ed.), *Advances in Hydrosience*, Vol. 7, Academic Press, New York, London, pp. 1–79.
- Le Mehaute, B., & Wang, S. (1996). Water waves generated by underwater explosions (Vol. 10): World Scientific.
- Liu, P. L.-F., Wu, T.-R., Raichlen, F., Synolakis, C. E., and Borrero, J. C. (2005) Runup and rundown generated by three-dimensional sliding masses, *J. Fluid Mech.*, 536, 107–144.
- Løvholt F, Pedersen G, Harbitz CB, Glimsdal S, Kim J. (2015) On the characteristics of landslide tsunamis. *Phil. Trans. R. Soc. A 373*: 20140376. <http://dx.doi.org/10.1098/rsta.2014.0376>
- Lynett, P., McCann, M., Zhou, Z., Renteria, W., Borrero, J., Greer, D., . . . Cinar, G. E. (2022). Diverse tsunamigenesis triggered by the Hunga Tonga-Hunga Ha’apai eruption. *Nature*, 609(7928), 728-733. doi:10.1038/s41586-022-05170-6
- Lynett, P.J., K. Gately, R. Wilson, L. Montoya, D. Arcas, B. Aytore, Y. Bai, J.D. Bricker, M.J. Castro, K.F. Cheung, C.G. David, G.G. Dogan, C. Escalante, J.M. González-Vida, S.T. Grilli, T.W. Heitmann, J.J. Horrillo, U. Kânoglu, R. Kian, J.T. Kirby, W. Li, J. Macías, D.J. Nicolsky, S. Ortega, A. Pampell-Manis, Y.S. Park, V. Roeber, N. Sharghivand, M. Shelby, F. Shi, B. Tehranirad, E. Tolkova, H.K. Thio, D. Velioglu, A.C. Yalçiner, Y. Yamazaki, A. Zaytsev, and Y.J. Zhang (2017) Inter-model analysis of tsunami-induced coastal currents. *Ocean Model.*, 114, 14–32, doi: 10.1016/j.ocemod.2017.04.003.
- Maeno, F., F. Imamura, and H. Taniguchi, (2006) Numerical simulation of tsunamis generated by caldera collapse during the 7.3 ka Kikai eruption, Kyushu, Japan. *Earth Planets and Space*, 58(8): 1013-1024.
- Maeno, F. and F. Imamura, (2011) Tsunami generation by a rapid entrance of pyroclastic flow into the sea during the 1883 Krakatau eruption, Indonesia. *Journal of Geophysical Research-Solid Earth*, 116.
- Mader, C.L. and Gittings M.L. (2006) Numerical model for the Krakatoa hydrovolcanic explosion and tsunami. *Science of Tsunami Hazards*, 24(3), p 174
- Morrissey, M., Gisler, G., Weaver, R., and Gittings, M.: (2010) Numerical model of crater lake eruptions, *Bull. Volcano.*, 72, 1169–1178.
- Omira, R., Ramalho, R.S., Kim, J. et al. (2022) Global Tonga tsunami explained by a fast-moving atmospheric source. *Nature* 609, 734–740 <https://doi.org/10.1038/s41586-022-04926-4>
- Pakoksung, K., Suppasri, A., and Imamura, F. (2021). Probabilistic Tsunami Hazard Analysis of Inundated Buildings Following a Subaqueous Volcanic Explosion Based on the 1716 Tsunami Scenario in Taal Lake, Philippines, *Geosciences*, 11, 92, <https://doi.org/10.3390/geosciences11020092>.
- Paris, R., Ulvrová, M., Selva, J., Brizuela, B., Costa, A., Grezio, A., Lorito, S., and Tonini, R. (2019). Probabilistic hazard analysis for tsunamis generated by subaqueous volcanic explosions in the Campi Flegrei caldera, Italy, *J. Volcanol. Geoth. Res.*, 379, 106– 116, <https://doi.org/10.1016/j.jvolgeores.2019.05.010>.
- Popinet, S. (2011) Quadtree-adaptive tsunami modelling. *Ocean Dynamics*, 61 (9), pp.1261-1285. [ff10.1007/s10236-011-0438-z](https://doi.org/10.1007/s10236-011-0438-z). [ffhal-01445423f](https://doi.org/10.1007/s10236-011-0438-z)
- Popinet S. (2012) Adaptive modelling of long-distance wave propagation and fine-scale flooding during the Tohoku tsunami. *Natural Hazards and Earth System Sciences* 12(4): 1213–1227.
- Proudman J (1929) The effects on the sea of changes in atmospheric pressure. *Geophys Suppl Monthly Notices Roy Astr Soc* 2:197–209

- Qin, X., LeVeque, R. J., & Motley, M. R. (2019). Accelerating an adaptive mesh refinement code for depth-averaged flows using GPUs. *Journal of Advances in Modelling Earth Systems*, 11, 2606–2628. <https://doi.org/10.1029/2019MS001635>
- Sato, H. and Taniguchi, H. (1997) Relationship between crater size and ejecta volume of recent magmatic and phreato-magmatic eruptions: Implications for energy partitioning, *Geophys. Res. Lett.*, 24, 205–208, <https://doi.org/10.1029/96gl04004>.
- Savage SB and Hutter K. (1989) The motion of a finite mass down a rough incline. *J. Fluid. Mech.* 199, 177–215. (doi:10.1017/S0022112089000340)
- Synolakis, C.E., E.N. Bernard, V.V. Titov, U. Kânoğlu, and F.I. González (2008) Validation and verification of tsunami numerical models. *Pure Appl. Geophys.*, 165(11–12), 2197–2228.
- Themens, D. R., Watson, C., Žagar, N., Vasylykevych, S., Elvidge, S., McCaffrey, A., et al. (2022). Global propagation of ionospheric disturbances associated with the 2022 Tonga volcanic eruption. *Geophysical Research Letters*, 49, e2022GL098158. <https://doi.org/10.1029/2022GL098158>
- Titov, V.V., U. Kânoğlu, and C. Synolakis (2016) Development of MOST for real-time tsunami forecasting. *J. Waterw. Port Coast. Ocean Eng.*, 142(6), 03116004, doi: 10.1061/(ASCE)WW.1943-5460.0000357
- Ulvrova, M., R. Paris, K. Kelfoun and P. Nomikou, (2014) Numerical simulations of tsunamis generated by underwater volcanic explosions at Karymskoye lake (Kamchatka, Russia) and Kolumbo volcano (Aegean Sea, Greece). *Natural Hazards and Earth System Sciences*, 14(2):401-412.
- Ulvrova, M., R. Paris, P. Nomikou, et al., (2016) Source of the tsunami generated by the 1650 AD eruption of Kolumbo submarine volcano (Aegean Sea, Greece). *Journal of Volcanology and Geothermal Research*, 321: 125-139.
- Vacondio, R., Dal Palu, A., Ferrari, A., Mignosa, P., et al. (2017) A non-uniform efficient grid type for GPUparallel Shallow Water Equations models, *Environmental Modelling & Software*, 88(4), p 119-137 doi: 10.1016/j.envsoft.2016.11.012
- Voellmy A. (1955) Über die zerstörungskraft von lawinen. *Schweiz. Bauzeitung* 73, 159–165, 212–217, 246–249, 280–285.
- Wang X, Power WL. (2011) COMCOT: a tsunami generation, propagation, and run-up model. Lower Hutt (NZ): GNS Science. 121 p. (GNS Science report; 2011/43).
- Watts, P., Grilli, S. T., Kirby, J. T., Fryer, G. J., & Tappin, D. R. (2003). Landslide tsunami case studies using a Boussinesq model and a fully nonlinear tsunami generation model. *Natural Hazards and Earth System Sciences*, 3(5), 391-402. Retrieved from <Go to ISI>://WOS:000208897600009
- Watts, P., and C. F. Waythomas (2003), Theoretical analysis of tsunami generation by 24pyroclastic flows, *J. Geophys. Res.*, 108(B12), 2563, doi:10.1029/2002JB002265
- Waythomas C.F. and Watts P. (2003). Numerical simulation of tsunami generation by pyroclastic flow at Aniakchak Volcano, Alaska. *Geophysical Research Letters* 30(14), 1751, doi:10.1029/2003GL017220
- Williams, D.A., Horsburgh, K.J., Schultz, D.M. et al. (2021) Proudman resonance with tides, bathymetry and variable atmospheric forcings. *Nat Hazards* 106, 1169–1194. <https://doi.org/10.1007/s11069-020-03896-y>
- Wright, C.J., Hindley, N.P., Alexander, M.J. et al. (2022) Surface-to-space atmospheric waves from Hunga Tonga–Hunga Ha’apai eruption. *Nature* 609, 741–746. <https://doi.org/10.1038/s41586-022-05012-5>
- Zhang, Y.J. and Baptista, A.M. (2008) An Efficient and Robust Tsunami Model on Unstructured Grids. Part I: Inundation Benchmarks. *Pure and Applied Geophysics* 165, 2229-2248 <https://doi.org/10.1007/s00024-008-0424-7>



### Chapter 3 – Volcanic Tsunami hazard assessment: Stromboli volcano example

Of the tsunamigenic volcanoes identified by the questionnaire and listed in Appendix 2, the Stromboli volcano (southern Tyrrhenian Sea, Italy) is well-known for its moderate, but persistent explosive activity, which has lasted most probably since the medieval age, one thousand years ago. The island of Stromboli rises 924 m above sea level, but the volcano has deep roots ~2000 m below the sea surface (Fig 2). The volcanic edifice is thus almost 3000 m high, making Stromboli one of the largest volcanic edifices in Europe. The volcano is two-thirds underwater and it has grown above the water in the last 100 ka as the result of a continuous sequence of eruptions together with a NNW-ward migration of the eruptive activity.

The early activity was associated with a series of large-scale gravitational sector collapses of the NW and SE facing slopes, facilitated by tectonically-controlled NE–SW-trending fissures (Rosi, 1980; Pasquarè et al., 1993). The NW-facing flank of Stromboli has experienced at least 3 large flank collapses (Figs 3 and 4), the largest one (*Vancori*) occurred 13 ka with volumes up to 2 km<sup>3</sup> (Tibaldi, 2001; Romagnoli et al., 2009, Lucchi et al., 2019). A dramatic series of sector collapses (*NeoStromboli*) took place ~5 ka ago generating the 3 km long and up to 2 km wide Sciara del Fuoco depression. Some of these collapses were associated with violent explosive events and phreato-magmatic water-magma interaction (Bertagnini and Landi, 1996). These collapses involved a total volume of ~1.2 km<sup>3</sup> (Kokelaar and Romagnoli 1995; Tibaldi, 2010). The actual shape of the Sciara del Fuoco is linked to a collapse in Roman age ~2 ka (*Pizzo*) with a volume of ~0.8 km<sup>3</sup> (Francalanci et al., 2013) that generated a tsunami with a run-up of ~50 m (Tinti et al. 2000).

Over the years, the continuous eruptive activity of Stromboli has partially filled the Sciara del Fuoco scarp with heterogeneous volcanoclastic deposits of lavas and scoria with sporadic coherent lavas. Today, the Sciara del Fuoco is a 35° (on average) steep scar extends ~ 700 m below the sea surface, and it represents the preferential runway of volcanic products generated by eruptive phenomena. Most of the eruptive material accumulates at a mean rate of ~10<sup>5</sup> -10<sup>6</sup> m<sup>3</sup>/year along the Sciara del Fuoco, providing the overloading condition for landslide and/or debris slide with volumes ranging between 10<sup>5</sup> and 10<sup>7</sup> m<sup>3</sup>. The most critical part for the development of landslides is the proximal submarine area characterized by an apron of volcanoclastic material in metastable conditions.

All the tsunamis that have occurred at Stromboli over historical time, were triggered by gravitational instabilities of the Sciara del Fuoco in response to violent explosive or effusive eruptions (Tinti et al., 2008). Recent work on paleo-events (Rosi et al., 2019) has identified three well-preserved *Medieval* (1300-1400) tsunami deposits linked to a collapse of ~180x10<sup>6</sup> m<sup>3</sup> of the Sciara del Fuoco, which seems to have destroyed the ports of Naples, Amalfi, and Pozzuoli in 1343, causing casualties throughout the Neapolitan Gulf (Rosi et al., 2019).

In the last century, in 1879, 1916, 1919, 1930, 1944, and 1954, large tsunamis were generated during periods of intense volcanic activity (Fig 5), some of them with marine ingression so large (hundreds of meters) heavily damaged buildings along the coast and cause casualties on Stromboli (Maramai et al., 2005). The 1930 tsunami is known to have had an ingression of almost 200 m and a run-up of 2–3 m at Stromboli and was also observed along the Calabrian coast (Maramai et al. 2005). This large tsunami was associated with one of the most violent explosive eruptions of the last century, with hot

avalanches also running outside the Sciara del Fuoco and heavily impacting the villages of Stromboli and Ginostra.

In more recent years, the largest tsunami occurred on 30 December 2002 and was caused by two landslides, one subaerial and the other submarine, along the Sciara del Fuoco slope, with a total volume of  $\sim 20 \times 10^6 \text{ m}^3$  (Chiocci et al., 2008). Buildings at 10 m elevation were badly damaged, indicating a run-up of at least  $\sim 11 \text{ m}$  and a marine ingress as far as  $\sim 130 \text{ m}$  on the nearby Stromboli coast, but also in the close ( $\sim 20 \text{ km}$ ) island of Panarea. The tsunami was observed in several places along the coast of Italy, from the Campanian in the north-east to the western part of Sicily southward (Tinti et al., 2005). The two landslides were the response in terms of volcano stability to a magma intrusion, which opened several vents along the Sciara del Fuoco and resulted in the largest effusive eruption of the last 60 years.

Gravitational mass-flow of the Sciara del Fuoco scarp induced by the volcanic activity are also responsible for a large number of tsunamis with an average of one event every 20 years since the beginning of 1900 (Table I). This makes Stromboli one of the main sites in the Southern Tyrrhenian Sea where non-earthquake-induced tsunamis can be generated.

Besides large sector collapses with volumes in the order of  $10^9 \text{ m}^3$ , the historical record thus suggests two main mechanisms of tsunami generation at Stromboli, both associated with a strong deviation from the “normal” and moderate explosive activity (Fig 5): i) Effusive; and ii) Violent explosive eruptions. Both cases can induce large subaerial and/or underwater mass movements of different volumes.

Effusive eruptions are generally linked to magma intrusion and to the opening of lateral effusive vents, which compromise the stability of the Sciara del Fuoco flank and involve the collapse of potential volumes of  $10^7$ - $10^8 \text{ m}^3$ . The opening of an effusive vent is generally associated with an increase of the magma input rate, which leads to a transition from the explosive to the effusive regime. This process can last several days and should give enough time to warn the population of the imminent possibility of a tsunami.

Conversely, violent explosive eruptions (paroxysms) can occur suddenly and without clear precursors, representing a real threat to the population and a challenge in managing the risk. Since 1900, Stromboli has experienced 20 large paroxysms, approximately one every 6 years (Bevilacqua et al., 2019), with the last ones in July and August 2019. These violent explosive eruptions are always associated with pyroclastic density current (PDC), triggered both by the collapse of the volcanic plume or by the partial collapse of the crater rim. PDCs run down the  $\sim 1200 \text{ m}$  long Sciara del Fuoco slope at a mean velocity of 50-70 m/s and generate tsunamis when they impact the sea surface. PDCs at Stromboli are more frequent than sector collapse or magma intrusion and involve smaller volumes of  $10^5$ - $10^6 \text{ m}^3$  like in July and August 2019 which have generated two tsunamis of  $\sim 1$ - $2 \text{ m}$  height.

The last PDC occurred on 4 December 2022 and triggered a tsunami recorded by the Tsunami Early Warning System (TEWS) with a height of 1.5 m at  $\sim 1100 \text{ m}$  from the splash zone. This tsunami was large enough to trigger the automatic alert system of the Italian Civil Defense.

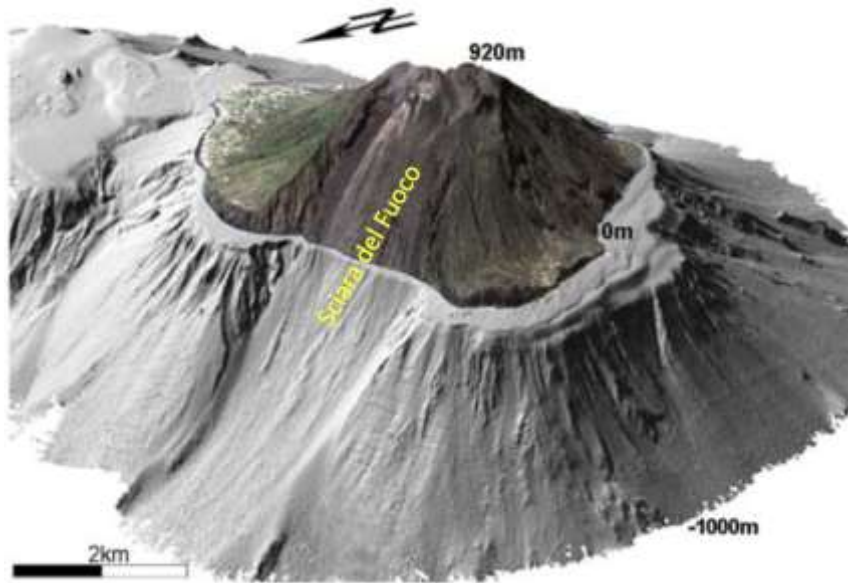


Figure 2. 3D map of Stromboli volcano showing the Sciara del Fuoco slope above and below the sea surface (Chiocci et al., 2008).

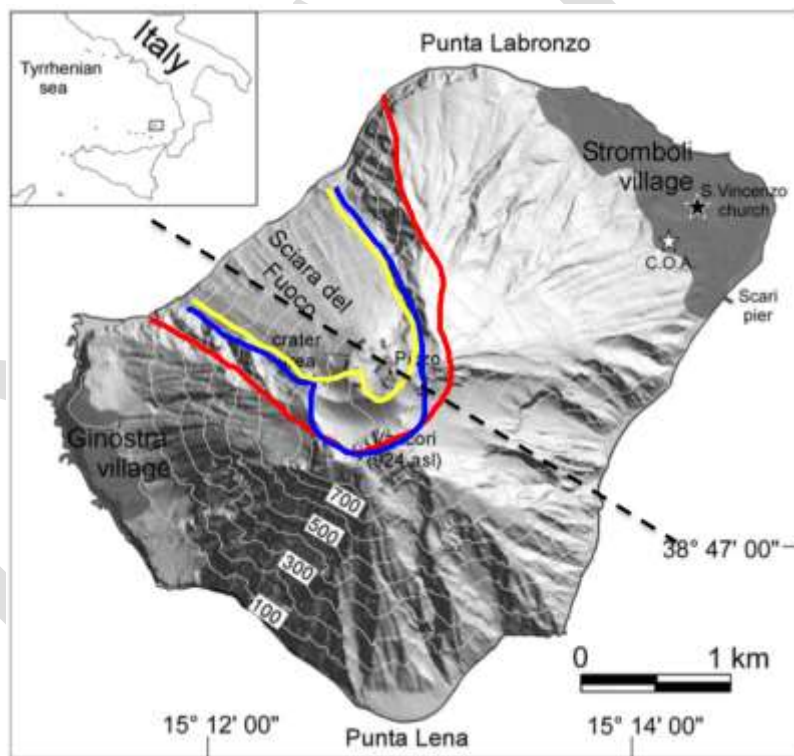


Figure 3. Stromboli volcano and the position of the 3 main collapses in the NW flank occurred ~13 ka (Vancori in red), ~5 ka (NeoStromboli in blue) and ~2 ka (Pizzo in yellow) in Roman age which have originated the present-day Sciara del Fuoco slope.

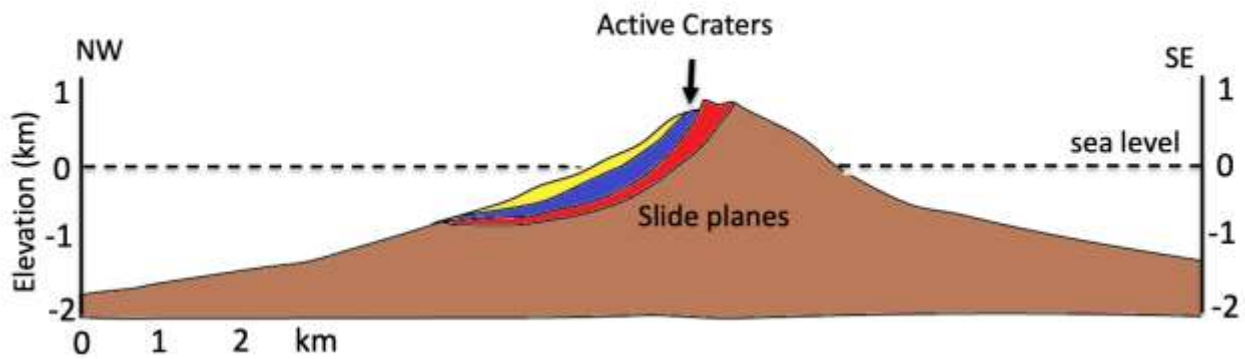


Figure 4. Section along the NW-SE profile of Stromboli volcano (see Figure 2) with the position of the sliding planes of the 3 main collapses (Redrawn from Tibaldi, 2001) of Vancori (in red), NeoStromboli (in blue) and Pizzo (in yellow).

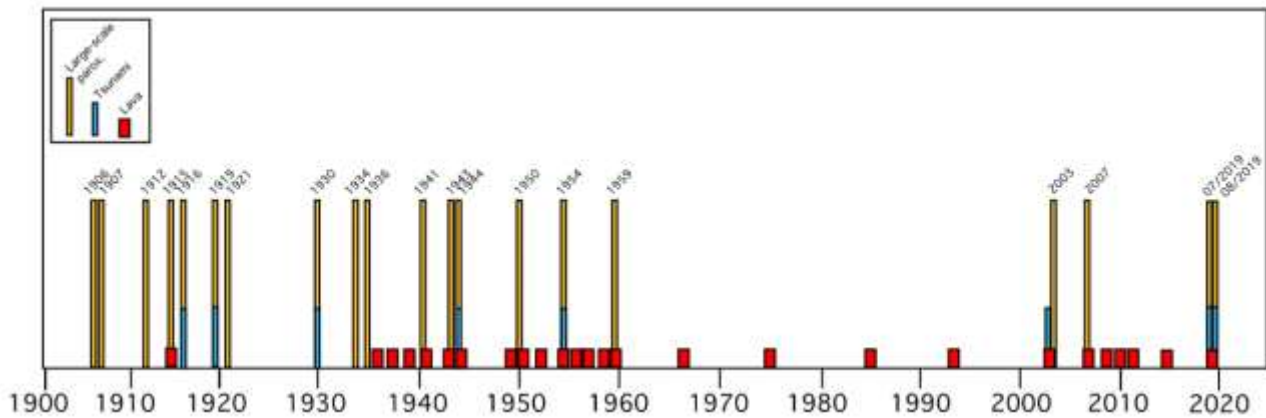


Figure 5. Relationship between volcanic activity and tsunamis at Stromboli (from Rosi et al., 2013). Number of explosive paroxysms (yellow), effusive eruptions (red) and tsunami (blue) that have occurred since 1900. The 1960 – 2003 is a period of relatively low activity, mainly characterized by the typical moderate explosive Strombolian activity. Most of the tsunamis (7) are associated with explosive paroxysms. The largest ones occurred in 1930 and 1944 with marine ingressions up to 300 m and a run-up of 3-4 m.

## Tsunami Hazard Assessment

At Stromboli, the risk of tsunami is estimated considering the scenario associated with the two landslides that occurred on 30 December 2002 at the beginning of a 9-months long effusive eruption. This was the largest tsunami recorded during the last century and it has been particularly well-studied in terms of generation and dynamics (Chiocci et al. 2008). The total landslide volume was greater than  $17\text{--}20 \times 10^6 \text{m}^3$  (Chiocci et al., 2003) and generated a wave with an amplitude of  $\sim 11$  m (Tinti et al. 2006a) with a maximum sea inundation of  $\sim 200$  m at Scari (Figure 6).



**Figure 6.** The 30 December 2002 flank collapse and tsunami at Stromboli. Images show the a) ash cloud generated by the landslide on the Sciara del Fuoco and b) and c) the marine inundation at Scari (see Figure 7) close to the harbor of Stromboli (photos of Philippe Guillemin).

Tsunami hazard is then evaluated by modelling the propagation of different tsunami waves triggered by different landslide scenarios [Fornaciai et al., 2019; Ongaro et al., 2021]. Simulating a landslide-generated tsunami is particularly complex and it depends on the aerial or submarine landslide dynamics (see Chapter 2), its interaction with the water surface, and the wave propagation and runup on the coast. Rigid and deformable (granular) submarine landslide models have been considered (Esposito Ongaro et al., 2022) to estimate their impact on Stromboli. They showed that solid slides cause larger waves and runup. Although it is likely that the granular model provides a better representation of gravitational flow processes potentially generated by submarine landslides at Stromboli, it is still difficult to define a priori which one is more realistic.

The non-hydrostatic three-dimensional model NHWAVE (Ma et al., 2012) was used (Fornaciai et al., 2019) to generate and propagate tsunami waves caused by eight different scenarios of flank collapse associated with submarine (with volumes of 7.1, 11.8, 17.6, and  $23.5 \times 10^6 \text{ m}^3$ ) and subaerial landslides (with volumes of 4.7, 7.1, 11.8, and  $35.3 \times 10^6 \text{ m}^3$ ).



**Figure 7.** Map of Stromboli with the location of Stromboli and Ginostra villages, the Sciara del Fuoco and the two sea floor tsunami sensors located to the Northeast (PLB) and Southwest (PDC) of the Sciara del Fuoco (see Chapter 5). b) Map of Stromboli zoomed on the zone impacted by 2002-tsunami (modified after Bonilauri et al., 2021).

The modelling shows a very good fit (Fig 8) with the marine inundation observed in 2002 (Tinti et al., 2006) for a  $17.6 \times 10^6 \text{ m}^3$  submarine landslide, which agrees with the volumes estimated by field surveys (Chiocci et al., 2003). Moreover, the model shows that a similar runup can be explained by a  $7.1 \times 10^6 \text{ m}^3$  subaerial mass flow, indicating that for the same volume, aerial landslides generate higher waves and runup than the submarine ones.

Models predicts also that the arrival time along the populated coast of Stromboli is quite similar through different scenarios. The first positive tsunami wave, not affected by interaction with previous waves, typically arrives over 1 minute at Spiaggia Lunga and almost 3.5 minutes at the Harbor (see Fig 8), while the wave with the largest amplitude hit the same shore between 2-2.5 minutes at Spiaggia Lunga) and 5-7 minutes at the Harbor) (Fornaciai et al., 2019).

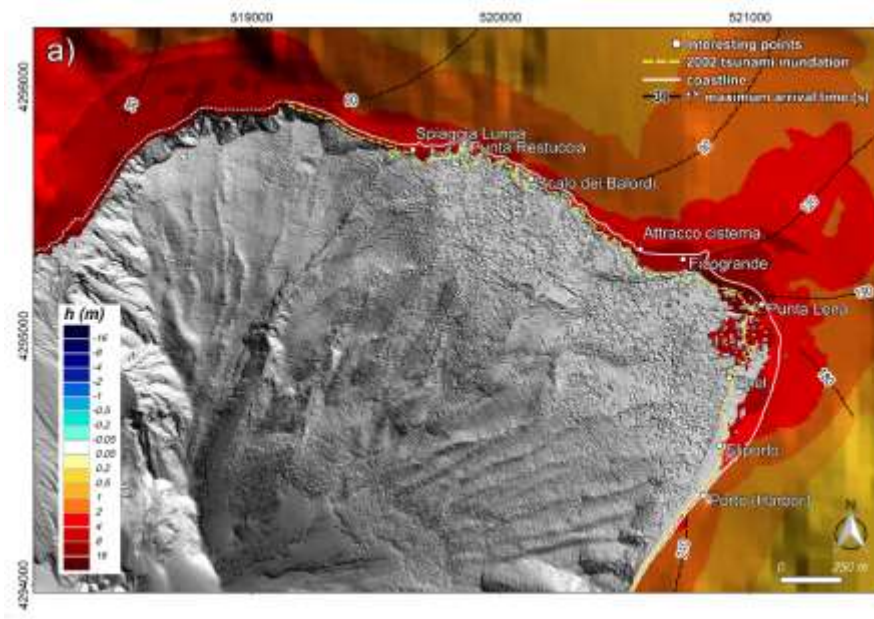


**Figure 8.** Observed and simulated tsunami wave heights and runups on Stromboli. (a) Stromboli map representing the maximum simulated inundation and wave height for a tsunami caused by a submarine slide along the SdF of  $17.6 \times 10^6 \text{ m}^3$ . (b) Comparison between the observed 2002 run-up (Tinti et al., 2006) and the simulated assuming a submarine scenario (Fornaciai et al., 2019).

Simulated tsunami waves generated by landslides in the Sciara del Fuoco by a submarine landslide of  $17.6 \times 10^6 \text{ m}^3$  (scenario 1) and a subaerial landslide of  $35.3 \times 10^6 \text{ m}^3$  (scenario 2) were used to calculate different intensity scenarios and the relative tsunami risk at Stromboli (Turchi et al., 2022). Tsunami intensity is calculated as the water depth above the terrain level, resulting from the difference between the wave height derived from the simulations (Fornaciai et al., 2019) and the elevation obtained from a 1-3 resolution digital elevation model (DEM) of the island. While scenario 1 is replicating the 30 December 2002 tsunami, the second scenario 2 is estimated to have the probability to occur in tens to hundreds of years (Schaefer et al., 2019).

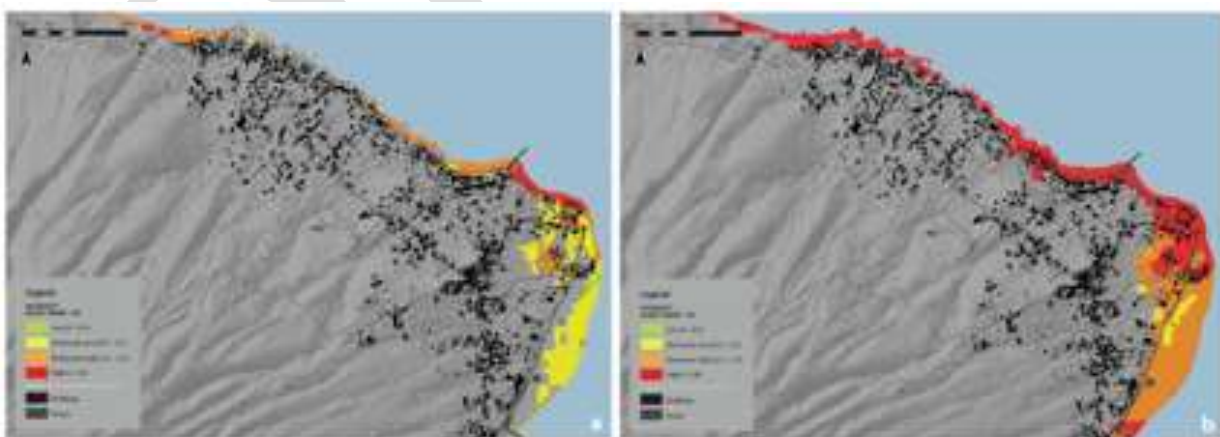


Figure 9

Besides the different subaerial or submarine origin of the tsunami-induced mass flow dynamics, there are also two possible volcanic triggers, which give different warning times (see also Chapter 4):

- A. Gravitational landslide induced by an increased magmatic activity (e.g., magma intrusion, effusive eruption), such as occurred in 2002.
- B. Entry of pyroclastic flow into the sea due to the collapse of a km-high explosive plume (e.g., paroxysm) like during the 2019 eruption.

In the first case, the sudden occurrence of the landslide will allow only a maximum 4-minutes warning compatible with the modelled travel time for the wave to travel from the source of the tsunami (the coast of the Sciara del Fuoco) to Stromboli village (Fig 6). In the second scenario, the actual warning system, based on the automatic detection of the explosive paroxysm by the inflation of the ground, will allow the origin of the possible tsunami to be anticipated by 4–5 minutes, increasing to 8-9 minutes the tsunami warning time with a great impact on our ability to reduce the associated risk.

### **Probabilistic Approach**

A probabilistic approach to evaluate the tsunami hazard (Selva et al.,2021) at Stromboli, and in general generated by volcanoes in the Tyrrhenian Sea, is still missing. Recently, the National Institute of Geophysics and Volcanology (INGV), in the framework of the operational monitoring activities for the National Department of Civil Protection (DPC), signed a Cooperation Agreement with the Universities of Pisa and Firenze to develop a probabilistic hazard map in harmony with the procedure used by the national Tsunami Alert Center (CAT) of the INGV to calculate the hazard related to earthquake-generated tsunamis. Tsunami hazard maps will be defined for different scenarios, and each will be identified with a different probability level. The project is in cooperation with the University Clermont-Auvergne (LMV), the NGI of Oslo, the University of Malaga, and CSIC of Barcelona. Hazard maps will be then used to evaluate inundation maps and will serve as a base to define in cooperation with the Italian Civil protection protocols for the mitigation of the risk associated with tsunami associated with volcanic activity. As an example, Bonilauri et al. (2021) assessed the ease of building evacuation, determined pedestrian evacuation times, proposed emergency evacuation plans, and evaluated the level of awareness of Stromboli residents on volcanic tsunamis.

### **REFERENCES**

Bertagnini A, Landi P (1996) The Secche di Lazzaro pyroclastics of Stromboli volcano: a phreatomagmatic eruption related to the Sciara del Fuoco sector collapse. *Bull Volcanol* 58:239–245.

Bevilacqua, A., Bertagnini, A., Pompilio, M., Landi, P., Del Carlo, P., Di Roberto, A., Aspinall, W., Neri, A. (2020). Major explosions and paroxysms at Stromboli (Italy): A new historical catalog and temporal models of occurrence with uncertainty quantification. *Scientific reports*, 10(1), 1-18.



Bonilauri, E., Harris, A.J.L., Morin, J., Ripepe, M., Mangione, D., Lacanna, G., Ciolli, S., Cusolito, M., Deguy, P., 2021. Tsunami evacuation times and routes to safe zones: a GIS-based approach to tsunami evacuation planning on the island of Stromboli, Italy. *Journal of Applied Volcanology*

Chiocci, F. L., Romagnoli, C., Tommasi, P., Bosman, A. (2008). The Stromboli 2002 tsunamigenic submarine slide: characteristics and possible failure mechanisms. *Journal of Geophysical Research: Solid Earth*, 113(B10).

Fornaciai, A., M. Favalli, L. Nanniperi, (2019). Numerical simulation of the tsunamis generated by the Sciara del Fuoco landslides (Stromboli Island, Italy). *Sci. Rep.* 9:18542. doi: 10.1038/s41598-019-54949-7

Kokelaar, P., Romagnoli, C. (1995). Sector collapse, sedimentation, and clast population evolution at an active island-arc volcano: Stromboli, Italy. *Bulletin of Volcanology*, 57(4), 240-262.

Lucchi, F., Francalanci, L., De Astis, G., Tranne, C. A., Braschi, E., Klaver, M. (2019). Geological evidence for recurrent collapse-driven phreatomagmatic pyroclastic density currents in the Holocene activity of Stromboli volcano, Italy. *Journal of Volcanology and Geothermal Research*, 385, 81-102.

Ma, G., Shi, F. & Kirby, J. T. Shock-capturing non-hydrostatic model for fully dispersive surface wave processes. *Ocean Modelling* 43, 22–35 (2012).

Maramai, A., Graziani, L., Alessio, G., Burrato, P., Colini, L., Cucci, L., Nappi, R., Nardi, A., Vilardo, G. (2005). Near-and far-field survey report of the 30 December 2002 Stromboli (Southern Italy) tsunami. *Marine Geology*, 215(1-2), 93-106.

Esposti Ongaro T., M. de'Micheli Vitturi, M. Ceraminara, A. Fornaciai, L. Nanniperi, M. Favalli, B. Calusi, J. Macias, M.J. Castro, S. Ortega, J.M. Gonz'alez-Vida, C. Escalante, Modelling tsunamis generated by submarine landslides at Stromboli Volcano (Aeolian Islands, Italy): a numerical benchmark study, *Front. Earth Sci.* 9 (2021) 1–21.

Pasquaré, G., Francalanci, L., Garduño, V. H. Tibaldi, A. 1993. Structure and geologic evolution of the Stromboli volcano, Aeolian Islands, Italy. *Acta Vulcanologica*, 3, 79–89.

Ripepe, M., Lacanna, G., Pistolesi, M., Silengo, M. C., Aiuppa, A., Laiolo, M., Massimetti, F., Innocenti, L., Della Schiava, M., Bitetto, M., La Monica, F.P., Nishimura, T., Rosi, M., Mangione, D., Ricciardi, A., Genco, R., Coppola, D., Marchetti E., Delle Donne, D. (2021). Ground deformation reveals the scale-invariant conduit dynamics driving explosive basaltic eruptions. *Nature communications*, 12(1), 1-8.

Risica, G., Speranza, F., Giordano, G., De Astis, G., Lucchi, F. (2019). Palaeomagnetic dating of the Neostromboli succession. *Journal of Volcanology and Geothermal Research*, 371, 229-244.

Romagnoli, C., Kokelaar, P., Casalbore, D., Chiocci, F. L. (2009). Lateral collapses and active sedimentary processes on the northwestern flank of Stromboli volcano, Italy. *Marine Geology*, 265(3-4), 101-119.

Rosi, M., 1980. The island of Stromboli. *Rend. Soc. Ital. Mineral. Petrol.*, 36, 345-368.

Rosi, M., Levi, S. T., Pistolesi, M., Bertagnini, A., Brunelli, D., Cannavò, V., Di Renzoni, A., Ferranti, F., Renzulli, A., Yoon, D. (2019). Geoarchaeological evidence of middle-age tsunamis at Stromboli and consequences for the tsunami hazard in the Southern Tyrrhenian Sea. *Scientific reports*, 9(1), 1-10.

Tibaldi, A. (2001). Multiple sector collapses at Stromboli volcano, Italy: how they work. *Bulletin of Volcanology*, 63(2), 112-125.

Tibaldi, A. (2010). A new geological map of Stromboli volcano (Tyrrhenian Sea, Italy) based on application of lithostratigraphic and unconformity-bounded stratigraphic (UBS) units. *GSA Spec. Pap.*, 464, 33-49.

Tinti, S., Pagnoni, G., Zaniboni, F., Bortolucci, E. (2003). Tsunami generation in Stromboli Island and impact on the south-east Tyrrhenian coasts. *Natural Hazards and Earth System Sciences*, 3(5), 299-309.

Tinti, S., Zaniboni, F., Pagnoni, G., Manucci, A. (2008). Stromboli Island (Italy): scenarios of tsunamis generated by submarine landslides. *Pure and applied geophysics*, 165(11), 2143-2167.

Turchi A., Di Traglia F., Gentile G., Fornaciai A., Zetti I., Fanti R., (2022) Relative seismic and tsunami risk assessment for Stromboli Island (Italy). *Int. J. Dis. Risk Red.*, 76.

DRAFT

## **Chapter 4 – Volcano monitoring requirements for tsunami warning**

The source of tsunamis generated by volcanoes is in general often very close to populated coasts. This gives a very short propagation time (in the order of minutes), which calls for a rapid detection system, able to issue an alert without human validation (see Chapter 5). In general, tsunami warning systems are not designed to deal with a large mass sliding in the water, like the case of many volcanic islands (see Chapter 1), nor to face tsunamis triggered by atmospheric disturbances like the recent Hunga Tonga Hunga Ha’apai eruption (Kubota et al., 2022). Most of the actual warning systems are built to handle earthquake-generated tsunamis, and even then only after the source and the magnitude of the earthquake have been defined. A tsunami warning is then issued based on the expected arrival time predicted by tsunami travel time software (e.g., TTT), with wave heights at coast possibly predicted by previous numerical simulations of wave propagation. These earthquake-generated tsunami warning systems are ineffective when the tsunami is generated by non-earthquake sources, such as volcanic eruptions, as the systems are initiated by earthquake events and propagate waves based on sea floor deformations.

Tsunamis generated by volcanoes are, on the other hand, mostly dependent on magma dynamics, which in most cases is a slower process than the brittle fracture dynamics associated with earthquakes. The source time functions of volcanic eruptions are somewhat longer (days to months) compared to earthquakes (seconds to minutes), and usually give rise to several forms of geophysical and geochemical indicators before the onset of the eruption.

Propagation of magma within the central feeding systems and/or along dykes (intrusion) causes changes in the local stress distribution, which is the main factor in volcanic edifice destabilization [Siebert, 1984]. Magma overpressure, in fact, exerts huge pressure on the edifice walls and decreases both the frictional resistance, as well as the effective stress of the poro-elastic medium [Voight and Elsworth, 1997].

The input of new magma from a deep reservoir into the shallower part of the volcanic edifice triggers an increase of the eruptive volcanic activity, which can help anticipate volcano instability from several days to months and is in general associated with a large number of geophysical and geochemical “anomalies”. This increase can be detected by monitoring networks and, contrary to the tsunami of earthquake origin, for specific volcanoes. In some cases, the population could be warned at times of heightened activity when volcanic tsunamis are more probable.

Various sources of volcanic tsunamis (see Chapter 1) are linked and triggered by the increase of magma or gas flow rate. Monitoring systems at volcanoes are already specifically designed to provide timely information on the transition between different activity regimes.

The transition is detected as a deviation of geophysical and geochemical parameters from the background level, and in case of Stromboli-type volcanic edifices it is generally linked to magma intrusion along fractures crossing the volcano edifice, or to an increase of the magma level within the feeding conduits. The first case generally induces instability of the volcano edifice before an effusive

eruption occurs (cases A, B, in Chapter 1), whereas the second case can lead to a more rapid and violent explosive eruption with the consequent collapse of the volcanic plume and/or of the crater rim (cases C, E, F and G in Chapter 1).

For Stromboli-type edifices, both eruptive scenarios are responsible for many of the phenomena described in Chapter 1 (refer to Fig 1 in Chapter 1), which can potentially generate a tsunami:

- Magma intrusion before effusive eruptions induce the instability of the volcanic flank and thus subaerial (case A in Fig 1) and submarine (case B) landslide. Depending on the magma composition or type of volcanism, this activity can be also responsible for intense pyroclastic flows activity (case C).
- Explosive eruptions are instead the source of different tsunamigenic phenomena (also described in Chapter 1), such as: i) Underwater explosions (in the case where the eruptive center is underwater) (case E); ii) Collapse of the eruptive plume (case F); and iii) Forcing of acoustic-gravity waves (case G).

These scenarios can have different preparation times and require different monitoring techniques. Magma migration towards the surface can last several days, or months, and the trigger mechanism has a long incubation time (from few to tens of days). Whereas explosive eruption is more controlled by fast magma dynamics (minutes to hours), which only allow a short notification time. From a risk management point of view, the effusive trigger mechanisms can give more time to prepare and warn the population of the imminent possibility of a tsunami than the rapid dynamics associated to explosive eruption. Besides, while magma intrusion is responsible for collapsing volumes of  $10^7$ - $10^9$  m<sup>3</sup> (Table 1 in Chapter 1), the explosive eruptions involve in general smaller volumes of  $10^5$ - $10^8$  m<sup>3</sup> (Table 2 in Chapter 1).

## **Processes And Monitoring Techniques**

The most common monitoring techniques used today on volcano observatories that could be used to anticipate possible tsunamigenic phenomena (other volcano monitoring techniques exist that are not included) can be listed. Volcano observatory best practices (VOBP) workshops were held in 2011, 2013, 2016, and 2019 to bring together representatives from the majority of the world's volcano observatories for the purpose of sharing information on the operation and practice of these institutions and making best practice recommendations (Pallister et al., 2019, Lowenstern et al., 2022a,b).

### **Volcano Seismicity**

Volcano seismicity is the most common parameter used to monitor volcanoes around the globe (e.g., McNutt et al., 2015). Seismic activity can be continuously recorded at a safe distance from the volcano (tens of kilometers), and it is independent of the ambient conditions. Seismic data are routinely processed automatically in near real-time by volcano observatories, providing updated information on earthquake location, type of seismicity, and/or seismic tremor amplitude (Pallister & McNutt, 2015).

### *Magma migration*

Magma migration is indicated by brittle fracture seismicity, which propagates along and/or away from the volcano. While magma migrates into fissures and approaches the surface, rates of seismicity increase, and earthquake locations become shallower. In general, seismicity is also associated with ground deformation, and both are considered as reliable precursors of volcanic eruptions (e.g., Peltier et al., 2018; Sigmundsson et al., 2022).

Caldera unrest, for example, is generally associated with inflation of the ground and a seismicity (Fig 1) contained within the ring faults delimiting the volcano structure, reflecting the increased level of overpressure in the magma chamber (Newhall & Dzurisin, 1988; Galletto et al., 2022). Whereas melt movement is accompanied by a rapid deflation of the caldera magma chamber and a rotation of the earthquake focal mechanisms (Roman et al., 2004). These events last from 1 day to 3 months, and the dike horizontal length varies between 1 and 60 km (Einarsson & Brandsdottir, 2021)

### *Magma fluid-dynamics*

Fluido-dynamics of the magmatic column generate seismic signals, which are different from normal earthquakes. While tectonic earthquakes are related to the brittle behaviour of rocks, this type of volcanic seismicity is caused by the movement of magma or gas in the volcanic conduit. Seismic signals of volcanic origin have lower frequency content than earthquakes and are generally named as LP (long- period) events (Kawakatsu & Yamamoto, 2007). Because of these characteristic waveforms, volcano seismic signals are easily recognized (Falcin et al., 2021) and in general are associated with the magma/gas flow in the conduit. An increase in volcanic seismicity most commonly anticipates an increase of volcanic activity (McNutt et al., 2015). Many observatories use volcanic seismicity as a reliable precursor of volcanic eruptions (Chouet et al., 1994). At Piton de la Fournaise, this type of system has allowed successful real-time early warning alerts a few minutes to hours before 22 eruptions (Roult et al., 2014)

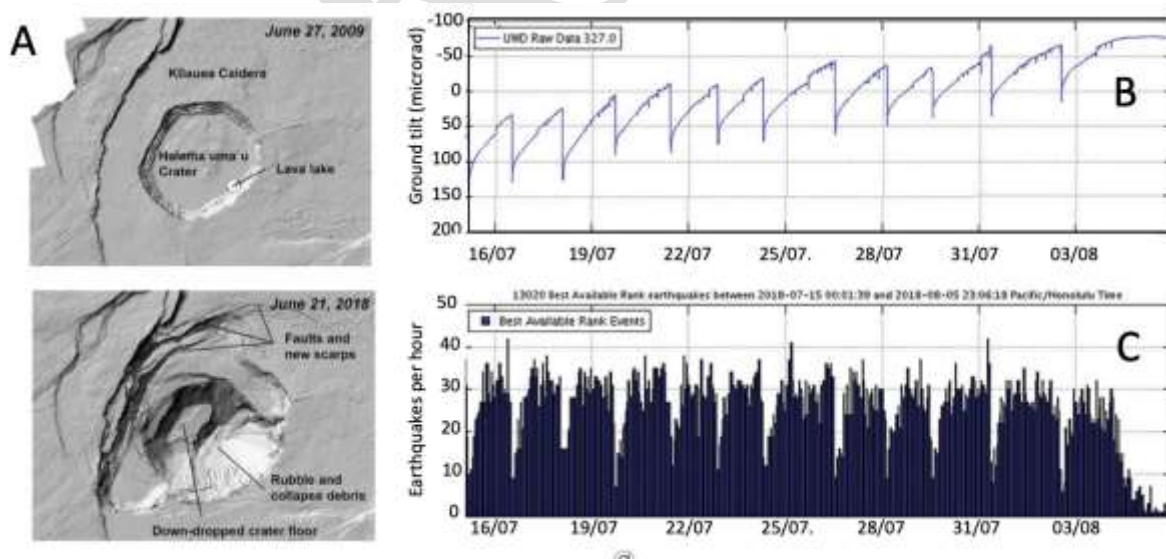


Figure 10. Ground deformation (tilt) and seismicity (earthquake counts) on Kilauea Volcano (A) between July 15 and Aug. 5, 2018. A cyclic pattern shows (C) the gradually increase of seismicity 1-3 days until the caldera floor suddenly dropped several meters in a matter of seconds. (B) The sharp steps on the tilt plot (B) reflect when summit collapses occurred, causing the ground deflation. (from USGS reports)

*Moving sources*

Seismic signal on volcanoes can also be generated by non-isotropic sources associated with a large mass flow moving down volcano slopes (Kanamori and Given, 1998), such as rockfalls (or rock avalanches), landslides or pyroclastic flows (Calder et al., 2002). Rockfalls and landslides have a distinctive seismic signal, both in the time and frequency domain, that could be used to track gravitational mass movements, and are therefore a key factor in detecting flank instabilities (such as at Stromboli, Montserrat, Piton de la Fournaise volcanoes). Rockfalls are usually concentrated along the unstable slopes where major flank instabilities are likely to occur [Allstadt et al., 2018]. Assuming that a proportional law exists between destabilization forces and failure mass, or volume, the occurrence of frequent smaller scale rockfalls can be considered as a potential precursor of larger flank failures that might evolve into flank collapses (Fig 2). From this perspective, rockfall monitoring could allow us to anticipate major flank instabilities (Hibert et al., 2014) or the likely occurrence of pyroclastic flow (De Angelis et al., 2002; Uhira et al., 1994).

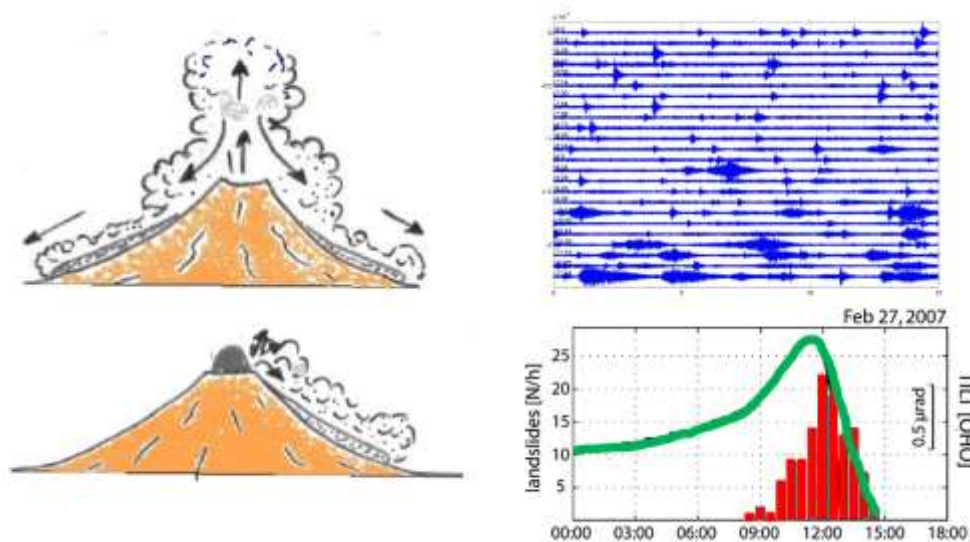


Figure 11- Collapse of the eruptive plume and/or crater rim/dome generates pyroclastic flows and rock avalanches along the steep volcano slope (from Francis, 1993). Magma intrusion inflates the volcano edifice (green line in D) which makes the flank unstable, generating rockfalls and pyroclastic flows which have characteristic cigar-shaped seismic transients, Tilt amplitude recorded by the radial component of tiltmeter (green line) and number of rockfalls per hour as recorded by seismic station (from Marchetti et al., 2009).

**Ground Deformation**

Volcanic eruptions are associated with inflation/deflation cycles caused by charge/discharge mechanisms of the magma reservoir and/or of the feeding magma system (Fig 10). Volcano deformation may occur through the migration, accumulation, and degassing of magma and can provide information about the size and geometry of magma reservoirs, as well as their temporal variability (Segall, 2013). When magma is intruded into the volcanic structure, the surrounding rock will deform in order to accommodate the new material and often results in ground deformation (Dzurisin, 2003). The inflation of a magma reservoir is a common precursor to an eruption (Dzurisin et al., 1983; Biggs & Pritchard, 2017), which may be followed by rapid deflation as magma is erupted (Fig 10). Magma intrusion can occur vertically (along the preexisting feeding

conduit system), or it can move laterally for kilometers along dykes (Duputel et al., 2019; Sigdmunsson et al., 2015).

Magmatic degassing may also cause ground deformation. Volatiles in magmas, such as water, carbon dioxide and sulphur dioxide, can exsolve as magma rises. After nucleation, gas separates from oversaturated melt and bubbles are formed. The bubble formation increases the pressure leading to intense periods of magmatic degassing (Girona et al., 2015). Approaching the surface, gas volume in the melt increase and gas becomes decoupled from the melt. Inflation of the ground before these explosive eruptions is generally explained as due to the increase of pressure induced by the volumetric expansion of magma in the shallow feeding system due to the rapid exsolution of the gas (Nishimura, 2009)

Improving our ability to detect the ground inflation will allow us to anticipate from days to minutes the eruptions on many basaltic, as well andesitic volcanoes (Iguchi et al., 2008; Bonaccorso et al., 2012; Peltier et al., 2011; Ripepe et al., 2021). Ground deformation was already used in the 1980s to automatically forecast most (~70%) of the vulcanian explosion at Sakurajima volcano [Kamo, 1989], making it possible to forecast days before the eruptive activity at Mount St. Helens in 1980 (Swanson et al., 1983). More recently, the ground tilt recorded at Stromboli during violent explosions (paroxysms) shows a systematic pattern in the way the volcano edifice inflates several minutes (10 minutes) before the explosions, which seems to be independent on the eruption intensity. This similarity in the ground deformation provided the robust statistical base to develop an Early Warning Alert System that automatically recognizes the deformation pattern preceding a paroxysm (Fig 3). A-posteriori analysis of the last 18 years (from 2005 to 2023) shows that large explosive eruptions can be automatically detected 4-5 minutes before onset (Ripepe et al., 2021), and almost 7 minutes before a tsunami generated by the collapse of the volcanic plume is detected by tsunami gauges (see Chapter 5). Ground deformation is opening new perspectives to explain the explosive dynamics and is providing a new way to monitor active volcanoes with great impact on the assessment of volcanic risk to society.

Ground deformation can be detected by several monitoring techniques using Global Positioning System (GPS) receivers, tiltmeters, strainmeters (Bonaccorso et al., 2012) and by radar interferometry using ground-based Synthetic Radar Aperture (GB-InSAR) instruments (Schaefer et al., 2019). These measurements have a large sensitivity but are limited to few points located on the Earth's surface.

### **Acoustic Pressure**

Among the monitoring techniques, infrasound is probably the one that more closely reflects the explosive process. Infrasound is, in fact, generated only when the volcano dynamics become coupled with the atmosphere, which mainly occurs during an explosive eruption. In addition, under the right propagation conditions, the limited attenuation in atmospheric waveguides makes infrasound travel long distances (Drob et al., 2003), thus providing evidence of ongoing eruptions even at long source-to-receiver distances (e.g., Campus, 2006; Dabrowa et al., 2011). During the last decade, pilot experiments on the automatic detection and notification of volcanic eruptions with infrasound arrays were performed in South America (Garcés et al., 2008) and in Italy (Ulivieri et al., 2013). Notifications were automatically delivered to the Volcanic Ash Advisory Centers (VAAC) at the onset and the end of large explosive eruptions at Tungurahua Volcano (Fee et al., 2010). More

recently, a fully automated and operational warning system based on local (<6 km) infrasound array data was developed for Etna volcano in Italy with a reliability rate of 96.5% and without negative false alerts (Ripepe et al., 2018). During favourable propagation conditions, global arrays are capable of identifying explosive activity and infrasound monitoring on a global scale and can provide timely input, even with a latency of ~1 hour due to propagation time is considered (Matoza et al., 2017; Marchetti et al., 2019).

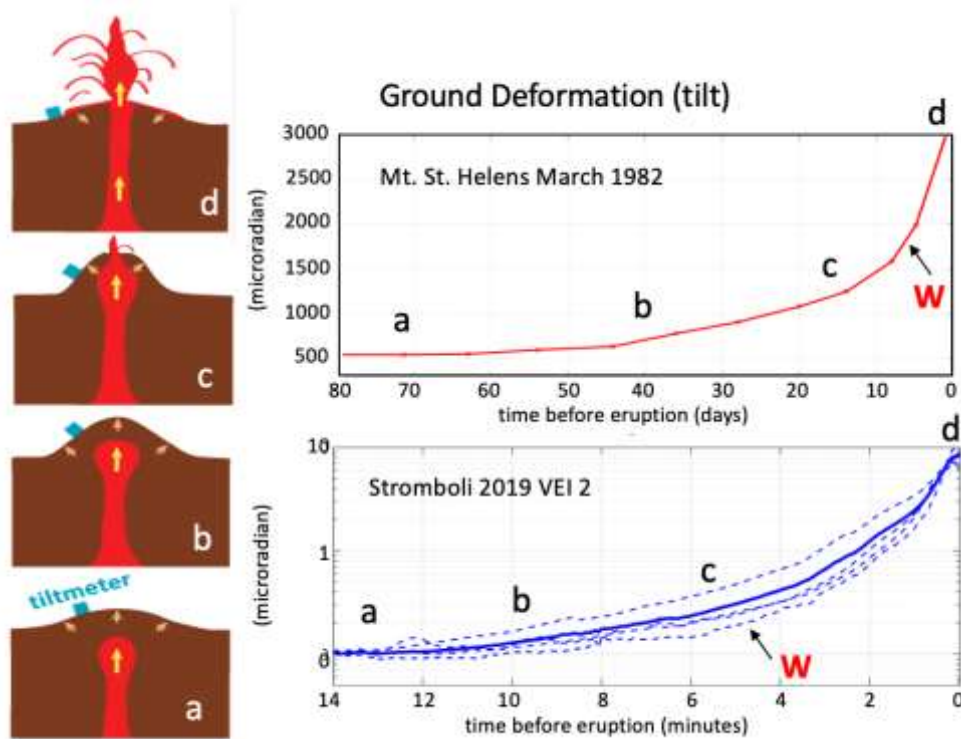


Figure 12. Before explosive eruptions, upward magma migration progressively inflates the ground. This inflation could be used to deliver a warning days or minutes before eruption. Inflation at Mt. St. Helens (upper panel) started several days before the 19 March 1982 eruption and allowed a warning to be given (indicated with the letter W) a few days before the explosion (from USGS report). At Stromboli (lower panel), ground inflation is smaller than St. Helens but follows a regular pattern which is used to automatically issue alerts 4-5 minutes before violent explosive events (Ripepe et al., 2021).

On volcanoes where tsunamis can be generated by pyroclastic flows, infrasound can be used to complement the seismic record to automatically detect in real-time the occurrence and trajectory of pyroclastic flows (Oshima & Maekawa, 2001; Delle Donne et al., 2014) or large mass movements. Recently, the atmospheric perturbation (Lamb wave) associated with the January 2022 violent eruption of HTHH volcano in Tonga (Matoza et al., 2022) triggered tsunami waves worldwide that globally surprised tsunami modellers, as they arrived almost 2 hours before the expected “normal” earthquake-generated tsunami onset (Kubota et al., 2022). The HTHH volcanic eruption was one of the most powerful events ever recorded, with audible sound detected more than 10,000 kilometers from the source, circumnavigating the globe in both directions (Fig13). The results highlight the capability of infrasound for near-real-time volcano monitoring at a regional and global scale and demonstrate how it could supplement other monitoring techniques in remote, poorly instrumented, areas.



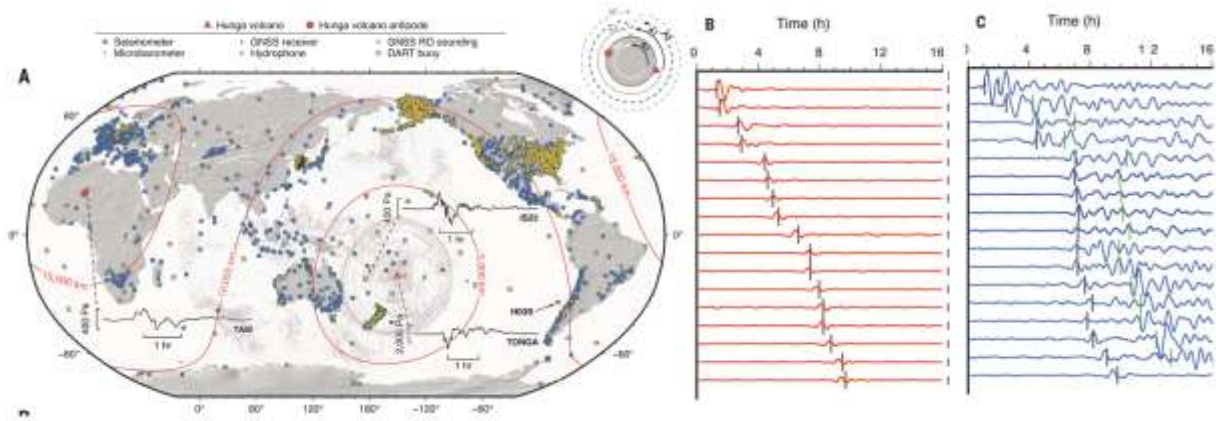


Figure 13. (A) Global distribution of recording geophysical sensors Background image is brightness temperature difference (Himawari-8) at 07:10 UTC on 15 January 2022. Selected 4-hour pressure waveforms are filtered from 10,000 to 100 s. Upper-right inset shows Hunga wave paths around Earth. (B) Observed barograms. (C) Observed ocean bottom pressure gauge waveform (Matoza et al., 2022; Kubota et al., 2022).

### Satellite monitoring

In recent years, there has been a dramatic increase in the number and capabilities of satellites to monitor the world’s volcanoes (Pollard et al., 2020; Pavolonis et al., 2022). Data from satellite instruments provide a cost-effective means of tracking activity and potentially forecasting hazards due to volcanoes around the world (Pritchard et al., 2022). A growing number of volcano monitoring parameters of the electromagnetic spectrum are now measurable from space. Ultraviolet, optical, infrared, and microwave (synthetic aperture radar) measurements can provide information on the volcanic thermal and gas emissions, ground displacement, and surface and topographic change before, during and after a volcanic eruption (e.g., Valade et al., 2019).

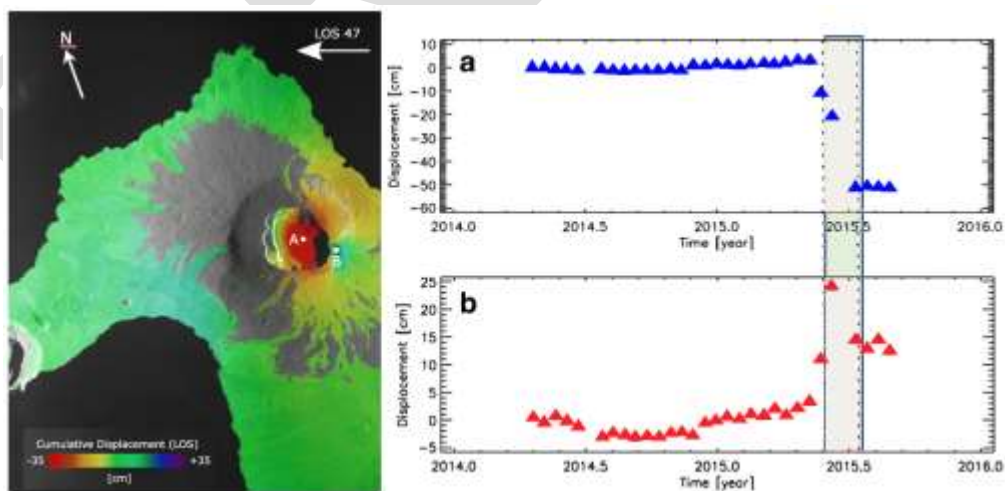


Figure 14. Ground deformation at Wolf volcano between 16 April 2014 and 25 August 2015 obtained from satellite data on descending track. The map shows the cumulative ground deformation; red color means movement away from the satellite, blue towards it. The time series of two selected points located on the tops of the volcano are also presented. Color bar shows the eruption time period. Time series (a) highlights a deformation of about 50 cm away from the satellite during the eruptive period (deflation) and (b), deformation is towards the satellite (inflation). (from Pritchard et al., 2018)

Satellite remote sensing has proven to be useful both in volcano monitoring (Fig 14) by detecting and tracking unrest and ongoing eruptions (Coppola et al., 2016), as well as for eruption forecasting (Hooper et al., 2012) and understanding the fundamental processes occurring at volcanoes (for example, Dean et al., 2015; Dehn & Harris, 2015; Biggs et al., 2014). As with ground-based data, using multiparameter satellite data (for example, thermal emissions, outgassing, and deformation) can precede eruptions, in some cases by months to years, and improve the chances of detecting anomalies and understanding underlying volcanic processes. Although we cannot yet quantitatively relate any given satellite-detected unrest event to an eruption, satellite data are being used to issue alerts (see examples in Schneider et al., 2000; Pallister et al., 2013; Pritchard et al., 2018).

When the timing between satellite detections and eruption is compared (Furtney et al., 2018), it is found that most thermal emission (~80%) and SO<sub>2</sub> outgassing (~95%) detections are co-eruptive while about 50% of satellite deformation detections preceded eruption. From 2000 to 2010, deformation was detected a mean of 1,001 days before an eruption, thermal anomalies were detected a mean of 36 days before an eruption, and SO<sub>2</sub> outgassing was detected a mean of 341 days before an eruption (Phillipson et al., 2013). Detected unrest preceded eruptions by 274, 51, and 797 days for satellite-detected thermal emissions, SO<sub>2</sub> outgassing, and deformation, respectively (Furtney et al., 2018). Remote sensing data will never replace terrestrial monitoring; rather, they provide a critical complement to ground monitoring,

#### **Alert System for Volcano Tsunamis**

Only ~10% of the historically active ~1,500 volcanoes (according to the database of the Global Volcanism Program of the Smithsonian Institution) are monitored in real-time (Pallister & McNutt, 2015). The accuracy assessment of the volcanic alerts issued by government agencies prior to eruptions reveals the complexity of the decision-making process and suggests improvements in our monitoring systems (Winson et al., 2014; Polland & Anderson, 2020). Currently, no instrumental network automatically provides the real-time onset and location of volcanic eruptions without human supervision.

This calls for the development of dedicated monitoring strategies possibly in the framework of international collaboration and/or already established initiatives, as USGS-VDAP (<https://volcanoes.usgs.gov/vdap/>) or Wovodat (<https://www.wovodat.org/>) (Lowenstern and Ewert, 2020; Newhall et al., 2017).

Interpretation of monitoring data in terms of volcanic hazard remains still empirical, although forecasts are becoming more quantitative based on an improved understanding of the physics of magmatic processes (Sparks [2003](#)) and the use of statistical methods (e.g., Newhall and Hoblitt [2002](#); Marzocchi and Bebbington [2012](#)).

Alert Level	Meaning
GREEN/NORMAL	Background
YELLOW/ADVISORY	Above Background
ORANGE/WATCH	Escalation of Parameters
RED/ALERT	Eruption imminent/Ongoing

Figure 15. Color code representing the Volcano Alert levels (VAL) typically used by Volcano Observatory to issue alerts, which could be integrated in the Tsunami Warning Systems to actuate pre-warning procedures.

Volcano Alert Levels (VAL) represent the most common worldwide method to communicate the state of activity for a volcano (Fig 15) and provide also short-term forecasts (e.g., Potter et al. 2014). Alert levels are usually defined by volcano observatories and represent the “official” communication of volcano status by scientists to civil protection authorities (Tilling, 2008).

Alert levels can be very effective as an immediate means of communication about the state of a volcano. They include a scale of four levels associated with a different colour scale of alerts (Papale, 2017). They are largely used when a change in the activity level should be communicated as fast as possible. The use of alert levels is also useful to communicate at the local or global level basic information on the state of unrest or ongoing eruption. For this reason, a similar four-level colour scale named VONA (Volcano Observatory Notice for Aviation) is used for communications by Volcano Observatory to the Volcanic Ash Advisory Centres (VAAC), which inform civil aviation authorities on the potential presence of ash clouds along airplane routes worldwide (Pallister et al., 2019).

We foresee a similar alert level notification to also mitigate the possible risk of tsunamis generated by volcano unrest (Fig 16). Following a similar strategy to that used by the ICAO for the ash dispersal in the atmosphere, the Volcano Tsunami Alert Notification (VOTAN) levels should indicate:

- a) Two levels of pre-eruption volcanic activities ; a significant unusual and/or increasing volcanic activity (YELLOW) or a larger increasing activity (ORANGE) which could presage a volcanic eruption.
- b) Ongoing volcanic eruption (RED); description of the eruption including whether flank instability or a large plume is occurring.
- c) Volcanic eruption cessation (GREEN).

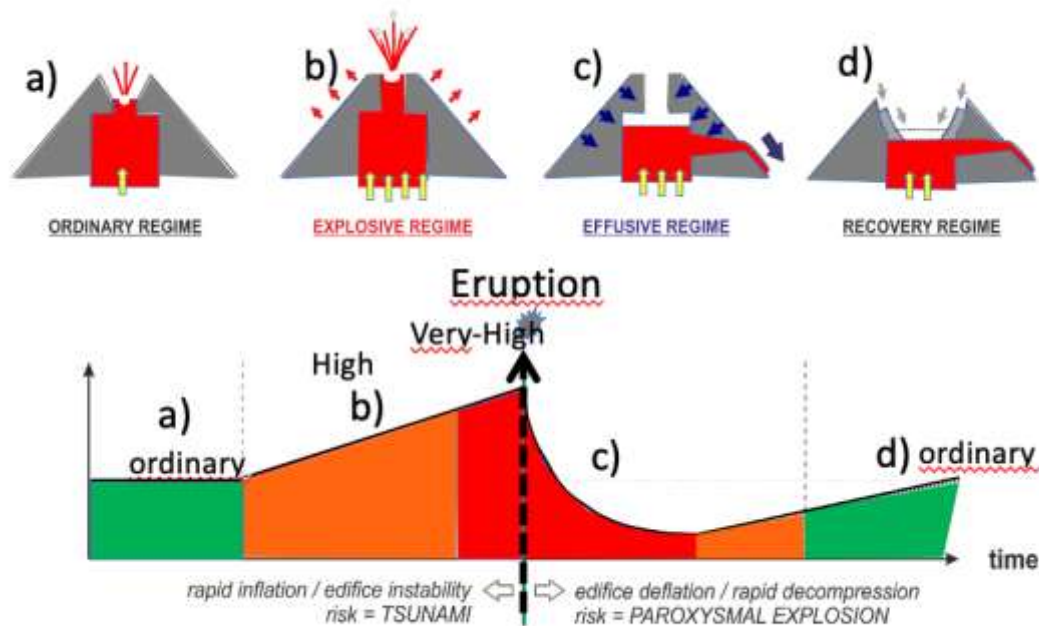


Figure 16. Conceptual model of the VAL color change as function of significant variations in the monitoring parameters, and implications for associated tsunami hazards (from Valade et al., 2016)

The VOTAN would be made available to IOC Tsunami Warning Focal Points (TWFP) and National Tsunami Warning Centers (NTWC) in potentially impacted Member States, as well as the IOC Tsunami Service Providers for that Region.

For volcanoes in remote poorly instrumented areas, a global monitoring network such as the Comprehensive Nuclear-Test-Ban Treaty Organization (CTBTO), designed to detect nuclear explosions anywhere on earth, could provide efficient information on seismic, infrasonic and hydroacoustic (for submarine) activity related to volcanic unrest which could cause a tsunami. The CTBTO global network is in fact already involved both in tsunami warning agreements with 19 countries and collaboration with VAAC for the testing of the volcanic information system (VIS), to establish a real-time operational system of volcanic eruptions warning. Nevertheless, the current agreement between CTBTO and UNESCO does not include infrasound data.

In most cases, the use of CTBTO's data for both seismic and volcanic tsunami has proven more reliable and speedier than data from some other sources.

## REFERENCES

Allstadt, K.E. et al. (2018). "Seismic and acoustic signatures of surficial mass movements at volcanoes". In: Journal of Volcanology and Geothermal Research.

Biggs, J., & Pritchard, M. E. (2017). Global volcano monitoring: what does it mean when volcanoes deform? Elements, 13(1), 17-22.

Biggs, J., Ebmeier, S.K., Aspinall, W.P., Lu, Z., Pritchard, M.E., Sparks, R.S.J., and Mather, T.A., 2014, Global link between deformation and volcanic eruption quantified by satellite imagery: *Nature Communications*, v. 5, article 3471, 7 p., <https://doi.org/10.1038/ncomms4471>.

Bonaccorso, A., Calvari, S., Linde, A., Sacks, S. & Boschi, E. Dynamics of the shallow plumbing system investigated from borehole strainmeters and cameras during the 15 March 2007 Vulcanian paroxysm at Stromboli volcano. *Earth Planet. Sci. Lett.* 357-358, 249–256 (2012).

Calder, E.S. et al. (2002). “Mechanisms of lava dome instability and generation of rockfalls and pyroclastic flows at Soufriere Hills Volcano, Montserrat”. In: Geological Society, London, *Memoirs* 21.1, pp. 173–190.

Campus, P.: Monitoring volcanic eruptions with the IMS Infrasound Network, *Inframatrics*, 15, 6–12, 2006.

Chouet, B. A., Page, R. A., Stephens, C. D., Lahr, J. C. & Power, J. A. Precursory swarms of long-period events at Redoubt Volcano (1989–1990), Alaska: their origin and use as a forecasting tool. *J. Volc. Geotherm. Res.* **62**, 95–135 (1994).

Coppola, D., Laiolo, M., Cigolini, C., Donne, D.D., and Ripepe, M., 2016, Enhanced volcanic hot-spot detection using MODIS IR data: results from the MIROVA system: Geological Society, London, *Special Publications*, v. 426, p. 181–205, <https://doi.org/10.1144/SP426.5>

Duputel, Z., Lengliné, O., & Ferrazzini, V. (2019). Constraining spatiotemporal characteristics of magma migration at Piton de la Fournaise volcano from pre-eruptive seismicity. *Geophysical Research Letters*, 46(1), 119-127.

Dzurisin, D. (2003). A comprehensive approach to monitoring volcano deformation as a window on the eruption cycle. *Reviews of Geophysics*, **41**(1), 1001. <https://doi.org/10.1029/2001RG000107>

Dabrowa, A. L., Green, D. N., Rust, A. C., and Phillips, J. C. (2011) A global study of volcanic infrasound characteristics and the potential for long-range monitoring, *Earth Planet Sc. Lett.*, 310, 369–379, <https://doi.org/10.1016/j.epsl.2011.08.027>.

De Angelis, S. , V. Bass, V. Hards and G. Ryan, “Seismic Characterization of Pyroclastic Flow Activity at Soufrière Hills Volcano, Montserrat, 8 January 2007,” *Natural Hazards and Earth System Sciences*, Vol. 7, No. 4, 2007, pp. 467-472. doi:10.5194/nhess-7-467-2007

Dean, K.G., Osiensky, J., Gordeev, E., Senyukov, S., Rybin, A.V., Karagusov, Y.V., Terentyev, N.S., and Guryanov, V.B., 2015, An overview of satellite monitoring of volcanoes, *in* Dean, K.G., and Dehn, J., eds., *Monitoring volcanoes in the North Pacific—Observations from space*: Berlin, Heidelberg, Springer, p. 261–302.

Dehn, J., and Harris, A.J.L., 2015, Thermal anomalies at volcanoes, *in* Dean, K.G., and Dehn, J., eds., *Monitoring volcanoes in the North Pacific*: Berlin, Heidelberg, Springer, p. 49–78.

Delle Donne, D., Ripepe, M., De Angelis, S., Cole, P. D., Lacanna, G., Poggi, P., & Stewart, R. (2014). Chapter 9 Thermal, acoustic, and seismic signals from pyroclastic density currents and Vulcanian explosions at Soufrière Hills Volcano, Montserrat. *Geological Society, London, Memoirs*, 39(1), 169-178.

Drob, D. P., Picone, J. M., & Garcés, M. (2003). Global morphology of infrasound propagation. *Journal of Geophysical Research*, 108(D21), 4680. <https://doi.org/10.1029/2002JD003307>

Dzurisin, D., Westphal, J. A. & Johnson, D. J. Eruption prediction aided by electronic tiltmeter data at Mount St. Helens. *Science* 221, 1381–1383 (1983).

- Einarsson P., and Brandsdóttir B., (2021). Seismicity of the Northern Volcanic Zone of Iceland. *Front. Earth Sci.*, vol.9. | <https://doi.org/10.3389/feart.2021.628967>.
- Falchin, A., Métaxian, J. P., Mars, J., Stutzmann, É., Komorowski, J. C., Moretti, R., ... & Lemarchand, A. (2021). A machine-learning approach for automatic classification of volcanic seismicity at La Soufrière Volcano, Guadeloupe. *Journal of Volcanology and Geothermal Research*, 411, 107151.
- Fee, D., Garcés, M., & Steffke, A. (2010). Infrasound from Tungurahua volcano 2006-2008: Strombolian to plinian eruptive activity. *Journal of Volcanology and Geothermal Research*, 193(1-2), 67–81. <https://doi.org/10.1016/j.jvolgeores.2010.03.006>
- Francis, P. (1993). *Volcanoes. A planetary perspective*.
- Furtney, M.A., Pritchard, M.E., Biggs, J., Carn, S.A., Ebmeier, S.K., Jay, J.A., McCormick Kilbride, B.T., and Reath, K.A., 2018, Synthesizing multi-sensor, multi-satellite, multi-decadal data sets for global volcano monitoring: *Journal of Volcanology and Geothermal Research*, v. 365, p. 38–56, <https://doi.org/10.1016/j.jvolgeores.2018.10.002>.
- Galletto F., Acocella V., Hooper A., Bagnardi M. (2022) Eruption at basaltic calderas forecast by magma flow rate. *Nature Geoscience*, <https://doi.org/10.1038/s41561-022-00960-z>
- Garcés, M., Fee, D., Steffke, A., McCormack, D. P., Servranckx, R., Bass, H., et al. (2008). Capturing the acoustic fingerprint of stratospheric ash injection. *EOS, Transactions*, 89(40), 377–378. <https://doi.org/10.1029/2008EO400001>
- Girona, T., Costa, F., and Schubert, G. (2015). Degassing during Quiescence as a Trigger of Magma Ascent and Volcanic Eruptions. *Sci. Rep.* 5, 1–7. doi:10.1038/srep18212
- Hibert, C. et al. (2014). “Automated identification, location, and volume estimation of rockfalls at Piton de la Fournaise volcano”. In: *Journal of Geophysical Research: Earth Surface* 119.5, pp. 1082–1105.
- Hooper, A., Prata, F., and Sigmundsson, F., 2012, Remote sensing of volcanic hazards and their precursors: *Proceedings of the Institute of Electrical and Electronics Engineers (IEEE)*, v. 100, no. 10, p. 2908–2930, <https://doi.org/10.1109/JPROC.2012.2199269>.
- Kamo, K. A. In *Volcanic hazards: assessment methods and monitoring* (Latter J. H. ed.) 585–598 (Springer, 1989)
- Kanamori, H. and J.W. Given (1982). “Analysis of long-period seismic waves excited by the May 18, 1980, eruption of Mount St. Helens—A terrestrial monopole?” In: *Journal of Geophysical Research: Solid Earth* 87.B7, pp. 5422–5432.
- Kawakatsu, H., & Yamamoto, M. (2015). Volcano seismology. *Earthquake Seismology*, 389-419.
- Kubota et al., *Science* 2022
- Iguchi, M., Yakiwara, H., Tameguri, T., Hendrasto, H. & Hirabayashi, J. Mechanism of explosive eruption revealed by geophysical observations at the Sakurajima, Suwanosejima and Semeru volcanoes. *J. Volcanol. Geotherm. Res.* 178, 1–9 (2008).
- Lowenstern, J.B., and Ewert, J.W., 2020, Volcano observatories reduce risk around the globe. Here’s how we can support them: *Temblor*, accessed September 3, 2020, at <http://doi.org/10.32858/temblor.085>
- Lowenstern, J.B et al. Strengthening local volcano observatories through global collaborations, *Bull. Volcanology*, **84**, 10 (2022a).

Lowenstern, J.B. et al. Guidelines for volcano-observatory operations during crises: recommendations from the 2019 volcano observatory best practices meeting, *J. Appl. Volcanol.* **11**, 3 (2022b).

Marchetti, E., Genco, R., & Ripepe, M. (2009). Ground deformation and seismicity related to the propagation and drainage of the dyke feeding system during the 2007 effusive eruption at Stromboli volcano (Italy). *Journal of volcanology and geothermal research*, 182(3-4), 155-161.

Marchetti, E., Ripepe, M., Campus, P., Le Pichon, A., Vergoz, J., Lacanna, G., Mialle, P., Hereil, P., and Husson, P.: Long range infrasound monitoring of Etna volcano, *Sci. Rep.-UK*, 9, 18015, <https://doi.org/10.1038/s41598-019-54468-5>, 2019.

Matoza, R. S., Green, D. N., Le Pichon, A., Shearer, M., Fee, D., Mialle, P., & Ceranna, L. (2017). Automated detection and cataloging of global explosive volcanism using the International Monitoring System infrasound network. *Journal of Geophysical Research: Solid Earth*, 122, 2946–2971. <https://doi.org/10.1002/2016JB013356>

Matoza, R. S., et al., (2022). Atmospheric waves and global seismoacoustic observations of the January 2022 Hunga eruption, Tonga, *Science*, 377, 95– 100, <https://doi.org/10.1126/science.abo7063>.

McNutt, S. R., Thompson, G., Johnson, J. B., De Angelis, S., & Fee, D. (2015). Seismic and infrasonic monitoring. In *The encyclopedia of volcanoes*, (2nd ed., pp. 1071–1099). London: Academic Press. <https://doi.org/10.1016/B978-0-12-385938-9.00063-8>

Newhall, C.G., and Dzurisin, D., 1988, Historical unrest at large calderas of the world: U.S. Geological Survey Bulletin 1855, 1,108 p.

Newhall, C.G., and Hoblitt, R., 2002, Constructing event trees for volcanic crises: *Bulletin of Volcanology*, v. 64, p. 3–20, <https://doi.org/10.1007/s004450100173>

Newhall CG, Costa F, Ratdompurbo A, Venezky DY, Widiwijayanti C, Thin Zar Win N (2017) WOVodat—an online, growing library of worldwide volcanic unrest. *J Volcanol Geoth Res* 345:184–199

Nishimura, T. Ground deformation caused by magma ascent in an open conduit. *J. Volcanol. Geoth. Res.* 187, 178–192 (2009).

Oshima, H., Maekawa, T., 2001. Excitation process of infrasonic waves associated with Merapi-type pyroclastic flow as revealed by a new recording system. *Geophysical Research Letters* 28 (6), 1099–1102.

Pallister, J., Papale, P., Eichelberger, J., Newhall, C., Mandeville, C., Nakada, S., Marzocchi, W., Loughlin, S., Jolly, G., Ewert, J., and Selva, J., (2019), Volcano observatory best practices (VOBP) workshops—A summary of findings and best-practice recommendations: *Journal of Applied Volcanology*, v. 8, article 2, 33 p., <https://doi.org/10.1186/s13617-019-0082-8>

Pallister, J., Schneider, D., Griswold, J.P., Keeler, R.H., Burton, W.C., Noyles, C., Newhall, C.G., and Ratdompurbo, A., 2013, Merapi 2010 eruption— Chronology and extrusion rates monitored with satellite radar and used in eruption forecasting: *Journal of Volcanology and Geothermal Research*, v. 261, p. 144–152.

Pallister, J., & McNutt, S. (2015). Synthesis of volcano monitoring. In *The encyclopedia of volcanoes*, (2nd ed., pp. 1151–1171). London: Academic Press. <https://doi.org/10.1016/B978-0-12-385938-9.00066-3>

Papale, P., 2017, Rational volcanic hazard forecasts and the use of volcanic alert levels: *Journal of Applied Volcanology*, v. 6, no. 13.

Peltier, A., Bachèlery, P., & Staudacher, T. (2011). Early detection of large eruptions at Piton de la Fournaise volcano (La Réunion Island): Contribution of a distant tiltmeter station. *Journal of Volcanology and Geothermal Research*, 199(1-2), 96–104. <https://doi.org/10.1016/j.jvolgeores.2010.11.006>

Peltier A, Villeneuve N, Ferrazzini V, Testud S, Hassen Ali T, Boissier P and Catherine P (2018) Changes in the Long-Term Geophysical Eruptive Precursors at Piton de la Fournaise: Implications for the Response Management. *Front. Earth Sci.* 6:104. doi: 10.3389/feart.2018.00104.

Poland, M.P., and Anderson, K.R., 2020, Partly cloudy with a chance of lava flows—Forecasting volcanic eruptions in the twenty-first century: *Journal of Geophysical Research—Solid Earth*, v. 125, no. 1, 32 p., <https://doi.org/10.1029/2018JB016974>.

Poland, M.P., Lopez, T., Wright, R., and Pavlonis, M.J., 2020, Forecasting, detecting, and tracking volcanic eruptions from space: *Remote Sensing in Earth Systems Sciences*, v. 3, no. 1, p. 55–94, <https://10.1007/s41976-020-00034-x>.

Potter SH, Jolly GE, Neall VE, Johnston DM, Scott BJ. Communicating the status of volcanic activity: revising New Zealand's volcanic alert level system. *J Appl Volcanol.* 2014;3:13

Phillipson, G., Sobradelo, R., and Gottsmann, J., 2013, Global volcanic unrest in the 21st century—An analysis of the first decade: *Journal of Volcanology and Geothermal Research*, v. 264, p. 183–196.

Pritchard, M.E., Biggs, J., Wauthier, C., Sansosti, E., Arnold, D.W.D., Delgado, F., Ebmeier, S.K., Henderson, S.T., Stephens, K., Cooper, C., Wnuk, K., Amelung, F., Aguilar, V., Mothes, P., Macedo, O., Lara, L.E., Poland, M.P., and Zoffoli, S., (2018), Towards coordinated regional multi-satellite InSAR volcano observations—Results from the Latin America pilot project: *Journal of Applied Volcanology*, v. 7, article 5, 28 p., <https://doi.org/10.1186/s13617-018-0074-0>.

Pritchard, M.E., Poland, M., Reath, K., Andrews, B., Bagnardi, M., Biggs, J., Carn, S., Coppola, D., Ebmeier, S.K., Furtney, M.A., Girona, T., Griswold, J., Lopez, T., Lundgren, P., Ogburn, S., Pavlonis, M., Rumpf, E., Vaughan, G., Wauthier, C., Wessels, R., Wright, R., Anderson, K.R., Bato, M.G., and Roman, A., (2022), Optimizing satellite resources for the global assessment and mitigation of volcanic hazards—Suggestions from the USGS Powell Center Volcano Remote Sensing Working Group: *U.S. Geological Survey Scientific Investigations Report 2022–5116*, 69 p., <https://doi.org/10.3133/sir20225116>.

Ripepe, M., Marchetti, E., Delle Donne, D., Genco, R., Innocenti, L., Lacanna, G., and Valade, S. (2018). Infrasonic early-warning for explosive eruption. *J. Geophys. Res., Solid Earth* **123**(11), 9570–9585, <https://doi.org/10.1029/2018JB015561>.

Ripepe, M., G. Lacanna, M. Pistolesi, M.C. Silengo, A. Aiuppa, M. Laiolo, F. Massimetti, L. Innocenti, M. Della Schiava, M. Bitetto, F.P. La Monica, T. Nishimura, M. Rosi, D. Mangione, A. Ricciardi, R. Genco, D. Coppola, E. Marchetti, D. Delle Donne, (2021). Ground deformation reveals the scale-invariant conduit dynamics driving basaltic explosive eruptions. *Nat. Comm.* 12:1683, <https://doi.org/10.1038/s41467-021-21722-2>

Roman, D.C., Moran, S.C., Power, J.A., and Cashman, K.V. (2004). Temporal and Spatial Variation of Local Stress Fields before and after the 1992 Eruptions of Crater Peak Vent, Mount Spurr Volcano, Alaska. *Bul. Seism. Soc. Am.* Vol.94, No.6, pp.2366-2379.

Roult, G. C., Beauducel, F., Ferrazzini, V., Boissier, P., & Villeneuve, N. (2014, December). The "Jerk" Method for Predicting Intrusions and Eruptions of Piton De La Fournaise (La Réunion Island) from the Analysis of the Broadband Seismological Rer Station. In *AGU Fall Meeting Abstracts* (Vol. 2014, pp. V43A-4844).

Segall P. Volcano deformation and eruption forecasting. In: *Geol. Soc. Lond., Sp. Pub.* 380; 2013. p. 22. <https://doi.org/10.1144/SP380.4>.



Siebert, L. (1984). “Large volcanic debris avalanches: characteristics of source areas, deposits, and associated eruptions”. In: *Journal of volcanology and geothermal research* 22.3-4, pp. 163–197.

Sigmundsson et al., 2022 Deformation and seismicity decline before the 2021 Fagradalsfjall eruption. *Nature* 609, 523-528

Schaefer, L.N., F. Di Traglia, E. Chaussard, Z. Lu, T. Nolesini, N. Casagli, Monitoring volcano slope instability with Synthetic Aperture Radar: a review and new data from Pacaya (Guatemala) and Stromboli (Italy) volcanoes, *Earth Sci. Rev.* 192 (2019) 236–257.

Schneider, D.J., Dean, K.G., Dehn, J., Miller, T.P., and Kirianov, V.Y., 2000, Monitoring and analyses of volcanic activity using remote sensing data at the Alaska Volcano Observatory—Case study for Kamchatka, Russia, December 1997, in Mouginiis-Mark, P.J., Crisp, J.A., and Fink, J.H., eds., *Remote sensing of active volcanism: American Geophysical Union, Geophysical Monograph Series*, v. 116, p. 65–85.

Sparks RSJ. Forecasting volcanic eruptions. *Earth Planet Sci Lett.* 2003;10:1–15. [https://doi.org/10.1016/S0012-821X\(03\)00124-9](https://doi.org/10.1016/S0012-821X(03)00124-9).

Swanson, D.A., Casadevall, T.J., Dzurisin, D., Malone, S.D., Newhall, C.G., and Weaver, C.S., 1983, Predicting eruptions at Mount St. Helens, June 1980 through December 1982: *Science*, v. 221, no. 4618, p. 1369–1376, <https://doi.org/10.1126/science.221.4618.1369>.

Tilling, R. I. The critical role of volcano monitoring in risk reduction. *Adv. Geosci.* **14**, 3–11 (2008).

Uhira, K., H. Yamasato, and M. Takeo (1994). “Source mechanism of seismic waves excited by pyroclastic flows observed at Unzen volcano, Japan”. In: *Journal of Geophysical Research: Solid Earth* 99.B9, pp. 17757–17773.

Ulivieri, G., Ripepe, M., & Marchetti, E. (2013). Infrasound reveals transition to oscillatory discharge regime during lava fountaining: Implication for early-warning. *Geophysical Research Letters*, 40, 3008–3013. <https://doi.org/10.1002/grl.50592>

Valade, S., G. Lacanna, D. Coppola, M. Laiolo, M. Pistolesi, D. Delle Donne, R. Genco, E. Marchetti, G. Ulivieri, C. Allocca, C. Cigolini, T. Nishimura, P. Poggi, M. Ripepe, (2016). Tracking dynamics of magma migration in open-conduit systems, *Bull. Volcanol.* 78.

Valade, S., Ley, A., Massimetti, F., D’Hondt, O., Laiolo, M., Coppola, D., Loibl, D., Hellwich, O., and Walter, T.R., 2019, Towards global volcano monitoring using multisensor sentinel missions and artificial intelligence—The MOUNTS monitoring system: *Remote Sensing*, v. 11, no. 113, article 1528, 31 p., <https://doi.org/10.3390/rs11131528>.

Voight, B., and D. Elsworth (1997). “Failure of volcano slopes”. In: *Geotechnique* 47.1, pp. 1–31

Winson, A. E. G., Costa, F., Newhall, C. G., & Woo, G. (2014). An analysis of the issuance of volcanic alert levels during volcanic crises. *Journal of Applied Volcanology*, 3(1), 14. <https://doi.org/10.1186/s13617-014-0014-6>

## Chapter 5 – Volcanic Tsunami Warning Systems: Stromboli and Anak Krakatau volcano examples

### 5.1 Stromboli Volcanic Tsunami Warning System

Numerical simulations (Fornaciai et al., 2019) provide evidence that a tsunami generated in the Sciara del Fuoco (see Chapter 3), will reach the populated coast of Stromboli in less than 3-4 minutes. After only 15-20 minutes the whole Aeolian Arc and the coast of Calabria and Sicily (at ~60 km) would be impacted. Waves would travel across the southern Tyrrhenian sea entering in the Neapolitan Gulf after 1 hour and 20 minutes.

For this reason, two elastic beacons were deployed by Laboratory of Geophysics of University of Florence (LGS) in 2008 and 2017 offshore the Sciara del Fuoco, at 260 m and at 350 m distance from Punta dei Corvi (PDC) and Punta Labronzo (PLB) capes (Fig 17) respectively. The systems have been developed since 2007 in response to the tsunamis generated by a partial flank collapse occurred in 30 December 2002. The short propagation time (3-4 min) of the populated coast of Stromboli and the densely inhabited nearby (<60 km) coast of Italy required the development of a system fully automatic, able to detect tsunamis as rapidly as possible.

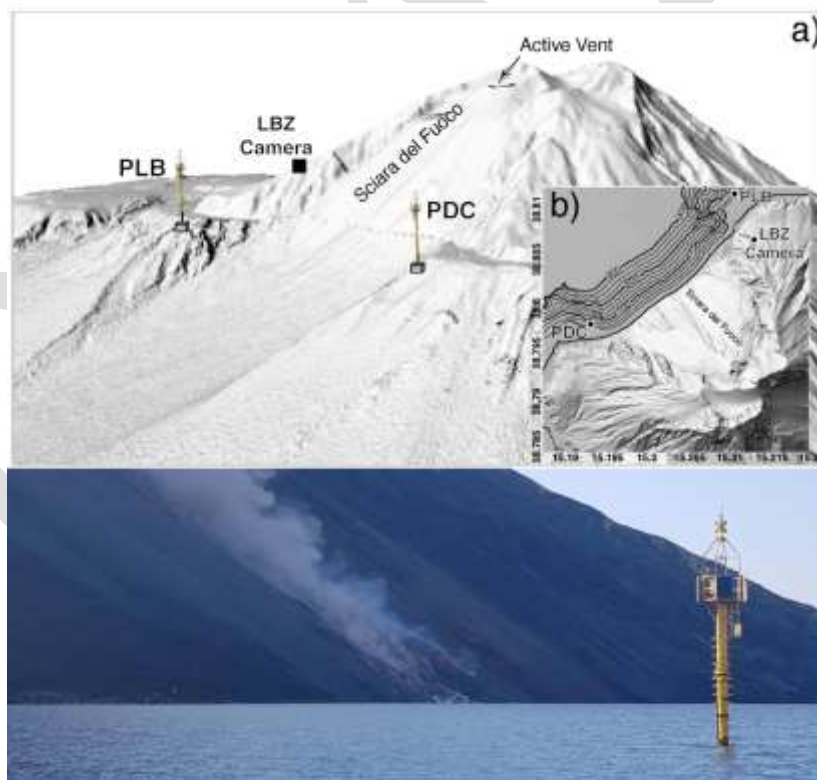


**Figure 17.** Position of the two elastic beacons (PLB and PDC) on 3D (a) and 2D (b) map of Stromboli volcano showing the Sciara del Fuoco slope above and below the sea surface. Photo of PLB elastic beacon at ~300 m in front of the Sciara del Fuoco during the 9 October 2022 effusive eruption. The structure stands ~9 m above the sea surface.

The system consists of two parts: i) Detection of the tsunami wave (by LGS); and ii) Activation of an acoustic alert system of sirens (by DPC) deployed at Stromboli, in the Aeolian islands, and in Sicily (Milazzo)

*The elastic beacons tsunami gauge system*

The TEWS operating at Stromboli is based on the sea level measurements at four pressure sensors installed along two elastic beacons at ~14 and ~48 m below the sea surface, placed at ~300 m offshore the Sciara del Fuoco. The elastic beacons are a semi-rigid structure with a 35 m long metallic pipe anchored with a concrete block of ~24 tons on the seabed with an anti-torsion steel cable (Fig 12). The elastic beacon has a small tower which stands ~10 m above the sea level, where the digitizer (Guralp – DM24S6EAMU), radio transmission system (5 GHz 10/100 Mbits) and power supply (4 solar panels 110 W) are placed. Both elastic beacons are equipped with two IDROMAR pressure sensors, sampled at 125 Hz. The depth of the pressure sensor on the seabed is optimal to reduce the effect of the sea waves at periods <13 s and to guarantee the best signal-to-noise ratio at the tsunami frequency band in near-field conditions (Fig 12).

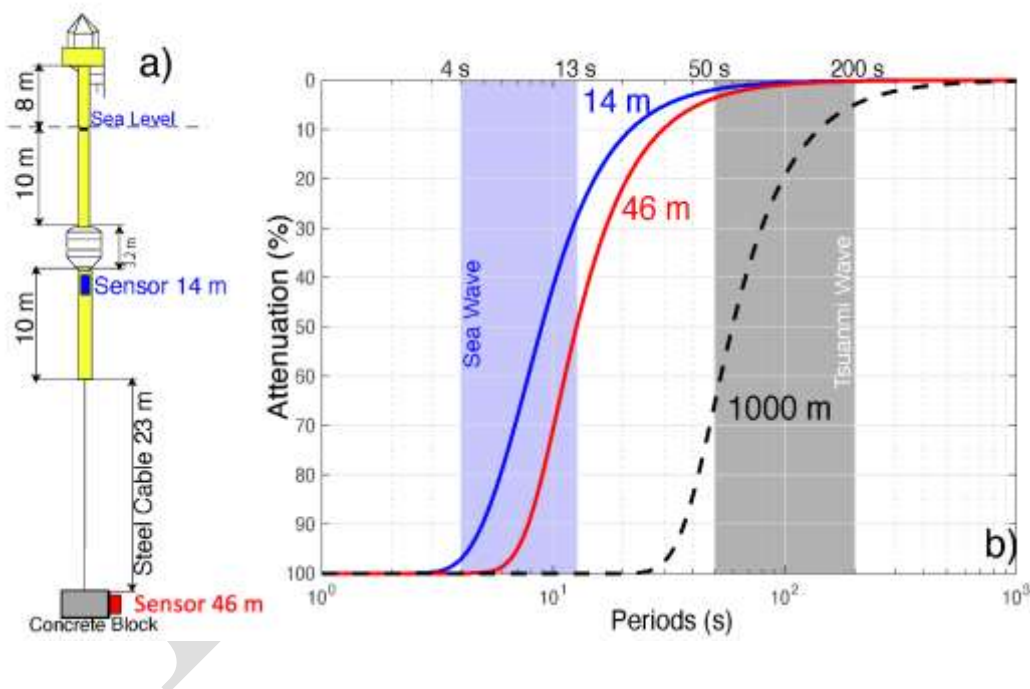


**Figure 18.** a) Schematic technical illustration of the main components of the elastic beacon. Pressure sensors used to detect the tsunami are at 14 (blue) and 46 m (red). b) wave dispersion calculated for the 14 and 46 m sensors show how this depth is optimal to reduce the contamination of the sea waves and maintain the best signal-to-noise ratio in the period range (50-200 s) typical of tsunami generated by landslide

*Tsunami detection algorithms*

The TEWS detection algorithm is grounded on the short-term average (STA) long-term average (LTA) ratio. Whereas STA is sensitive to rapid fluctuations in the sea wave amplitude, the LTA provides information on the background noise. The algorithm was calibrated considering synthetic tsunami waves modelled for the reference scenario of 30 December 2002 and assuming periods ranging between 30 s and 165 s, larger than those expected for the tsunami occurred at Stromboli in 2002 and at Anak Krakatau volcano in 2018. The detection algorithm operates on 5 consecutive steps (Fig19):

1. Spike removal: Spikes or sudden high frequency signal are usually the result of transmission error in the telemetry, disturbance from short electronic glitches, or in the case of Stromboli also by fishing activities around the elastic beacons. Spikes can contaminate the record resulting in the sudden increase of the STA and thus possible false detection.
2. Detrending the signal for tide removal: Linear detrend removes the tidal and/or barometric oscillations from the signal.
3. Low-pass filtering: The sea waves component is filtered using a FIR low-pass filter with a cut-off frequency  $f_c=0.067$  Hz and a bandwidth of 0.04 Hz to increase the signal-to-noise ratio.
4. Data decimation: Data are decimated from a 125 sampling rate down to 1 sample per second.
5. STA/LTA ratio: Finally, the STA/LTA ratio is calculated on the resampled data. To assure the correct description of the sea state and to reduce the statistical scatter, the LTA window should contain at least 300 times the larger sea wave period of 15 s (typical of rough sea state in the southern Mediterranean), which gives a LTA window of 4500 s. The STA window length depends instead strictly on the period of the tsunami wave to be detected. It was fixed at 40 s, which gives the larger value of the STA/LTA ratio at the onset of tsunami for periods ranging between 50 and 200 s (Fig 14).

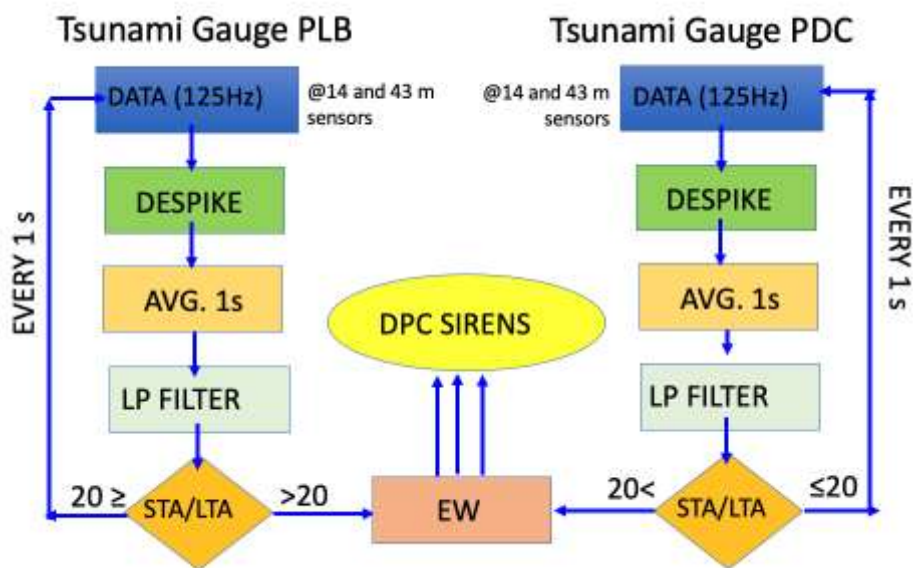


**Figure 19.** Chart flow of the automatic tsunami detection algorithm operating at Stromboli

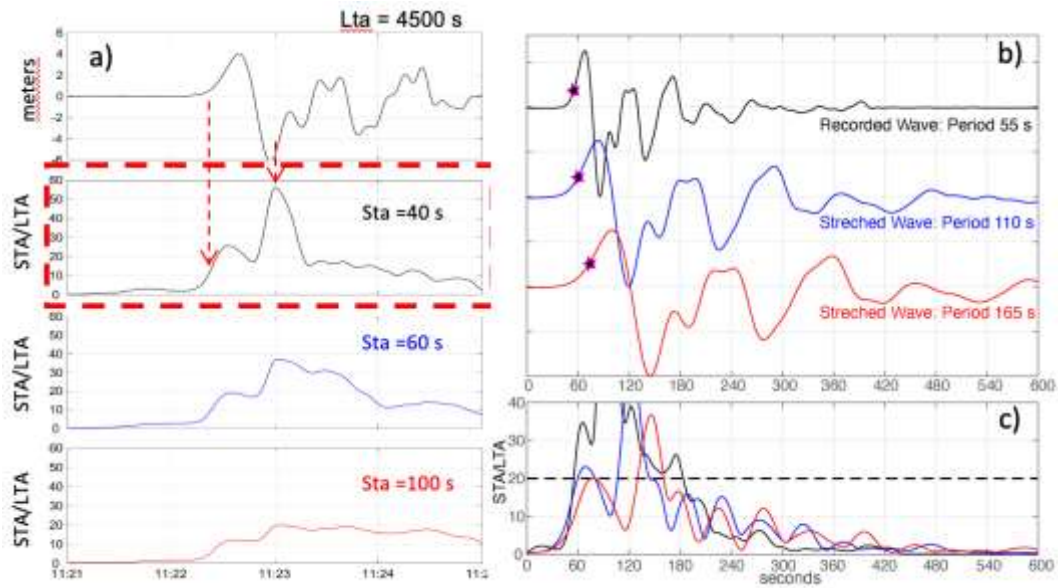


**Figure 20.** a) STA/LTA ratio calculated for LTA=4500 s and different STA time window shows the best performance with STA=40s to detect the onset of the tsunami. Signal used to test the algorithm is the tsunami wave modeled for the December 2002 landslide (Fornaciai et al., 2019). The 40 s large time window for the STA is also giving the best performance when b) different period of the tsunami ranging from 50 to 165 s are considered. c) Larger the period of the tsunami larger the STA time window or smaller the STA/LTA ratio should be for the most rapid detection of the tsunami onset.

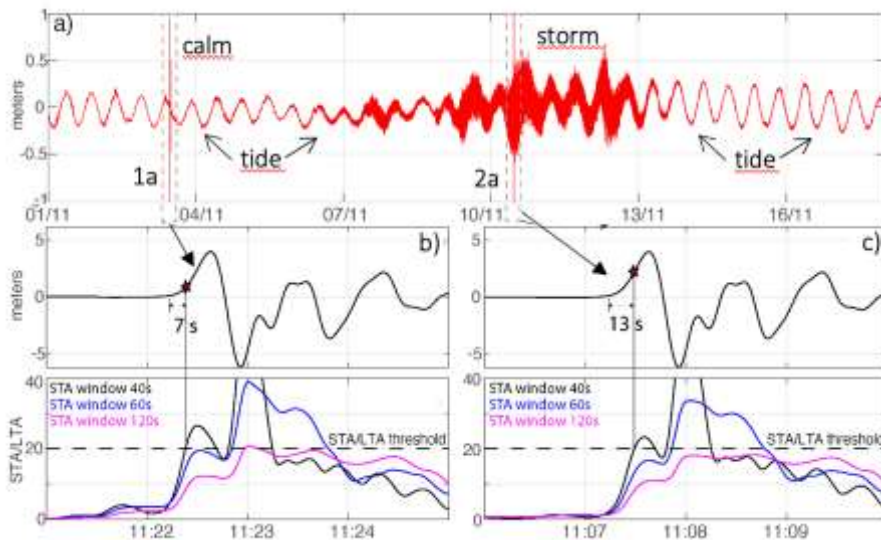


**Figure 21.** Sensitivity of the STA/LTA ratio to the sea condition has been tested by superimposing the theoretical waveform modeled for the December 2002 tsunami (Figure 4a) to calm (1a) and stormy (2a) sea conditions with waves up to 9 m. Onset of the tsunami is detected b) 7 s after the onset (STA=40s) but with a delay c) of only 6 s during the sea storm.

*Calibrating the TEWS sensitivity*

The detecting efficiency of the TEWS was calibrated by contaminating the synthetic tsunami wave modelled occurred during the 2002 Stromboli eruption with the noise relative to the most energetic sea storm recorded at Stromboli in the last 15 years that generated waves of ~1 m with periods of ~12 s at 46 m depth below sea level. The threshold ratio for the alert was then fixed at  $STA/LTA = 20$ , which also provides the best performance in rough sea conditions (Fig 15), with no false detections during unpredictable malfunctions of pressure sensor. The automatic alert is issued only when the  $STA/LTA$  ratio is larger than the detection threshold ( $STA/LTA > 20$ ) at both tsunami gauges for at least 90 s (Fig 19). This last logical filter increases the reliability of the system by minimizing the possibility of false detection and guarantees to automatically alert if a tsunami as large as 40 cm will occur in the worst sea conditions and with no false alert.

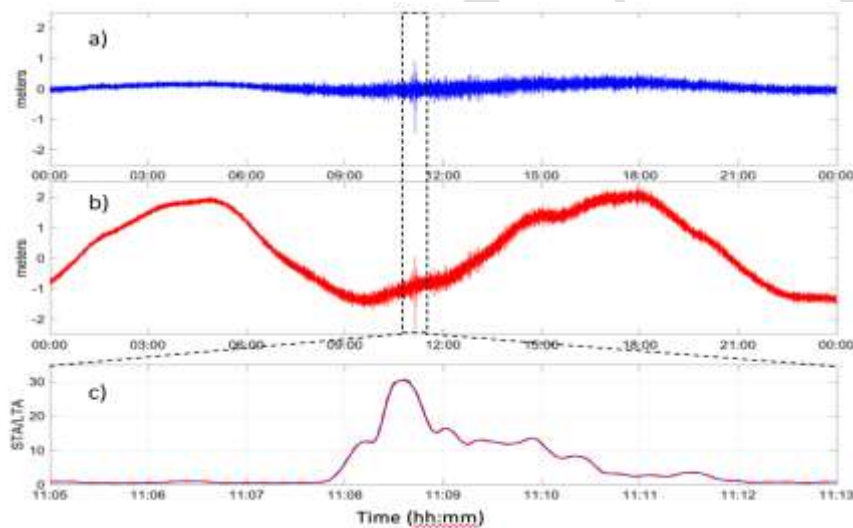


**Figure 22.** The TEW algorithm a) developed at Stromboli with tide of ~40 cm and sea waves of <15 s period was tested b) also for sea basins different than Mediterranean using larger tide (~2 m) and longer wave period and it shows c) how marine contaminations are removed and the  $STA/LTA$  ratio remains the same.

**Operational TEWS**

On August 28, 2019 the tsunami early warning alert was still being tested using only one gauge, but it allowed Civil defence authorities to activate the acoustic alert manually only 11 s after the tsunami onset and 3-4 minutes before the tsunami reached the populated coast of Stromboli. Since 9 September 2019, the early-warning system is fully operative and automatically linked to the acoustic alert system of the Italian Civil Defence. On December 4, 2022, a pyroclastic flow generated by a small (~ $10^5$  m<sup>3</sup>) collapse of the summit crater (Fig 23) that triggered a 1.4 m (peak-to-trough) height tsunami, which was automatically detected by the TEWS ~20 s after the onset and 9 s before the maximum negative amplitude of 1 m was reached (Fig 20). The detection automatically activated the

acoustic alert system of Italian DPC deployed in the Aeolian islands and in Sicily, triggering the emergency procedure along Sicily and Calabrian coasts.



**Figure 23.** Sequence of frames taken from the LBZ camera (see Figure 1) of the December 4, 2022, pyroclastic flow which moving downslope the Sciara del Fuoco at a speed of ~50 m/s generated a small tsunami visible in the lower right corner of each frame while propagates along the shore.

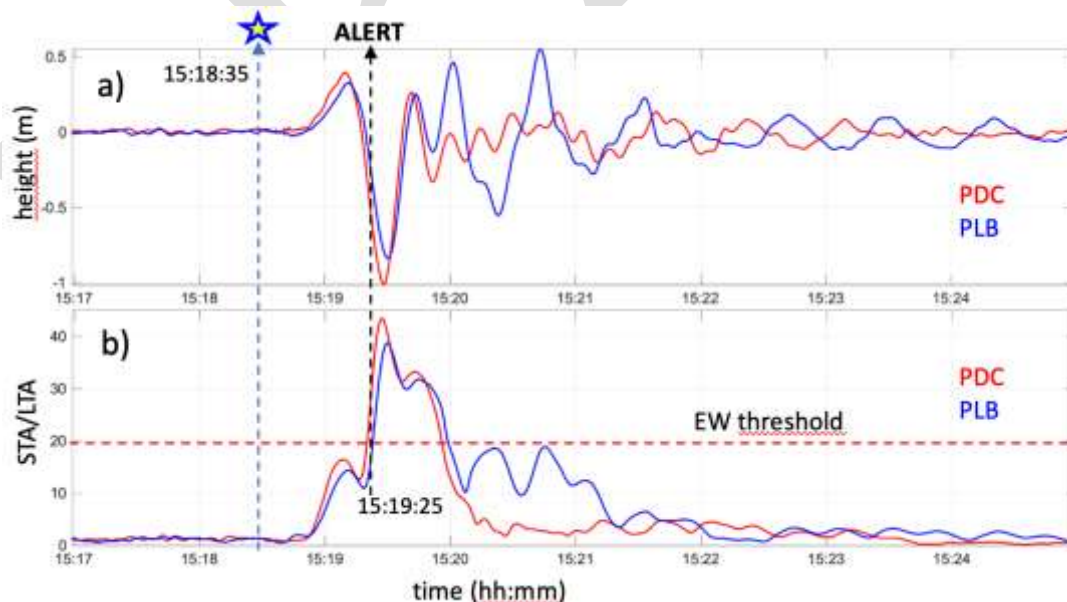


**Figure 24.** a) The small tsunami generated by the impact of the pyroclastic density current occurred at Stromboli on December 4, 2022 and recorded at the two elastic beacons (PDC and PLB) at a distance of ~1300 m from the splash zone. b) The STA/LTA ratio increased above the fixed warning threshold of 20 at 15:19:25, triggering the alert system 9 seconds before the maximum height and 50 seconds after the PDC onset



**Figure 25.** Position of the COA and the Acoustic Alert (siren) system used to warn population on the possible occurrence of a tsunami.

### ***Risk Mitigation at Stromboli***

The 30 December 2002 tsunami and the following eruptive emergency in 2003 at Stromboli was the most dangerous to have occurred on the island in the past three centuries, and the second most dangerous to have occurred in Italy during the last century after those of 1906 and 1944 at Vesuvius.

By pure chance the crisis caused just a few light injuries and panic, but no victims. The impact of the tsunami on residents and public opinion was considerable and resulted in the declaration of the “State of Emergency” by the National Government. This led to the set-up of a National Civil Defense project for the structural reduction of risk, financed by the National Government (Bertolaso et al., 2009). The main achievements were: i) Creation of the Centro Operativo Avanzato (COA) located in the village of Stromboli (Fig 19), a permanent civil protection and volcano real-time monitoring structure for a rapid safety response; ii) Installation of a siren system in the islands of Stromboli, Panarea, and Lipari, and in the Milazzo Harbor (Fig 25) triggered both manually or automatically by the TEWS (Bertolaso et al. 2009; Lacanna and Ripepe 2020); and iii) Organization of an information campaign on safety procedures for residents and tourists.

Risk mitigation activities were undertaken with the installation of signage, following the UNESCO standard design indicating the hazard areas expected to be inundated by the tsunami, which include indications on the behavior response “in case of” several sources of early alert (i.e., environmental cues/natural warnings and sirens sounding). Several waiting (evacuation) areas were identified on the island (see Fig 26). Signs show the direction of the safe “Escape route” and the direction to waiting areas (from Bonilauri et al., 2021). Note that the use of “escape routes” rather than “evacuation



routes” does not conform to the new international standards established in terms of tsunami evacuation (International Tsunami Information Center 2021).

A detailed analysis using a GIS-based risk analysis/mapping tool allowed a macroscopic evacuation model to determine the evacuation capabilities on the island of Stromboli in case of a volcanogenic tsunami. The considered high-risk zone to be evacuated involves 123 individual buildings over an area of 0.18 km<sup>2</sup>. The results show that 33% of the buildings can be evacuated in 4 min, and that a 10-min warning time is required for a complete and well-distributed evacuation in non-congestion situation (Bonilauri et al., 2021).



**Figure 26.** Tsunami signage at Stromboli indicating a) the limit of the Tsunami Hazard zone, b) the direction of the safer “Escape route” and c) the direction to waiting areas (from Bonilauri et al., 2021).

### **Emergency Response Plan**

In case of a tsunami detection by the TEWS (Fig 19) the Department of Italian Civil Protection (DPC) has defined in cooperation with the Sicily Regional Civil Protection, the Lipari Municipality, the monitoring centers of INGV and University of Florence (LGS), a national emergency response plan for non-conventional tsunami, such as volcano tsunamis. Given the short alert time (<4 minutes), the TEWS will send the alert before tsunami wave will be fully developed (generally within the first 20 s from the onset). This gives no time to run models to estimate the possible effects on the nearby coast. Therefore, regardless of the amplitude of the tsunami wave, once received the notification has been received from the TEWS, the DPC will automatically activate for three minutes the acoustic alert (sirens) at Stromboli and Ginostra villages, Panarea and Lipari island, and in the control room of the Harbour Office of Milazzo (see Fig 15) with a continuous

monotone sound. In addition, emails and SMS messages will be automatically sent to a list of previously selected Authorities with the following text: “Tsunami wave in progress at Stromboli”.

The early-warning message is thus automatically delivered to the emergency control rooms for the: i) National Civil Protection; ii) Sicily Regional Civil Protection; iii) Lipari Municipality; and iv) Prefecture of Messina. In coordination and cooperation with the National Department of Civil Protection, the Authorities in-charge will keep contact with: i) Mayor’s delegates for the islands of Stromboli, Vulcano, Panarea, Alicudi, and Filicudi; ii) Municipalities along the Sicily and Calabria coast, iii) Operational bodies present in the territory (e.g. Police, Firefighters, Forestry Corps, etc.) ;and iv) Voluntary structures of Civil Protection present on the different islands. The aim is to inform people, apply the safety procedures at local level, and regulate the navigation and the docking of boats.

Once the tsunami risk is declared over, the Lipari Municipality, with the support of the Regional Department of Civil Protection, will evaluate the opportunity to inform the population of Stromboli, Ginostra, and Panarea by using the same acoustic alert system in “voice” mode. The Department of Civil Protection, will monitor the possible effects of the tsunami along the coasts, and in agreement with the Sicilian Region, it will evaluate the activation of the emergency national civil protection plan.

### **Self-protection measures**

Due to the alert time being as short as 4 minutes at Stromboli and less than 15-20 minutes for the other islands and the coast of Sicily and Calabria, self-protection is, to date, the most effective civil protection measure for the risk reduction. However, due to the nature of the island and the location of the settlements, it cannot be zeroed.

The Department of Civil Protection is involved in activities (program “Io Non Rischio”) to inform local residents on the risk involved and on the self-protection measures to be taken in the case of a tsunami alert. If implemented promptly, self-protection measures can reduce, but do not eliminate, the risk for the population present on the island of Stromboli, but it can serve as the correct behaviour to follow. The efficacy of these self-protection measures also depends on the degree of the population knowledge, on the geographical location on the island, on their health conditions, and on their psycho-physical abilities.

At Stromboli, Civil protection is strongly recommends also actuating the self-protection measures in case the monotone sound of the sirens indicating a tsunami is not heard, if the following phenomena are observed:

- A very strong explosion with the formation of a big dark cloud that rises very high (a few kilometers) above the volcano;
- A big dark cloud that rises from the Sciara del Fuoco, indicative of a large landslide;
- A strong earthquake that you have felt directly or received news of;
- A sudden and unusual withdrawal of the sea followed by a rapid rise in the sea level;

In such case, the actions to follow are:

- Move away from the coast and reach as quickly as possible a safe altitude of 15-20 meters above sea level following the civil protection signs, but do not climb along the slopes of the volcano that could be hit by the fallout of volcanic materials;
- If you are on a boat move quickly from the coastline towards the open sea;
- If you are docking in the harbour, leave the boat immediately and get quickly to an elevated site on land following the civil protection signs, where present;
- If you realize that around you there are people that did not understand the alert signal, invite them to follow the correct actions.

After the tsunami:

- Stay in the area you have reached; after the first tsunami wave, others waves may follow, and be even more dangerous;
- Keep yourself informed and follow the instructions of the authorities and the Civil Protection volunteers to understand when leaving the safe place where you are and what to do.

### **Standard Operating Procedures**

The TEWS implemented at Stromboli is the first early warning system developed to automatically deliver an alert in case of a tsunami generated by volcanic activity (Lacanna & Ripepe, 2020) and is at the moment operating outside the Standard Operating Procedures (SOPs) developed for earthquake-generated tsunamis. However, on August 2022 the University of Florence (LGS) and the National Institute of Geophysics and Volcanology (INGV), in the framework of the operational monitoring activities for the National Department of Civil Protection (DPC), signed a Cooperation Agreement to integrate the TEWS of Stromboli within the activities of the national Tsunami Alert Center (CAT) of the INGV. The CAT-INGV operates as a Tsunami Service Provider certified by the ICG/NEAMTWS (Intergovernmental Coordination Group for the Tsunami Early Warning and Mitigation System in the North-Eastern Atlantic, the Mediterranean and connected seas), which is an integral part of the global tsunami risk warning and mitigation system, established and coordinated by the Intergovernmental Oceanographic Commission (IOC) of UNESCO.

At the moment, the signals recorded by the tsunami systems at Stromboli are transmitted in real-time in a standard format to the CAT-INGV in Rome. The information received will be soon integrated within the standard procedures of the NEAMTWS, both at national as well as at international level.

### **5.2 Anak Krakatau Volcanic Tsunami Warning System**

Following the flank collapse of Anak Krakatau and the associated tsunami in the Sunda Strait on December 22, 2018, an Indonesian Presidential Decree (n°93/2019) ordered the strengthening and development of earthquake and tsunami early warning information system in Indonesia to accommodate such non-seismic generated tsunamis. Different agencies and ministries were involved in enacting this new decree: BMKG, BPPT, KKP, ESDM, BIG, BPPT, LIPI, and, since 2022 the new BRIN (see list of abbreviations below). The BMKG initiated the implementation of a non-tectonic tsunami system (Inatnt) for Indonesia, with the aim of developing SOPs for landslide and volcanic tsunami sources.

Regarding Anak Krakatau, a new local tsunami early warning system was created in 2019, thanks to a collaboration between the KKP and the JCR (Joint Research Center, European Commission). The system is based on inexpensive devices for sea level measurement (IDSL). Different partners later joined the project (BRIN, BIG, PVMBG) and BMKG was designated as the TEWS authority. As of 2022, the system relied on a network of eight IDSL stations delivering data in near real-time. Six stations are located on the coasts of Java and Sumatra, one station on Sebesi Island (Sunda Strait), and one station on Rakata Island (this latter one being located at 5 minutes tsunami travel time from the volcano). Additional stations will be soon added to the network in the proximity of other volcanoes (one on Sertung Island, and another one on Panjang Island). The Ministry of Communication and Information (BAKTI) installed a dedicated satellite system that provides internet connection to the IDSL stations, thus allowing high-frequency real-time transfer to the remote server. Data is accessible in real time on the website of the JCR ([https://webcritech.jrc.ec.europa.eu/TAD\\_server](https://webcritech.jrc.ec.europa.eu/TAD_server)). BMKG monitors the data and will be able to issue alerts utilising its Indonesian Tsunami Early Warning System (InaTEWS) before the waves reach the coasts of Java and Sumatra, assuming a typical tsunami travel time of 20-40 minutes. Local communities are involved in the installation and maintenance of the stations, thus promoting community-based preparedness. In a major German government funded collaboration (Tsunami Risk Project), German scientist and engineers are working with their Indonesian counterparts to further develop the InaTEWS (also developed with German support following the 2004 Indian Ocean Tsunami for seismic generated tsunamis) to also monitor and warn for tsunamis generated by non-seismic and complex sources, such as volcanoes and submarine landslides.

Since the 2018 disaster, the PVMBG (ESDM) has also implemented new equipment on the volcano itself (2 seismic stations, 3 GNSS receivers, an infrasound station, 2 tiltmeters, and a webcam), on nearby islands (seismic stations on Rakata and Sertung Islands), and an infrasound station on the eastern coast of Sumatra.



Figure 27 - IDSL stations installed on the coasts of the Sunda Strait to detect tsunamis from the Anak Krakatau volcano (source: BRIN).

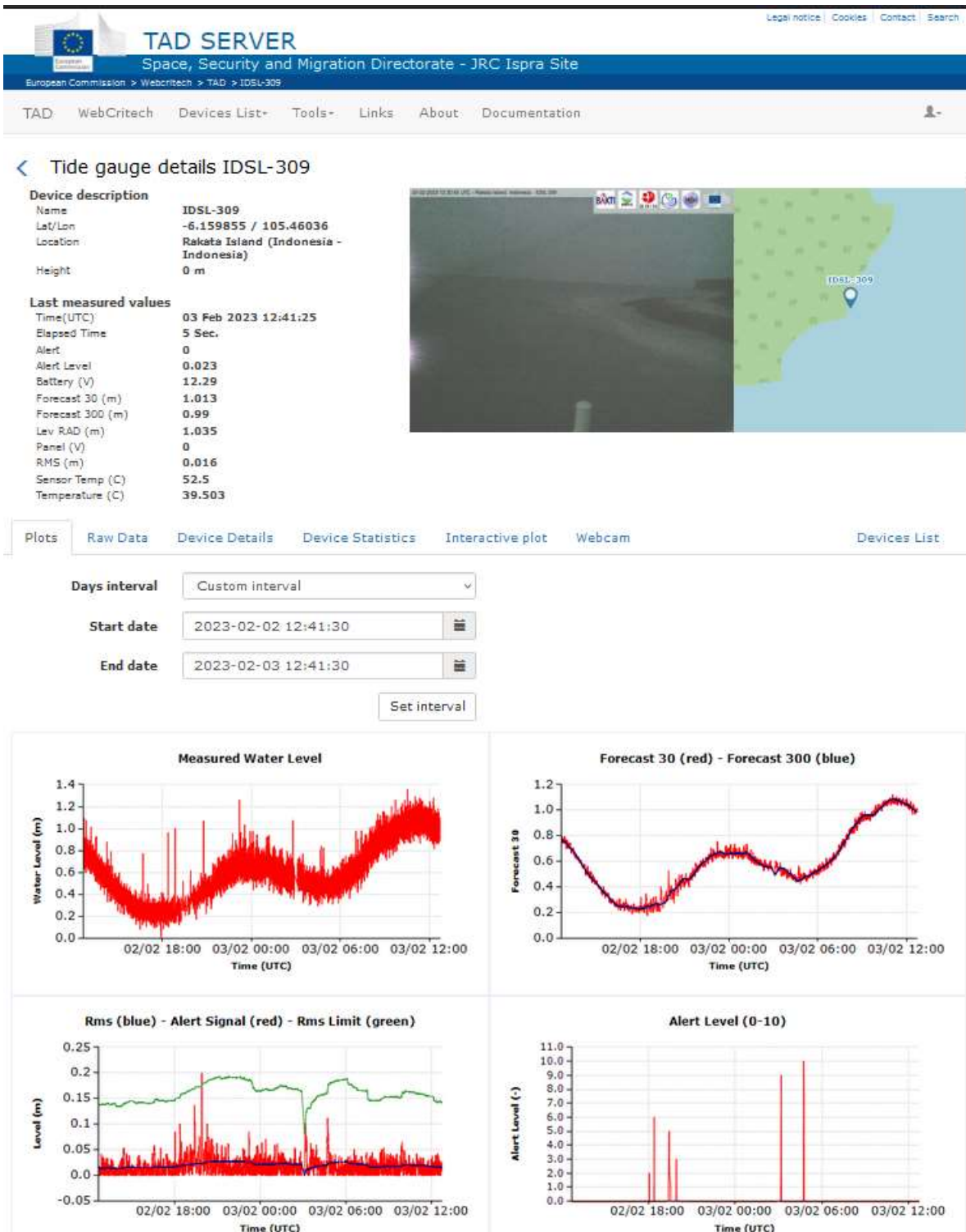


Figure 28 – Live data from the IDSL station at Rakata Islands (source: JCR website).

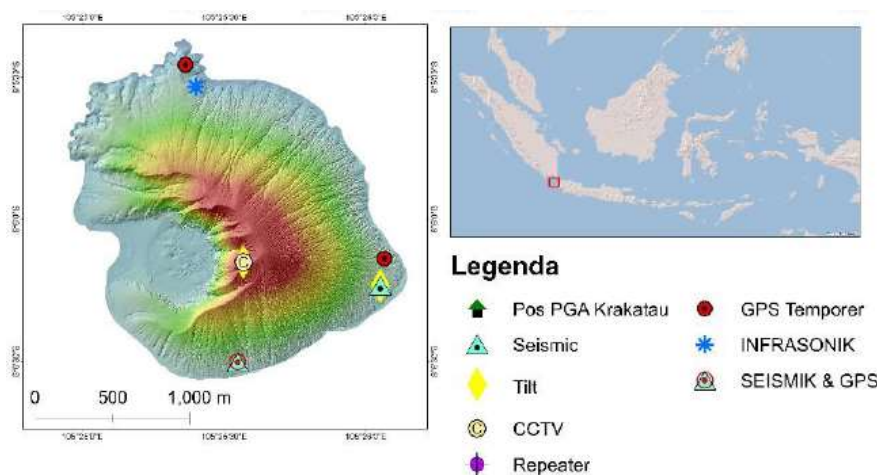


Figure 29 – Monitoring equipment installed on Anak Krakatau volcano (source: PVMBG).

## ABBREVIATIONS

BMKG: Badan Meteorologi, Klimatologi, dan Geofisika / Meteorological, Climatological, and Geophysical Agency.

BPPT: Badan Pengkajian dan Penerapan Teknologi / Agency for the Assessment and Application of Technology).

KKP: Kementerian Kelautan dan Perikanan / Marine and Fisheries Ministry.

ESDM: Energi dan Sumber Daya Mineral / Ministry of Energy and Mineral Resources.

PVMBG: Pusat Vulkanologi dan Mitigasi Bencana Geologi / Center for Volcanology and Geological Hazard Mitigation.

LIPI: Lembaga Ilmu Pengetahuan Indonesia / Indonesia Institute of Science.

BIG: Badan Informasi Geospasial / Geospatial Information Agency.

BRIN: Badan Riset dan Inovasi Nasional / National Research and Innovation Agency.

## REFERENCES

Bertolaso G, De Bernardinis B, Bosi V et al (2009) Civil protection preparedness and response to the 2007 eruptive crisis of Stromboli volcano, Italy. *J. Volcanol Geotherm Res* 182(3-4):269–277. <https://doi.org/10.1016/j.jvolgeores.2009.01.022>

Bonilauri, E.M., Harris, A.J.L., Morin, J., Ripepe, M., Mangione, D., Lacanna, G., Ciolli, S., Cusolito, M. and Deguy, P., (2021). Tsunami evacuation times and routes to safe zones: a GIS-based approach to tsunami evacuation planning on the island of Stromboli, Italy. *J. Applied Volcanol.*, <https://doi.org/10.1186/s13617-021-00104-9>

Lacanna, G., and Ripepe, M. (2020). “Genesis of tsunami waves generated by pyroclastic flows and the early-warning system,” in Rittmann Conference 2020, Session S13. The Summer 2019 Stromboli Paroxysms: A Precious Opportunity to Expand the Knowledge on the Volcano (Catania).

## Chapter 6 – Recommendations/Gaps

### Recommendations to IOC-UNESCO Member States:

#### Monitoring and Warning:

1. As a first step, organisation(s) should be designated for monitoring and warning of Tsunamis Generated by Volcanoes (TGV) . The second and third steps are to install monitoring instrumentation and develop Standard Operating Procedures (SOPs) to handle volcanic tsunamis.
2. The TGV monitoring and warning system should be implemented by, or in cooperation with the National Tsunami Warning Centre (NTWC) and regional Tsunami Service Provider and national and regional Volcano Service Providers , where such exist.
3. All volcanoes mentioned in the TGV report should be monitored and have processes in place to warn for tsunamis. Should other, potentially tsunamigenic volcanoes begin erupting, these should also be monitored and included within the tsunami warning process.
4. Detect/warn geophysical (seismology, GNSS, tiltmeter, barometric and sea level data streams need to be available to designated the tsunami monitoring/warning agency (and possibly also to the volcano monitoring agency)
5. As well as monitoring systems for volcano activity and potential far-field propagation of sea level signal, a sea level gauges network with real-time continuous data transmission should be deployed close to each identified volcano to verify risk and then ongoing monitoring and warning. One second sampling with 1 cm accuracy (< 1 mm sampling) is recommended sampling is recommended for recording and automatic detection. Data transmission through radio or microwave links, fiber optic, or dedicated telephone lines, or other modes should be implemented to ensure the data is transmitted and received and widely shared with international community in a timely manner.
6. Methods to also specifically alert persons in remote areas (such as scientific teams in the field, or recreational hikers) should be considered.
7. TGV SOPs for tsunami warning should be linked with existing Volcano Alert Activity scales.

#### Risk Assessment and Preparedness:

8. A TGV hazard and risk assessment should be undertaken to determine vulnerable areas.
9. For TGV, multi-stakeholder meetings should be convened that included science agencies, volcano and tsunami warning operations centres, and disaster management agencies. For each identified potential source, worst-case and credible scenario planning discussions should start as soon as possible.
10. During a period of heightened TGV hazard, consider closing access to vulnerable areas. When eruption is imminent and then tsunami hazard is high, consider evacuating populations from vulnerable locations.
11. Specific TGV signage and evacuation routes should be implemented in all areas that may be impacted by tsunamis generated by volcanoes.
12. TGV public awareness campaigns should be conducted regularly – the type and frequency of awareness activities may be different for the local population compared to transient populations such as tourists.

**Recommendation to TOWS-WG:**

13. TGV warning notification systems should be considered and coordinated as part of the IOC-UNESCO Global Tsunami Warning and Mitigation System, and also when possible be part of a Multi-Hazard Early Warning System (MHEWS).
14. TOWS-WGs recommend ICGs examine TGVs in region of responsibility and review TGV hazard monitoring and warning requirements, including costs of deploying and maintaining such systems.
15. TOWS-WG recommend, where identified TGVs may impact multiple Member States, Tsunami Service Providers (TSPs) for the relevant ocean basin tsunami warning and mitigation systems consider if they need to be involved in monitoring and provision of threat advice.
16. IOC-UNESCO Ad hoc Team on TGV should continue and finalize the TGV Report by mid-2023.

**Recommendation to IOC-UNESCO Secretariat:**

17. IOC Secretariat to help inform Member States widely on the potential tsunami hazard from volcanoes:
  - a. Publish the TGV report as an IOC-UNESCO publication in 2023
  - b. Provide the TGV Report, including the List of Tsunamigenic Volcanoes to Volcano Observatories
  - c. Provide the TGV Report, including the List of Tsunamigenic Volcanoes to IOC-UNESCO Member States



## APPENDIX 1

### Volcano Observatory Questionnaire

#### 16 countries responded:

- Italy submitted from multiple agencies that are involved and/or multiple volcanoes/regions.
- France provided a single questionnaire gathering information from all 4 observatories.
- Notably missing were Philippines, Tonga (new monitoring post-HTHH), USGS/HVO (for Hawaii, American Samoa – note that tsunami warnings are provided by Pacific Tsunami Warning Center (PTWC)).
- PTWC Tsunami Inundation Detection System (TIDS) for Hawaii island, USA is used as criteria for Hawaii tsunami warning when there is either no earthquake or an earthquake less than their M6.9 earthquake tsunami warning criteria. This system has been in place for about 20 years and is able to alert the PTWC within one minute after the sensor is flooded. The PTWC conducts a ‘wet’ sensor communication test daily.

#### IOC Tsunami Service Providers (for regional alerts):

- The ICG/PTWS through the PTWC has implemented TGV interim SOPs for the Hunga Tonga – Hunga Ha’apai Volcano, Tonga. The SOPs (IOC Circular letter No 2902 17 August 2022) are expected to be formally adopted at the next ICG/PTWS-XXX (September 2023).
- The ICG/CARIBE-EWS through its Task Team on Tsunami Procedures for Volcano Crises will be testing several Volcano Observatory Notice for Tsunami Threat (VONUT) message products in its next CARIBEWAVE exercise in March 2023 (Mount Pelée flank collapse scenario). Messages are to be issued by countries and the PTWC. The messages have a Volcanic Activity Summary and share information on where the closest sea level gauges are located.
- ICG/IOTWMS is investigating the development of a TSP product for tsunamis generated by volcanoes, based on the VACC related procedures developed and operated by the Joint Australian Tsunami Warning Centre (TSP-Australia)

#### General Comment:

- TGV tsunami warnings currently follow a ‘Detect, then Warn’ procedure only. This procedure requires detection and confirmation of a wave, and so the warning may be too late to be useful unless there are many wave detection sensors between the volcano and coastal communities. However, if heightened volcanic unrest with precursor activity is known in advance, then tsunami warning centres can be on heightened pre-alert to watch for Eruption/Flank collapse-related tsunamis. For a significant tsunami to be generated, the eruption or flank collapse needs to be ‘massive,’ but this is yet to be quantitatively defined.

#### Hazard assessment:

- TGV tsunami hazard assessments (eruption history, numerical modelling of historical events or worst-case scenarios) in general have not been conducted for all potential volcanoes.

#### Monitoring – instrumentation:

- Volcano Observatories generally monitor in real time seismicity, surface deformation (tilt, movement), and geochemistry as eruption indicators.
- Most Volcano Observatories do not host sea level stations, and thus are not monitoring the sea level for tsunamis.

**Warning – procedures:**

- Only Stromboli, Anak Krakatau, and Tonga (Hunga Tonga – Hunga Ha’apai volcano) have dedicated EWS instrumentation for volcanic tsunamis, with Standard Operating Procedures (SOPs). Hawaii Island (also known as Big Island) of State of Hawaii has TIDS ‘wet sensor’ system to detect tsunami inundation (from any source).
  - Stromboli has custom-designed elastic beacons deployed in the ocean to detect tsunami waves. Automatic detection is followed by siren sounding. Testing indicates that it can detect a tsunami wave within about 15 seconds. It was deployed in 2018 and has detected three tsunamis since then with no false alerts.
  - At Stromboli, early warning based on ground deformation was demonstrated in the 3 July 2019 eruption; with an alert issued to Civil Defense in Rome, Sicily, and at Stromboli five minutes before the eruption, six minutes before the tsunami was generated and 10 minutes before the first wave reached the coast in Stromboli.
  - Since 2019, Anak Krakatau has had sea level stations installed on the nearby islands and the coasts of Java and Sumatra (Sunda Strait) which deliver near-real-time data to a remote server.
  - On Hawaii Island, PTWC monitors for tsunami inundation using TIDS on-land ‘wet sensors,’ deployed at elevations and distances inland where evacuation from a tsunami would be needed. When the floodwater reaches the sensor then it triggers. When the earthquake magnitude is less than 6.9, and especially if it is much smaller, but a TIDS triggers or sea level fluctuations above 1 meter amplitude are observed nearby, then a Local Tsunami Warning is issued.
  - HTHH Volcano:: the PTWS through the PTWC has implemented tsunami threat alert SOPs based on the detection of tsunami waves at the nearest coastal sea level gauge (Nuku’alofa, Tongatapu, Tonga) or the nearest DART deep-ocean sensors. The threat message assumes that the HTHH is the volcanic tsunami source, and the forecast amplitudes are scaled linearly based on the observations from the 15 January 2022 volcanic tsunami.
- Only Australia has documented SOPs for non-seismic sources that depend upon VAAC notifications.
- Most observatories have discussed the potential threat of tsunamis, but do not yet have SOPs. Stromboli, Anak Krakatau, Australia, and Hawaii island (Hualalai, Kilauea) do. Japan has SOPs that have been developed on a case-by-case basis.
- Monitoring instruments are coastal sea level gauges and in-water pressure sensors (Elastic beacon, DART or DART-like)
- Two types of triggers:
  - VAAC notice of activity. Information exchange between VO and VAAC. This describe volcanic activity only – it does not include tsunami hazard potential nor does it confirm that a tsunami wave was generated. Therefore, it could be considered a pre-alert to be on the watch for a tsunami.
  - Wave detection at coastal or in-water sensors. . This confirms that a wave was generated, and if large enough would result in a Tsunami Warning.
- Tsunami Warnings are usually issued by Tsunami Warning Centres (TWC), which receive real-time sea level data for tsunami monitoring. In general, since most Volcano Observatories do not have 24x7 operations, they cannot serve as Tsunami Warning Centres.
  - To date, Volcano Observatories have not in general worked closely with TWCs. However, earthquake, tsunami, volcano monitoring are part of same department / agency in some countries (e.g. New Zealand). In other countries, they are not. so the monitoring data streams and their associated SOPs may not be coordinated (seamless) to enable efficient warnings. This is the similar situation for science agencies and universities, which may not be aware of the tsunami early warning process and or the tsunami warning SOPs.
  - Only very recently has the Stromboli Volcano Observatory been working with the Italian NTWC (INGV) to manage tsunami monitoring and warning.



### QUESTIONNAIRE: Tsunamis Generated by Volcanoes

<b>Name of respondent:</b>	
<b>Institution :</b>	
<b>Email address :</b>	
<b>A : VOLCANO</b>	
1. How many volcanoes do you have to monitor?	
2. Name of the volcanoes, coordinates and which ones are potentially tsunamigenic?	
3. Based on your expertise, can you identify one or several eruptive and/or gravitational processes that could generate a tsunami from each of these volcanoes?	
4. Have you ever had discussions about volcanic tsunami in your group/observatory/institute, and how to address this hazard?	
<b>B: MONITORING</b>	
5. Have you implemented networks to monitor the various eruptive/gravitational processes? If yes, please describe the networks	
6. In your opinion, what could be the best pool of monitoring techniques for the early detection of volcanic tsunami?	
7. Did you build and implement instruments (e.g., tide gauges, instrumented buoys) designed specifically to monitor volcanic tsunamis?	
8. Have you, or do you plan to implement a volcano tsunami monitoring system? If yes for which volcano and when?	
9. Do you currently share any monitoring data for volcanoes, earthquakes, or other geophysical/geological phenomena with a tsunami warning center or with an international group (eg IRIS, UNESCO/IOC, ...)?	
10. Have you ever recorded a tsunami of volcanic origin? When, and are the data available or published?	
<b>C: WARNING</b>	
11. Is a volcanic tsunami hazard included in your standard operating procedures	

<p>(early detection, alert, evacuation)? If yes, could you provide documentation related to the method of detection, characterization, and procedures for alerting?</p>	
<p>12. Have you ever been in contact with a local, national or regional tsunami warning centre? If yes, which one?</p>	
<p>13. What procedures have been established in conjunction with Volcanic Ash Advisory Centers (VAACs)?</p>	
<p>14. Do you monitor and provide alerts for sub-marine volcanoes to VAACs?</p>	
<p><b>D: References</b> Please provide references to any relevant papers or reports related to this questionnaire. If possible, please also email copies.</p>	
<p><b>E: Additional Information</b> Please provide any additional information or requests.</p>	

DRAFT

APPENDIX 2

LIST OF TSUNAMIGENIC VOLCANOES (TGV + VO)

A	B	C	D	E	F	G	H	I
NAME	COUNTRY	REGION	SUBREGION/ISLAND	BAIN	LONG, LAT (WGS84)	VOLCANO TYPE	DISTANCE / COAST (km)	LAST 0000 0000 year
Mount Pelée	FRANCE	WEST INDIES	MARTINIQUE	CARIBBEAN	-61.16488,14.80937	A	5.8	1852
Mount de la Feuillade	FRANCE	INDONESIA	REUNION ISLAND	INDIAN	53.70798,-21.24288	B	9	2021
Kulambé	GREECE	AEGEAN SEA	ME SANTORINI	MEDITERRANEAN	25.48477,36.52648	C	0	1692
Santorini	GREECE	AEGEAN SEA	SANTORINI	MEDITERRANEAN	25.49594,36.40419	C	0.8	1956
Blackburn Jorjy	SPAIN	WEST INDIES	NA SPAINADA	CARIBBEAN	-61.64121,12.29880	C	0	2017
Vestmannaeyjar	ICELAND	ICELAND	WESTMANA ISLANDS	NE ATLANTIC	-20.2646,65.4188	C	0	1873
Barren Island	INDIA	ANDAMAN ISLANDS	BARREN ISLAND	INDIAN	93.88073,11.27905	A	1.1	2020
Anak Krakatau	INDONESIA	JAWA-SUMATRA	SUNDA STRAIT	INDIAN	108.42572,-6.18119	B	0.8	2020
Banda Api	INDONESIA	BANDA SEA	BANDA	PACIFIC	128.88248,-4.52215	A	1.8	1988
Batu Tara	INDONESIA	FLORES SEA	KOMBA	PACIFIC	122.58594,-7.78819	A	1	2022
Belatunda	INDONESIA	FLORES SEA	FALUNGH	PACIFIC	121.70889,-8.22125	A	2.5	2021
Sangeang Api	INDONESIA	FLORES SEA	SANGEANG	PACIFIC	118.07565,-8.18806	A	5.2	2022
Ilawung	INDONESIA	HALA TENGISARA EAST	LEMBATA	PACIFIC	123.57281,-8.59105	A	1.8	2021
Luwatolo	INDONESIA	HALA TENGISARA EAST	LEMBATA	PACIFIC	123.58788,-8.27514	A	4	2022
Kaw	INDONESIA	SULAWESI	SANGHE	PACIFIC	125.44882,2.09011	A	5.5	2004
Sangeang	INDONESIA	SULAWESI	SANGHE	PACIFIC	125.48985,2.78888	A	4	2020
Ruang	INDONESIA	SULAWESI	SANGHE	PACIFIC	125.38987,2.30081	A	1.8	2003
Stromboli	ITALY	MEDIAN ISLANDS	STROMBOLI	MEDITERRANEAN	15.3239,38.7919	A	1.8	2022
Vulcano	ITALY	MEDIAN ISLANDS	VULCANO	MEDITERRANEAN	14.88134,38.40033	B	0.8	1880
Myiako-jima	JAPAN	IJU ISLANDS	MYIAKE	PACIFIC	138.52850,34.08279	A	2	2020
Myiashiro-jima	JAPAN	IJU ISLANDS	MYIASHIRO	PACIFIC	138.81800,33.31888,11.0	C	0	1879
Nishino-jima	JAPAN	IJU ISLANDS	NISHINO	PACIFIC	140.87387,27.24735	B	0.2	2021
Sentou	JAPAN	IJU ISLANDS	SENTOU	PACIFIC	140.85,31.488	C	0	1918
Tori-jima	JAPAN	IJU ISLANDS	TORI	PACIFIC	140.30281,28.48421	A	1.1	2002
Oshima-Oshima	JAPAN	JAPAN SEA	OSHIMA	PACIFIC	138.36710,41.51001	A	1	1789
Iki	JAPAN	IYUZU ISLANDS	IYUZU	PACIFIC	138.84526,36.79218	B	1	2020
Awajishiro-jima	JAPAN	IYUZU ISLANDS	AWAJISHIRO	PACIFIC	129.71988,29.69847	A	5.2	2020
Seitoko-jima	MONTERRAT	WEST INDIES	MONTERRAT	CARIBBEAN	-62.17988,-16.70217	A	8.3	2022
White Island	NEW ZEALAND	BAY OF PLENTY	WHITE ISLAND	PACIFIC	177.20557,-37.51937	A	0.8	2020
Mount St. Helens	USA	WASHOOSH	WHITE ISLAND	PACIFIC	-86.32806,46.42115	A	2.5	2018
Calgaigine	PAPUA-NEW GUINEA	BI-SMARK SEA	BI-SMARK	PACIFIC	-87.57081,11.86146	A	6.1	1854
Ben	PAPUA-NEW GUINEA	BI-SMARK SEA	BEN	PACIFIC	144.81881,-5.41275	A	1.1	1860
Eden	PAPUA-NEW GUINEA	BI-SMARK SEA	EDEN	PACIFIC	144.58906,-5.83734	A	0.5	2020
Moran	PAPUA-NEW GUINEA	BI-SMARK SEA	MORAN	PACIFIC	145.02742,-4.37890	A	3	2020
Watu Island	PAPUA-NEW GUINEA	BI-SMARK SEA	WATU ISLAND	PACIFIC	148.11472,-5.51817	C	0	2007
Belau	PAPUA-NEW GUINEA	NEW BRITAIN	BELAU	PACIFIC	152.29399,-4.27081	B	0.8	2024
Belau	PHILIPPINES	SARAYAN ISLANDS	NE CAGAYAN	PACIFIC	122.29254,-18.07189	B	0.2	1978
Compin	PHILIPPINES	BOHOL SEA	CAMPAN	PACIFIC	124.7251,8.1754	B	4	1853
Tal	PHILIPPINES	LUZON	TAL	PACIFIC	120.8938,14.0070	B	3.2	2021
Belau	RUSSIA	RUSSIAN ISLANDS	RUSSIA	PACIFIC	153.24978,48.29220	A	0.2	2019
Tuvaiti	SOLOMON ISLANDS	EAST SOLOMON	TUVALUA	PACIFIC	166.80182,-10.88840	A	1.1	2020
Wanatu	SOLOMON ISLANDS	WEST SOLOMON	WANATU	PACIFIC	157.878884,-8.990990	C	0	2021
St Vincent	ST VINCENT	WEST INDIES	ST VINCENT	CARIBBEAN	-61.08091,13.23104	A	2.5	2020
Mount Raui	TONGA	TONGA	WEST NGAUFU	PACIFIC	-174.77517,-18.89182	C	0	2008
Mount 'Apai	TONGA	TONGA	NORTH TONGATAPU	PACIFIC	-175.06677,-20.54491	B	0.1	2022
Lavaia / Mount Hood	TONGA	TONGA	WEST NGAUFU	PACIFIC	-174.869984,-19.289928	C	0	2019
Tofua	TONGA	TONGA	TOFU	PACIFIC	-175.07000,-19.76323	A	3	2024
Unamau	TONGA	TONGA	WEST TONGATAPU	PACIFIC	-175.55041,-20.85174	C	0	2022
Augustine	USA	ALASKA	AUGUSTINE	PACIFIC	-153.45023,59.38003	A	4	2004
Agulof	USA	ALUTIAN ISLANDS	AGULOF	PACIFIC	-168.03348,58.84010	A	0.2	2017
Crater	USA	ALUTIAN ISLANDS	CRATER	PACIFIC	-179.30883,52.17454	A	0.4	2008
Mount Loa	USA	CALIFORNIA	LOA	PACIFIC	-119.02655,38.00242	B	0.8	1790
Alava	USA	HAWAII	BIG ISLAND	PACIFIC	-155.2888,19.4201	B	14	2022
Laki	USA	HAWAII	SOUTH BIG ISLAND	PACIFIC	-155.2888,18.8281	B	0	1886
Asahi	USA	MARIANA ISLANDS	ASAHU	PACIFIC	145.47488,16.28819	A	1.8	1998
Mount Taal	USA	MARIANA ISLANDS	WEST SAMPALU	PACIFIC	144.73498,14.00084	C	0	2020
Baby	USA	MARIANA ISLANDS	NORTH SAMPALU	PACIFIC	145.58974,15.81975	C	0	1995
South Sargen	USA	MARIANA ISLANDS	SARGEN	PACIFIC	145.77988,14.57878	C	0	2020
Vanuatu	VANUATU	VANUATU	SE VANUATU	PACIFIC	168.34584,-16.93700	A	5.2	2007
Yasur	VANUATU	VANUATU	TANNA ISLAND	PACIFIC	169.44985,-16.93188	B	5.1	2020
Eastern Central	VANUATU	VANUATU	SOUTH ANATOM	PACIFIC	170.28844,-20.88807	C	0	1888

A	B	C	D	E	F	G	H	I
NAME	COUNTRY	REGION	SUBREGION/ISLAND	BAIN	LONG, LAT (WGS84)	VOLCANO TYPE	DISTANCE / COAST (km)	LAST 0000 0000 year
East Eye	VANUATU	VANUATU	EAST EYE	PACIFIC	168.27887,-18.88888	C	0	2020
Erasm	VANUATU	VANUATU	SOUTH EYE	PACIFIC	169.53700,-18.82028	C	0	1974
Mount St. Helens	ST. HELENA, NEVIS	WEST INDIES	ST. HELENA	CARIBBEAN	-62.88886,17.37000	A	4.8	1843
Saba	NETHERLANDS	WEST INDIES	SABA	CARIBBEAN	-65.28815,17.89988	A	1.9	1840
The Gulf	NETHERLANDS	WEST INDIES	ST. EUSTATIUS	CARIBBEAN	-62.88888,17.47784	A	1.2	2020
Saint Pierre	FRANCE	WEST INDIES	SAINT PIERRE	CARIBBEAN	-61.64339,14.04370	A	6.7	1876
Fort Macaulay	FRANCE	COMORES	MAOULAI	INDIAN	49.40180,-11.17710	C	0	2020
Delonze	PAPUA-NEW GUINEA	NEW BRITAIN	DELONZE	PACIFIC	150.10007,-4.05447	B	0.2	1880
Long Island	PAPUA-NEW GUINEA	BI-SMARK SEA	LONG ISLAND	PACIFIC	147.11781,-6.35215	A	7	1880
Ulakan	PAPUA-NEW GUINEA	NEW BRITAIN	ULAKAN	PACIFIC	151.30889,-5.18818	A	10.9	2022
Tulaman	PAPUA-NEW GUINEA	NEW BRITAIN	SOUTH HANAU	PACIFIC	147.20281,-2.45518	C	0	1957
Pyroch	RUSSIA	KURIL ISLANDS	PYROCH	PACIFIC	143.20000,48.09158	A	2.8	2021
Yasur	SOLOMON ISLANDS	WEST SOLOMON	NORTH GUADALCANAL	PACIFIC	159.80748,-8.13400	A	2.8	1847
Merapi	INDONESIA	HALUJAU	MERAPI	PACIFIC	107.53883,7.78334	A	4.8	2007
Merapi	INDONESIA	HALUJAU	MERAPI	PACIFIC	107.53883,7.78334	A	4.3	2018
Merapi	INDONESIA	BANDA SEA	EAST MERAPI	PACIFIC	128.34371,-8.87822	A	1.8	1904
Vesuvius	ITALY	CAMPANIA	VEVUVIUS	MEDITERRANEAN	15.21487,40.78995	A	5.6	1844
Etne	ITALY	SICILIA	ETNE	MEDITERRANEAN	15.00181,37.75128	A	2.7	2020
Campi Flegrei	ITALY	CAMPANIA	CAMPI FLEGREI	MEDITERRANEAN	14.18877,40.82574	B	0	1538
Tasor	NEW ZEALAND	NORTH ISLAND	TASOR	PACIFIC	175.81888,-38.88887	B	0	2020
Okatape	NEW ZEALAND	NORTH ISLAND	OKATAPE	PACIFIC	175.58817,-38.12027	B	0	1881
Mount Hood	NEW ZEALAND	REPMARIC	HOOD ISLAND	PACIFIC	-177.81881,-39.88817	A	1.8	2008
Cambo Viejo	SPAIN	CANARY ISLANDS	LAPALMA	ATLANTIC	-17.89715,28.58862	B	1.2	2021
San Jorge	PORTUGAL	AZORES ISLANDS	SANTO JORGE	ATLANTIC	-28.07794,38.05123	B	1.2	1881
Kilauea	ICELAND	ICELAND	KILAUEA	NE ATLANTIC	-18.02328,69.40888	A	29.4	1918
Fuquajima-Okanabe	JAPAN	IJU ISLANDS	FUQUAJIMA	PACIFIC	141.48834,24.77891	C	0	2021